UNIVERSITÉ DU QUÉBEC À MONTRÉAL

# GOLD MINERALIZATIONS AT THE SYENITE-HOSTED BEATTIE GOLD DEPOSIT AT DUPARQUET, NEOARCHEAN ABITIBI BELT, QUEBEC, CANADA

THESIS

PRESENTED

AS PARTIAL REQUIREMENT

OF THE MASTERS OF EARTH SCIENCES

BY

LUDOVIC BIGOT

DECEMBER 2012

UNIVERSITÉ DU QUÉBEC À MONTRÉAL

# LES MINÉRALISATIONS AURIFÈRES DU GISEMENT ARCHÉEN DE BEATTIE À DUPARQUET, ABITIBI, QUÉBEC, CANADA

MÉMOIRE

PRÉSENTÉ

COMME EXIGENCE PARTIELLE

DE LA MAÎTRISE EN SCIENCES DE LA TERRE

PAR

LUDOVIC BIGOT

DÉCEMBRE 2012

# AVANT-PROPOS

Ce mémoire est rédigé sous la forme d'un article scientifique qui sera soumis à la revue *Economic Geology* sous le titre *Gold Mineralizations at the Syenite-Hosted Beattie Gold Deposit at Duparquet, Neoarchean Abitibi Belt, Quebec, Canada.* Sa présentation est différente des mémoires habituellement présentées à l'UQAM; la rédaction est en anglais, et les figures et tableaux sont situés à la fin de l'article. Michel Jébrak, le directeur de maîtrise, est co-auteur de cet article. Ce format de mémoire a été choisi car il donne l'opportunité de transmettre de nouvelles connaissances à la communauté scientifique à l'échelle internationale.

REMERCIEMENTS

Je tiens à remercier en premier lieu Michel Jébrak, mon directeur de maîtrise, pour ses précieux commentaires, son enthousiasme, et ses multiples idées qui ont permis l'accomplissement de ce projet de maîtrise.

Je remercie la Corporation Minière Osisko, le CRSNG, et le FQRNT pour le financement. Un grand merci aux géologues d'Osisko pour leurs conseils techniques, tout particulièrement Carl Corriveau pour son aide sur le terrain et nos nombreuses discussions très enrichissantes. Un gros merci à Claude Gagnier, Olivier Nadeau, Julie Bourdeau, André Lalonde, Jean Goutier, Silvain Rafini, et Stéphane Faure pour leurs commentaires très constructifs qui ont grandement amélioré la qualité de ce travail. Merci aux correcteurs, Robert Wares et Michel Gauthier, pour la relecture du document. Je pense aussi à Raynald Lapointe, Dirk Schuman, et Lang Shi pour leur aide dans l'acquisition de données respectivement au MEB, au TEM, et à la microsonde. Un grand merci à Michelle Laithier pour les illustrations, à Jeffrey Vaillancourt et Denise Roy pour la gestion, et à Stéphanie et Killian pour la relecture de l'anglais. Merci à Christophe pour l'échantillonnage des veines. Je suis également très reconnaissant envers la SEG pour m'avoir octroyé des bourses et permis de prendre une super expérience au Chili.

Finalement, un énorme merci à Sylvie, ma copine, pour son soutien incroyable et sa compréhension durant cette aventure. Un grand merci à la famille, ainsi qu'aux collègues et amis, Stépane, Noémie, Laura, Émilie, Raph, Yona, Stéphanie, PA, Sam, et Misa.

TABLE DES MATIÈRES

LISTE DES FIGURES

LISTE DES TABLEAUX

RÉSUMÉ

Le gisement de Beattie est situé dans la ceinture de roches vertes de l'Abitibi, à proximité de la faille Porcupine-Destor, et est associé à une syénite porphyrique. Les corps minéralisés ont une ressource totale inférée de 2,77Moz contenu dans 56,2Mt de minerai à 1,53g/t d'or. Dans le gisement de Beattie, deux styles de minéralisation sont présents, à contrôle lithologique et à contrôle structural. La minéralisation à contrôle lithologique est limitée exclusivement à la syénite altérée en carbonates de fer. Cette minéralisation représente du minerai à basse teneur mais fort tonnage, dans lequel l'or est porté par la pyrite arsénifère et l'arsénopyrite. L'or est « invisible »; il se présente sous la forme de solution-solide dans le cœur poreux et riche en arsenic des pyrites. La minéralisation à contrôle structural est présente uniquement dans des zones de cisaillement adjacentes et incluses dans la syénite. Le minerai est à haute teneur dans des zones de brèches silicifiées à caractère hydraulique et tectonique, dans des veines de quartz cherteux, dans des veines polymétalliques intensément silicifiées, et dans des dykes de syénite trachytique très altérée. L'or y est visible sous forme d'éléctrum dans les microfractures des pyrites bréchifiées. Les deux styles de minéralisation et les altérations font partie d'une évolution paragénetique commune dans un environnement magmatique-hydrothermal. Des phases initiales oxydantes ont évolué en conditions réduites à la faveur de fluides magmatiques et externes riches en $CO_2$. Ce changement d'état d'oxydation a entrainé la précipitation des sulfures et la cristallisation de l'or « invisible » dans la pyrite arsénifère et l'arsénopyrite. Une phase d'altération ultérieure, dominée par des fluides hydrothermaux riches en silice, a pour résultat la bréchification des sulfures et leur redistribution dans des corridors siliceux, ainsi que la remobilisation de l'or dans les microfractures des pyrites bréchifiées. Les compositions calculées de $\delta^{18}O$ et $\delta D$ sur les veines de quartz associées à cet évènement tardif sont respectivement 7.67‰ et - 66‰, indiquant une dominance des fluides magmatiques avec une probable composante métamorphique. Cet évènement syn-métamorphique (transition D2-D3) est associé à un fort enrichissement en Hg, Te, Mo, Ag, Sb, As, et Se. Le style de cristallisation de l'or dans le gisement de Beattie est une conséquence de la dominance des régimes en systèmes ouverts, tant au niveau de l'incorporation dans le magma de l'arsenic qui contrôle la précipitation de l'or « invisible », que de la circulation tardive de fluides hydrothermaux riches en silice qui sont à l'origine de la remobilisation de l'or. Le gisement de Beattie partage des affinités avec des gisements associés aux intrusions (*Intrusion Related Gold Deposit*), des gisements épithemaux à tendance neutre à intermédiaire, et des gisements de type mésothermaux.

MOTS CLÉS : Gisement d'or, porphyre Archéen, or invisible, remobilisation de l'or

# INTRODUCTION GÉNÉRALE

La fertilité aurifère des couloirs de déformation en Abitibi (e.g., Porcupine-Destor, Larder-Lake-Cadillac) est bien reconnue, et notamment avec le style de gisements d'or orogénique (Rabeau, 2010). Cependant, l'exploration de l'or en Abitibi dans ces corridors de déformation porte de plus en plus sur des gisements aurifères porphyriques (Legault et Lalonde, 2009; Lafrance, 2011). Cette tendance s'est concrétisée par la découverte du gisement de Canadian Malartic par Osisko, et sa mise en production au printemps 2011. Avec le développement du modèle de gisements associés aux intrusions (*Intrusion Related Gold Deposit* ; Lang et Baker, 2001), et une certaine remise en cause de la classification de nombreux gisements d'or orogéniques (Groves et al., 1998), les modèles génétiques ont évolué ou ont été précisés. Ainsi, une origine commune dans un large système magmatique-hydrothermal est proposé pour les gisements de Canadian Malartic, Beattie, ou encore Douay (Robert, 2001). Ces gisements présentent des particularités communes, telles que des minéralisations disséminées dans de grands volumes de roches alcalines porphyriques, ou encore des altérations à carbonate, séricite, et silice; mais ils ont aussi des caractères atypiques bien distincts, tels que le style de cristallisation de l'or, des phases différentes de minéralisations, ou encore des associations d'éléments qui mettent en avant l'hétérogénéité de gisements pourtant classés sous une même appellation.

Les récents travaux effectués sur la propriété de Beattie démontrent une dominance du caractère disséminé et à basse teneur de la minéralisation dans l'intrusion, mais aussi un contrôle structural bien marqué le long de failles cisaillantes avec des teneurs élevées en or (Dupéré, 2011). Lorsque la mine Beattie était en opération (1933-1956), l'exploitation se faisait uniquement sur les corps minéralisés à haute teneur le long des failles (Davidson et Banfield, 1944); 33 t d'or ont été produit de 9,26 Mt de minerai à 3,86g/t Au. À la différence, le projet proposé par Corporation Minière Osisko et Clifton Star Resources Inc. portait sur une exploitation à faible teneur mais fort tonnage dans la syénite et ses bordures; les ressources inférées indiquent 83 t d'or pour 56.2 Mt de minerai à 1.53g/t Au (Dupéré, 2011). De même que pour ces deux types d'opérations, les pensées sur le modèle génétique du gisement ont évolué. En effet, Davidson et Banfield (1944) considèrent le gisement de

Beattie comme mesothermal, ou possiblement épithermal, alors que les études plus récentes (Robert, 2001 ; Legault et al., 2005) regardent la minéralisation comme génétiquement liée à la syénite.

L'objectif de ce projet de recherche est d'approfondir la compréhension métallogénique du gisement de Beattie, en déterminant la nature et les contrôles de la minéralisation. Pour cela, différents volets de la géologie ont été étudiés. La caractérisation minéralogique de la minéralisation s'est faite par l'analyse de sections polies au microscope optique, au microscope à balayage éléctronique, au microscope éléctronique à transmission, ainsi qu'à la microsonde. Cette étude a permis d'établir une séquence paragénétique détaillée pour le gisement. Par ailleurs, des analyses géochimiques de la minéralisation ainsi que des analyses isotopiques ont permis de tirer des conclusions quant à la nature précise des minéralisations et des fluides. Un volet modélisation 3D, avec l'utilisation du logiciel Leapfrog 3D®, a été développé pour différents aspects du gisement, particulièrement les altérations. Cela a permis une visualisation de la géométrie des paramètres lithologiques et structuraux, ainsi qu'une quantification des volumes. La dernière étape est une étude structurale sur les failles et veines du gisement avec l'utilisation du logiciel T-Tecto®. Cela a abouti à une reconstitution du tenseur des contraintes pour les phases tardives de déformation. L'approche pluridisciplinaire de cette recherche a permis d'apporter des précisions d'ordre minéralogique, chimique, et temporel sur le modèle génétique proposé par Robert (2001).

Ce mémoire est présenté sous forme d'un article scientifique qui sera soumis dans une revue scientifique qui traite de la géologie économique. L'article a été rédigé par le premier auteur. Le second auteur est Michel Jébrak qui est le directeur de maîtrise. Son implication s'est faite par la génération de pistes de recherches, l'aide sur le terrain, le suivi de la recherche, la relecture de l'article, et le soutien financier.

Dans l'article, la problématique du projet de recherche est d'abord exposée. Ensuite, la géologie régionale est présentée. La géologie de la propriété est par la suite décrite et comprend la stratigraphie, la pétrologie de la syénite, la géologie structurale, et se termine par une typologie des veines. S'ensuit l'étude de la minéralisation : tout d'abord la typologie des styles de minéralisation, puis l'étude de la paragenèse métallique, l'étude des caractéristiques de l'or et la géochimie de la minéralisation, vient ensuite l'analyse des altérations, suivit par la caractérisation des phases tardives cassantes et les résultats des analyses isotopiques. Une discussion aborde le volet précipitation et évolution de l'or, suivit par les nouvelles conclusions quant au modèle génétique proposé, et se termine par une comparaison avec d'autres gisements aurifères. La conclusion met en avant les points importants et les avancées réalisées au cours de ce projet de recherche.

Des données complémentaires sont présentent à la suite de l'article en appendice. Elles comprennent respectivement dans l'ordre, la méthodologie pour les analyses géochimiques et les résultats lithogéochimiques, l'étude de modélisation 3D, l'analyse des brèches, l'apport de la susceptibilité magnétique à l'exploration du gisement de Beattie, l'étude structurale des phases tardives cassantes, l'analyse quantitative des fluides d'altération, et l'analyse de l'or au microscope éléctronique à transmission.

**Référence**

Davidson, S., et A. F. Banfield. 1944. «Geology of the Beattie Gold Mine, Duparquet, Quebec». *Economic Geology*, vol. 39, p. 535-556.

Dupéré, M., C. Duplessis, et J. Gagné (2011). NI 43-101 Technical Report Mineral Resource Estimation Duparquet – Beattie Property For Osisko Mining Corporation and Clifton Star Resources Inc.: 125 p.

Groves, D.I., R.J. Goldfarb, M. Gebre-Mariam, S.G. Hagemann, et F. Robert. 1998. «Orogenic gold deposits: A proposed classification in the context of their crustal distribution and relationship to other gold deposit types». *Ore Geology Reviews*, vol. 13, p. 7–27.

Lafrance, B. 2011. «À la recherche d'IOCG et de porphyres à Cu-Au alcalins-calciques en Abitibi: utilisation de la typologie des intrusions». In *Forum Technologique Consorem-Divex,* Rouyn-Noranda, Québec.

Lang, J.R., et T. Baker. 2001. «Intrusion-related gold systems : the present level of understanding». *Mineralium Deposita*, vol. 36, p. 477-489.

Legault, M., J. Goutier, G. Baudoin, et M. Aucoin (2005). Synthese-metallogenique-de-la-faille-Destor-Porcupine, Ministère des Ressources Naturelles et de la Faune, Québec; ET 2005-01: 37 p.

Legault, M., et A.E. Lalonde (2009). Discrimination des syenites associées aux gisements aurifères de la sous province de l'Abitibi, Québec, Canada, Ministère des Ressources Naturelles et de la Faune, Québec; RP 2009-04: 10 p.

Rabeau, O. 2010. «Distribution de l'or de type orogénique le long de grands couloirs de déformation archéens: modélisation numérique sur l'exemple de la ceinture de l'Abitibi». Université du Québec à Montréal et Institut National Polytechnique de Lorraine (France), 155 p.

Robert, F. 2001. «Syenite associated disseminated gold deposit in the Abitibi greenstone belt, Canada». *Mineralium Deposita,* vol. 36, p. 505-516.

CHAPITRE 1

# GOLD MINERALIZATIONS AT THE SYENITE-HOSTED BEATTIE GOLD DEPOSIT AT DUPARQUET, NEOARCHEAN ABITIBI BELT, QUEBEC, CANADA


## Abstract

The Beattie deposit is located in the Abitibi greenstone belt, near the Porcupine-Destor Fault Zone, and is associated with a porphyric syenite. Several ore bodies possess a total inferred resource of 56.2 Mt at 1.53g/t gold, for a total of 2.77Moz. In the deposit, two distinct mineralization styles are present: lithologically-controlled, and structurally-controlled. Lithologically-controlled mineralization is limited to the iron-carbonatized syenite. Ore consists of bulk tonnage low-grade mineralization where gold-bearing arsenian pyrite and arsenopyrite are the dominant sulfides. Gold is "invisible"; it occurs as solid solution in the spongy As-rich core of pyrite. Structurally-controlled mineralization is present within shear zones which are within and adjacent to the syenite. This ore consists of relatively high-grade mineralization in silicified breccia with both hydraulic and tectonic features, cherty veins, polymetallic silica veins, and trachytic syenitic dykes. In this facies gold is visible as electrum filling microfractures of brecciated pyrite. The mineralization styles demonstrate a paragenetic evolution in a magmatic-hydrothermal environment. Initial oxidizing stages produced martite. Reducing conditions, marked by $CO_2$-rich magmatic and extrenal fluids, led to sulfides precipitation and gold deposition as "invisible" in the As-rich pyrite and arsenopyrite. A later-stage alteration event, dominated by silica-rich hydrothermal fluids produced sulfides brecciation and their redistribution in silica corridors, and gold remobilization in microfractures of brecciated pyrite. Calculated composition for $\delta^{18}O$ and $\delta D$ on quartz veins associated with this late event are respectively 7.67‰ and - 66‰, indicating a dominance of magmatic fluids with a probable metamorphic component. This event is associated with a strong enrichment in Hg, Te, Mo, Ag, Sb, As, and Se. The speciation of gold in the Beattie deposit is a consequence of the dominance of open-system regimes, both

for the incorporation in the fluid of arsenic that controlled the early gold deposition, and for the circulation of silica-rich fluids that characterized the late fracture-controlled gold mineralization. The Beattie deposit share characteristics with intrusion-related gold deposit, low to intermediate sulfidation epithermal deposit, and mesothermal deposit.

KEYWORDS: Gold deposit, Archean porphyry, invisible gold, gold remobilization

## 1.1 Introduction

The Beattie gold deposit occurs on the north-side segment of the Porcupine-Destor Fault Zone (PDFZ) in the Archean Abitibi Sub-Province (Figure 1.1a), and is associated with a syenitic intrusion. The PDFZ is east-west trending for 200 km. It is one of two main breaks in southern Abitibi, along with the Cadillac – Larder Lake Fault Zone. With a total gold production about 2446 tons (Legault et al., 2005), the PDFZ hosts several gold mines including the Timmins mining camp (Figure 1.1a). Despite the large gold production along the PDFZ, several metallogenic models of deposits remain poorly understood or need to be clarified (Robert et al., 2005).

The Beattie deposit, named in the honor of its discoverer John Beattie in 1910, is located in Duparquet township, in northwestern Quebec, approximately 40 kilometers northwest of the city of Rouyn-Noranda. The mining production of the Beattie deposit started in 1933, followed in 1943 by the mining of the Donchester property, and then the Central Duparquet property, both located in the eastern part of the Beattie deposit (Figure 1.1b). The total production at the Beattie mine, until its closure in 1956, was 32 tons of gold extracted from 9 257 321 tons of ore material, at an average grade of 3.86g/t Au (Bevan, 2009). Arsenic and silver were recovered as secondary products. Recent exploration work, conducted by Osisko Mining Corporation and Clifton Star Resources Inc., was performed on the Beattie deposit. It included geological mapping with a focus on alteration and structural features (Figure 1.1b, Figure 1.2c), geophysical surveys (Figure 1.2a), and an intensive drilling program which established inferred resources of 2.77 Moz gold (56.2 Mt @ 1.53g/t Au).

In the Abitibi greenstone belt, the majority of gold deposits along main fault zones have been recognized as mesothermal (e.g., Val d'or) according to the orogenic gold model of Colvine (1989), and Groves et al. (1998). Hydrothermal mineralized fluids circulating along first and lower-order structures in accreted terranes would be the origin of gold-bearing quartz-carbonate veins and lodes, both typical of orogenic gold deposits. However, several examples of felsic intrusion-related gold deposits occur along major fault zones and share geological features with the orogenic gold model, including metal association, wall-rock alteration, ore fluids, and structural controls (Groves et al., 2003). In Abitibi, the spatial association between small porphyry felsic intrusions and gold deposits has been either interpreted as a structural relation in which the intrusion is acting as a competent trap for mineralized fluids (Colvine, 1989; Witt, 1992), or as a genetic link between gold and the porphyry intrusion (Cameron and Hattori, 1987; Robert, 2001). The former interpretation has been commonly used, whereas the latter interpretation, referring to complex magmatic processes which imply redox reactions, is less prevalent. On the basis of geological relations and geochronological constraints, Robert (2001) distinguished a new group of syenitic gold deposits in the Abitibi greenstone belt, including Beattie, Canadian-Malartic, Holt-McDermott, Young-Davidson, and Douay. These deposits share common characteristics regarding the age of crystallization, the spatial association, the depth of emplacement, the mineralization, and their origin: they crystallized between about 2680 and 2672 Ma near major faults; they occur in association with the Timiskaming sedimentary Group; they were emplaced at shallow depth, typically lower than 2km; the mineralization consists of disseminated sulfides and structural control is an important feature; they are mostly oxidized intrusions and a genetic link between these deposits is proposed. Despite this classification, two questions need to be clarified about the Beattie deposit: How was gold precipitated? What is the evolution of the deposit in terms of petrology, geochemistry, and deformation?

The goal of this paper is a better understanding of the metallogeny of the Beattie deposit by identifying the nature and the controls of the gold mineralization. This will also improve the genetic model proposed by Robert (2001) for syenite-hosted gold deposits in the Abitibi.

## 1.2 Regional geology

The Archean Abitibi sub-province is located within the south-eastern part of the Superior Province. It is the largest continuous volcano-plutonic belt of the Canadian Shield, extending 700 km long E-W and 300 km wide N-S (Figure 1.1a). A Proterozoic structure, the Grenville orogenic front, truncates this belt in its eastern part. The Abitibi greenstone belt shares several characteristics with Archean greenstone belts in the Yilgarn craton regarding the age and the type of deposits (Robert et al., 2005; Duuring et al., 2007).

The Porcupine-Destor Fault Zone (PDFZ) is interpreted as a tectonic suture of allochtonous terranes (Mueller et al., 1996; Daigneault et al., 2002). It represents a geological boundary between the North Volcanic Zone (NVZ) and the South Volcanic Zone (SVZ). Chown et al. (1992) interpret the NVZ as an intact arc segment with two volcanic cycles, whereas Dimroth et al. (1982) consider the SVZ as a homoclinal oceanic floor-to-arc succession. An alternative model proposes the PDFZ is a consequence of anticlines folds detachment in a large autochtonous terrane (Benn and Peschler, 2005; Bedart et al., 2012).

Boivin (1974) considers a prehnite-pumpellyite metamorphic facies in the Duparquet area. The regional metamorphism in the area of Rouyn-Noranda ranges the subgreenschist-facies to greenschist-facies and locally amphibolite-facies around plutons (Powell et al., 1995). The age of regional metamorphism can be bracketed between 2677 and 2643 Ma, with average pressures of approximately 200 MPa.

A polyphased tectonic event in the southern Abitbi sub-province is proposed by Bleeker and Parrish (1996), and Daigneault et al. (2002). A first contractional deformation (D1) is marked by tilting, folding and local thrusting. A second event (D2), involving a major north-south shortening, is responsible for the development of east-west grain of lithologies, upright folds and penetrative foliation. It evolved gradually into D3 dextral faults and shear zones mainly localised along major fault zones. These deformational events started at 2687 Ma and ended around 2662 Ma with a breaking period between about 2680 and 2672 Ma.

## 1.3 Local geology

The Beattie syenite extends E-W for a length over 3300m, and a width N-S about 500m (Figure 1.1b). Both syenite and mineralization dip 35 to 40° to the E. Several smaller syenitic stocks, spatially associated with the Beattie syenite, occur in the E-W trend in the area of Duparquet.

### 1.3.1 Stratigraphy

The oldest unit in the area of Duparquet is the Kinojevis group where the main assemblage is the Deguisier formation (2718-2722 Ma; Zhang et al., 1993). Lithologies comprise abundant Fe-Mg tholeiitic massive and pillow basalts, with minor andesites and lapilli tuffs (Goutier and Lacroix, 1992). These volcanic rocks are interpreted as oceanic crust in a backarc rift (Kerrich et al., 2008). The Porcupine group (2692-2696 Ma) overlies previous units. It consists of greywacke, siltstone and mudstone indicating predominantly distal deposition by turbidity currents in a deep basin. U-Pb dating on zircon suggests that erosion of calc-alkaline to tholeiitic mafic volcanic rocks from the oldest assemblages of the south Abitibi greenstone belt would be the source for Porcupine group sediments (Ayer et al., 2002; Ayer et al., 2005). The youngest assemblage, the Duparquet formation, which belongs to the Timiskaming sedimentary group, consists of conglomerate to sandstone (Figure 1.1b) that record deposition in a stream dominated alluvial fan, fan-delta and/or braid delta adjacent to the sea or lakes (Mueller et al., 1996). These rocks are unconformably deposited on older assemblages. The Duparquet formation forms an easterly trending corridor along the Porcupine-Destor fault zone (Benn and Peschler, 2005; Peschler et al., 2006). Its maximal deposition age is 2678.9±2.8 Ma (David et al., 2006), and it lasts until 2672 Ma. This sedimentary period is known as the Timiskaming event. Based on U-Pb dating and petrological setting, David et al. (2006) suggest a proximal provenance for the volcanic and syenitic fragments.

A period of plutonism occurred during the Timiskaming event (Robert, 2001). The Beattie syenite (Figure 1.1b) has been dated at 2681.6 ± 1 Ma (U/Pb on zircon; Mueller et al.,

1996) indicating a pre-Timiskaming age, however this date is comprised in the uncertainty bracket of the sedimentary event. The age constraint based on field geology remains obscure; work by Robert (2001) outlines evidences that the Duparquet formation sediments unconformably truncate the Beattie syenite (Figure 1.1b), however Graham (1954) reports numerous conglomerate xenolith in the syenite. This uncertainty of the relative age between the alkaline rocks and the sediments highlights their sub-contemporaneous formation.

### 1.3.2 Petrology of the Beattie syenite

The Beattie syenite is a composite stock; several types of syenite differ in texture, composition, and morphology. Bourdeau et al. (2011) recognized five distinct syenites composing the Beattie intrusion: (1) Unaltered syenite in the core of the Beattie intrusion. This unit is magnetite and amphibole-rich but gold free; (2) The Beattie syenite porphyry, the main syenitic unit of the intrusion in terms of volume. It is strongly altered in carbonate and sericite, and contains most of the gold mineralization; (3) The Central Duparquet syenite porphyry, located in southeastern part of Duparquet. Phenocrysts size increase about twice, ranging from 5 to 16 mm, compared to the Beattie syenite porphyry, and it contains some gold; (4) The megaporphyritic syenite, related in space to the Central Duparquet syenite, and characterized by significant feldspar megacrysts of 1 to 6 cm in size. This syenite is gold free; (5) Trachytic syenite dykes, composed of 85-95% feldspar, and consisting of feldspar laths in a red aphanitic matrix of othoclase. This unit is usually strongly altered to carbonate and is gold-bearing. Furthermore, these dykes usually crosscut mineralized zones. Despite the variability of composition and texture of syenites and phenocrysts morphologies, all five syenite units share a common geochemical signature suggesting a same magmatic source.

The dominant intrusion, the Beattie syenite porphyry, is a porphyritic rock mainly characterized by light-grey K-felspar phenocrysts, microcline and orthoclase, 2 to 10 mm in size, set in a grey to reddish aphanitic groundmass of an aggregate of anhedral anorthoclase crystals (Figure 1.5a, b). Feldspar minerals comprise about 80% of all minerals in the syenite (Davidson and Banfield, 1944). The groundmass also contains some clinopyroxene relicts, but mostly hornblende which is largely altered to calcite, chlorite, and to a lesser amount epidote; green muscovite (sericite) is also common in the matrix. Accessory minerals include euhedral titanite, epidote, titaniferous magnetite and apatite.

### 1.3.3 Structural geology

In the area of Duparquet, stratigraphic units are deformed (Figure 1.1b). Major folds with E-W axial planes occur in the Kinojevis group; Deguisier formation layers are upright with younging to the south (Goutier and Lacroix, 1992). Sedimentary rocks of the Duparquet formation have strongly accommodated the deformation. The main structural characteristics include: A N-S flattening with L/l ratio of about 4 to 5 as measured on clasts (Figure 1.3c), E-W to ENE-WSW tight synclinal folds plunging 40° to 60° to the west, and an ENE-trending cleavage which steeply dips to the south. In addition, stretching lineations plunge shallowly to the east. In the Beattie syenite, except for local flattening, deformation is not well recorded.

Faulting is a major structural characteristic in the area of Duparquet. The PDFZ trends N110 with a dip ranging from 50° to 80° to the south (Graham, 1954). The Beattie syenite is bound to the north and to the south by two faults which branch away from PDFZ (Figure 1.1b, Figure 1.2c). The former is the Beattie fault which is mainly a thrust fault with a dextral component; the latter is the Donchester fault which is regarded as a shear fault. Both faults dip steeply sub-vertically to the north. An E-W to ENE-WSW sub-vertical shear zone (named the "Fracture zone" from Davidson and Banfield, 1944; Figure 1.1b, Figure 1.2c, Figure 1.3b), of about 10 to 20 meters width, occurs within the intrusion. In the Beattie syenite, foliation only exists in the Fracture zone. Major conjugated NW-SE dextral and NNE-SSW sinistral strike-slip movements crosscut the deposit (Figure 1.1b, Figure 1.20). In addition to these main strike-slip faults, several minor faults are present in the deposit. Furthermore, jointing is common in the syenite; a widespread joint system steeply dips to the S and W (Figure 1.3a).

### 1.3.4 Veins

Veins are locally abundant, but are not a key feature of the deposit. Veins are mostly present within the syenite and the Timiskaming sediments; only few have been observed in the volcanic rocks. Studied veins have three main orientations: ENE-WSW, ESE-WNW and NNW-SSE (Table 1.5; Figure 1.20, Figure 1.21a).

ENE-WSW veins occur in the Fracture zone. They consist of mineralized cherty quartz veins steeply dipping to the south (Figure 1.6e, f). Quartz is subhedral and forms a mosaic of very fine equigranular crystals, usually 10 to 15 µm.

ESE-WNW veins consist of flat extension barren quartz-carbonate veins, presenting open-space crystallisation, pseudo-colloform texture, and filled partially by chlorite (Figure 1.22a, b, c). Quartz is subhedral and forms a mosaic of medium grained crystals, ranging from 0.5 to 1.5 mm; the smallest quartz crystals form a cryptocrystalline groundmass. Interstitial sericite is locally present. Medium grained calcite is commonly present, and locally massive dissolution occurs (Figure 1.22c). These quartz-carbonate veins are irregular and their width range from 1 to 20 cm. They usually dip shallowly to the north. These veins locally display slight curves, suggesting crystallisation in ductile environment. Hydraulic breccia with sharp fragments of altered syenite is a common feature (Figure 1.22d).

NNW-SSE trending veins are mainly present in the Fracture zone within the syenite where sericitization, and locally silicification, is strong. Veins consist of tension veins filled with quartz and iron-carbonate (Figure 1.22e, f). These veins are not mineralized. Quartz is mostly subhedral and medium grained. Iron-carbonate consists mainly on euhedral to subhedral medium grained ankerite crystals that usually display a brown oxidized color on surface. Partial carbonate dissolution occurs in the strongest sericitization zone (Figure 1.22e, g). Most veins have a periodic spacing, with the same dimensions of about 10 to 20 cm length and 0.3 to 1 cm width; spacing usually ranges from 2 to 8 cm. Sinistral movements on NNW-SSE veins locally occur in the Fracture zone (Figure 1.22g). Cross-cutting evidences indicate NNW-SSE trending veins postdate ENE-WSW trending veins (Figure 1.22f).

### 1.4 Deposit geology

In the Beattie deposit, mineralization is hosted both in the Beattie syenite and in the Beattie and Donchester faults zones and the Fracture zone. Several mineralized zones within and adjacent to the Beattie syenite are recognizable (Figure 1.2b). The main ore body is located along the Beattie fault which marks the north contact between the Beattie syenite and the volcanic rocks of the Deguisier formation. The style of mineralization depends on the location in the deposit, either in the faults zones, or in the intrusion. All mineralization, regardless of their location, share a common paragenetic evolution in a magmatic-hydrothermal environment. Gold mineralization is generally correlated with the fineness of sulfides (pyrite and arsenopyrite) and their abundance.

#### 1.4.1 Mineralization styles

Mineralization styles in the Beattie deposit are twofold: (i) lithologically-controlled, limited to the syenite, and (ii) structurally-controlled, associated with the Beattie and Donchester fault zones and the Fracture zone (Table 1.1; Figure 1.4). Disseminated ore is widespread in the deposit and occurs both in the lithologically-controlled facies and in the structurally-controlled facies. However, gold content, mineralogy, alteration, and volume of ore are different depending on the facies. Ore in the lithologically-controlled facies is almost the same everywhere in the Beattie syenite; ore in the structurally-controlled facies displays several types of mineralization including breccia, replacement, veins, and dyke.

##### 1.4.1.1 Lithologically-controlled facies

Lithologically-controlled facies occurs exclusively within the Beattie syenite porphyry, and out of the Beattie and Donchester faults zones and the Fracture zone. Rock consists of a grey massive syenite (Figure 1.5a), occasionally reddish (Figure 1.5b), resulting from medium to intense iron-carbonatization. Phenocrysts are usually smaller than 1 mm in size, and fine chlorite stockworks as well as small veins of calcite have developed (Figure 1.5a, b). Ore is always disseminated. This facies represents a bulk-tonnage of low-grade material. Some mineralized zones are roughly continuous on 100m, and 83% of the overall ore in the deposit is below 2.5g/t Au (Dupéré et al., 2011). Mineralization generally grades from 0.3g/t Au to 2.5g/t Au; the sulfide concentration is about 5 to 8% (always <10%). The only important sulfides in the ore are gold-bearing arsenian pyrite and arsenopyrite; pyrite is about six times more abundant than arsenopyrite.

#### 1.4.1.2 Structurally-controlled facies

Structurally-controlled facies comprises the majority of the historically mined ore in the Beattie deposit. The mineralization zones are present either along the Beattie and Donchester faults zones, or within the Fracture zone, or both. Most of the mineralization grades >2.5g/t Au, with regular anomalous zones above 10g/t Au; the sulfide content ranges from 10 to 20%, and high-silica value is typical. Dupéré et al. (2011) indicate that ore grading 5g/t Au and more account for only 4.5% of the total ore in the deposit. In the deposit, four types of mineralization belong to the structurally-controlled facies.

Breccia ore was the main mined ore in the Beattie deposit (Davidson and Banfield, 1944). Rock consists of a greyish blue to yellowish colored breccia of angular to sub-angular fragments cemented in an abundant silicified groundmass, and cut by a network of tiny quartz stringers (Figure 1.6a, b, d). The fragments are usually monogenic and consist of altered syenite or altered volcanic rocks. The particles size distribution is normal, ranging from a few mm to a few cm. The motion of the fragment is usually very low, indicating a low mobility; occasionally the dilatation increases and the fragments are matrix supported. The fabric is mostly inherited. The complexity of the fragments (i.e., irregularity of the margins of the clasts; Jébrak, 1997) is low, however some fragments can have a significant complexity (Appendice C). These characteristics provide a better understanding of the fracturing processes. Silicification is a key feature of the breccia ore (Figure 1.6b, c, d). The ore bodies are similar to dykes. They form sub-vertical narrow volumes extended E-W along the Beattie faults and the Fracture zone (Figure 1.4). Ore is both included in the syenite and in the volcanic rocks. The mineralization of breccia ore type consists of fine disseminated pyrite mainly, with small clusters of pyrite; grade is usually >5g/t Au.

Cherty quartz veins (Figure 1.6e, f) occur only within the Fracture zone among foliated syenite. Rock consists of irregular grey-blue cherty quartz veins of about 10 to 20 cm width. Pyrite grains are very fine and disseminated. Small amount of sericite is occasionally present in the veins. The mineralization of cherty quartz veins usually grades >10g/t Au.

Polymetallic veins occur along the Beattie fault and the Fracture zone, but are rare. They consist of Au-As-S-Cu-Hg-Te rich semi-massive veins and are related to intensive silicification (Figure 1.6g). The mineralogical assemblage comprises pyrite, enargite, tennantite-tetrahedrite, and coloradoite. These narrow veins comprise the highest metallic values in the deposit such as 119.5g/t Au and 341g/t Au.

Trachytic syenite dykes (Figure 1.6h) form small ore bodies, about 6 meters width and irregular in length, which truncate both the syenite and the Fracture zone. They occur exclusively near the Beattie and Donchester fault zones and the Fracture zone. Unlike breccia ore, cherty quartz veins, and polymetallic veins, high-silica content is not a significant characteristic of trachytic syenite dykes. Carbonatization and sericitization are the dominant alterations. Mineralization consists of fine disseminated sulfides, mainly pyrite with small amount of arsenopyrite. Trachytic syenite usually grades >5g/t Au. These mineralized and structurally-controlled syenitic dykes have been named *Bostonite* by O'Neill (1932). The alteration and ore of trachytic syenite dykes appear as the lithologically-controlled facies; however, their occurrence related to the Beattie and Donchester faults and the Fracture zone highlights its structural control.

### 1.4.2 Magmatic-hydrothermal paragenesis

The paragenetic sequence in the Beattie deposit is divided into four stages (Figure 1.7): (1) Fe-Ti assemblage, (2) martitization, (3) sulfidation, and (4) breccia facies. Ore mineral paragenesis presents an evolution from magmatic phase to hydrothermal event.

(1) Fe-Ti assemblage consists of subhedral porphyric K-feldspar, and anhedral K-feldspar groundmass, with subhedral titaniferous magnetite (0.1-0.25 mm; up to 2% Ti in magnetite) which accounts for more than 55% of all metallic minerals (Figure 1.8a). Euhedral titanite (0.15-0.35 mm) is usually twinned and widespread (Figure 1.8a), and comprises more

than 40% of all metallic minerals. Very fine inclusions of apatite (0.005 mm) with submicron barite crystals locally occur in titanite crystals (Figure 1.8b, c, d), and in the matrix. Anhedral ilmenite (<0.05 mm) is present as trace mineral, <2%. Leucoxene, 4-5%, results of partial alteration of titanite, and titaniferous magnetite to a lesser extent. This Fe-Ti-oxide rich phase is altered by subhedral chlorite and a low Ca-carbonatization which grows mainly within hornblende crystals.

(2) The martitization phase consists of the gradual oxidation of magnetite grains (Figure 1.9a). Fine hematite crystals, representing about 35% of metallic minerals, form as exsolutions in magnetite which accounts for 50% of the overall metallic minerals. Leucoxene is widespread with 15% of all metallic minerals. It appears under various forms associated with various alteration styles: as pseudomorphs of titanite (Figure 1.9b), as replacement of ilmenite, and as a coronitic texture around titaniferous magnetite.

(3) Sulfidation phase is characterized by the abundance of fine sulfides, mainly pyrite. Euhedral pyrite (0.02-0.125 mm; Figure 1.10a, b, c, d, e, f), locally subhedral, is disseminated within the stock. It is the most abundant sulfide comprising 75% of all metallic minerals. Three overgrowth generations of pyrite can be identified: (G1) gold-bearing porous arsenian pyrite (Figure 1.10a, b, c, d, f). (G2) and (G3) non-porous, arsenic-poor and gold free pyrite. Very fine subhedral arsenopyrite (<0.015 mm) accounts for 12% and appears mainly as inclusions in G1 pyrite (Figure 1.10a, b, c, d, f). Galena (<0.01 mm; 1%) and sphalerite (<0.01 mm; 1%) also occur as inclusion in G1 pyrite (Figure 1.10a, b, c, d, f). In the sulfidation stage, neither titanite pseudomorphs, nor iron-oxide crystals exist. They are broken-down and result in widely disseminated leucoxene (12%). Locally, hematite dust occurs in the matrix and gives the reddish-wine color of the syenite (Figure 1.5b). Carbonatization is the dominant alteration. Sulfidation phase is controlled by the intrusion as it happens exclusively within the syenite and out of fault zones. Sulfidation phase represents the lithologically-controlled facies.

(4) The breccia stage is dominated by the fracturing of rocks and the brecciation of sulfides within silica corridors of decimeter to meter in width. In these corridors, the sulfide concentration is about two times more abundant than in the sulfidation phase. The three generations of euhedral to suhedral pyrite (G1, G2, G3) are recognised and all have

undergone brecciation. Pyrite is still the dominant sulfide, composing 70% of the overall metallic minerals (Figure 1.11a, b). In addition, the margins of the pyrite usually display alteration zones with irregular shapes (Figure 1.11a, e). Very fine subhedral arsenopyrite (<0.015 mm) accounts for 10% of metallic minerals, and mostly occurs as inclusion in G1 pyrite. However, both pyrite and arsenopyrite have recrystallized in minor amount. In addition to galena (<0.01 mm; 1%) and sphalerite (<0.01 mm; 1%), new metallic minerals (0.002-0.01mm) are present in microfractures and in the porosity of the pyrite crystals, as well as in the matrix: chalcopyrite (Figure 1.11h), enargite (Figure 1.11g, j), tennantite-tetrahedrite (CuAsS-CuSbS; Figure 1.11a, i), coloradoite (HgTe; Figure 1.11a, j), hessite ($Ag_2Te$; Figure 1.11a), and electrum (AuAg; Figure 1.11a, c, d, e, f). These minerals individually amount to less than 1%. Significant leucoxene concentrations (10%) happen locally. Barite crystals (0.02-0.03 mm; 2%) are present in the matrix. The breccia episode is controlled by the structure as it occurs only in the Beattie and Donchester faults zones, and the Fracture zone. Breccia stage represents the structurally-controlled facies.

A late-hydroxidation event led to goethite crystallisation, locally displaying coronitic texture around euhedral pyrite (Figure 1.11j), and ultimately pseudomorphic textures.

### 1.4.3 Gold features and ore mineralogy

Gold distribution in sulfides is directly related to the mineralization control, either lithological or structural. Gold texture evolves from "invisible" in pyrite and arsenopyrite to free-state, and gold concentration in host minerals ranges from insignificant to several hundreds of ppm. Furthermore, ore mineralogy changes significantly depending on gold features.

In the lithologically-controlled facies, gold appears in arsenian pyrite (G1) and arsenopyrite as "invisible" gold. This distribution is the dominant style in the Beattie deposit. Microprobe assays indicate that gold concentration usually increases from arsenian pyrite (G1) to arsenopyrite (Table 1.2; Appendice A); gold contents in arsenian pyrite (average 2% As, and up to 4.7% As) range from 80 to 270 ppm Au, whereas gold values range from 100 to 420 ppm Au in arsenopyrite. Arsenian pyrite is S deficient (50-51% wt%), whereas arsenopyrite is characterized by lower As content (34.2 – 40.5 wt%) and higher content of S (21.5 – 27.6 wt%) and Fe (36.3 – 36.6 wt%). Significant amount of gold and arsenic coincide with the high porosity of G1 pyrite. Hence, a correlation between gold, arsenic, and the level of porosity is highlighted in G1 pyrite.

Transmission Electron Microscope data (TEM; Appendice G), in G1 arsenian pyrite (Figure 1.12a) of the lithologically-controlled facies, shows heterogeneity in the lattice fringes (Figure 1.12b) which highlights the porous characteristic of this pyrite. In addition, the range of grey to dark color in the pyrite (Figure 1.12b) indicates respectively lower and higher arsenic concentration. Despite a high magnification (x470000), no gold particles have been found in the studied gold-bearing thin sections.

In the structurally-controlled facies, gold has distinct features of occurrence and texture. Most pyrite and arsenopyrite host minor to negligible invisible gold content, regularly lower than 70 ppm Au (Table 1.3). Gold is mainly visible but small, ranging from 2 to 15 μm. It appears as electrum (≈ 85% Au, 15% Ag; Table 1.4) which crystallises by filling microfractures in the pyrite, and in rare occurrences appears as free-state in the silica corridors (Figure 1.11a, c, d, e, f). In this facies, pyrite is still carrying gold but arsenic is not a significant gold marker anymore (Figure 1.13a). New arsenopyrite is still As deficient (42 wt%), but less than in the lithologically-controlled facies.

Ore mineralogy and elemental association are substantially different in the lithologically-controlled facies than in the structurally-controlled facies. Cu, Pb, Zn, and Bi concentrations are approximately the same in both facies, with a tendency for enrichment for Bi and Zn in the lithologically-controlled facies, and a slightly increase for Cu in the structurally-controlled facies. Structurally-controlled facies are marked by a strong increase of Hg, Te, and Mo (Figure 1.14), and to a lesser degree of Ag, As, Au, Sb, and Se. Structurally-controlled facies are polymetallic facies. Mineral ratios change in ore bodies; when lithological control is predominant, Au/Ag ≈ 1.2, whereas for structural control, Au/Ag ≈ 0.8. On the basis of gold concentration, two populations may be recognized (Figure 1.13a, b): (1) Au < 4 ppm: there is a linear correlation with As. In addition, when Ag < 2 ppm gold is linearly correlated with Ag, whereas above this threshold Ag distribution is scattered. (2) Au > 4 to 6 ppm: both As and Ag populations are uncorrelated and heterogeneously distributed. Minerals crystallization is significantly different depending on the mineralization facies. Unlike the lithologically-controlled facies, where metallic minerals crystallize as micrometric to nanometric inclusions in G1 pyrite, crystallisation styles of ore minerals in the structurally-controlled facies are heterogeneous. They either occur as filling microfractures and porosity of pyrite for enargite, coloradoite, tennantite-tetrahedrite, hessite, electrum (Figure 1.11a, c, d, e, g, i), or as veins for enargite and coloradoite (Figure 1.11g, i), or as free-state usually in silica corridors for chalcopyrite, electrum, and late-barite (Figure 1.11a, f, h).

### 1.4.4 Alteration

Alteration is widespread in the Beattie deposit (Figure 1.2c, Figure 1.15a, Figure 1.16a, Figure 1.17a, Figure 1.18a). The main alteration features are carbonatization, hematization, sericitization, and silicification. They always occur within the syenite, and along its margins. In addition, previous work identified a local sodic and potassic feldspathization along the Beattie fault. Furthermore, bleaching has been observed near ore bodies in the basalts (Davidson and Banfield, 1944). The four main alterations have been recognized in regard to their significant volume using 3D modeling with Leapfrog3D® (Appendice B), their enrichment or depletion of elements using isocon diagram (Grant, 2005), and their style of replacement.

Carbonatization is the dominant alteration in the deposit in terms of its volume. It comprises more than 151 million cubic metres of rock (Figure 1.16a), compare to 248 million cubic metres of syenite; 62% of this carbonatization happens in the syenite, and the remaining 38% is in the basalts and andesites of the Kinojevis group, and turbidites of the Porcupine group. Two carbonatization phases are recognized: (1) early, Fe-Ti assemblage-related. This carbonatization is a low degree of alteration consisting mainly of localised amphibole replacement. Altered rock is usually grey with a greenish tint. These altered rocks occur in small and distinct areas, near anomalous magnetic zones (>0.0293 $nT/m^2$; Figure 1.2a, c). (2) syn-sulfidation is the most abundant carbonatization phase of the deposit. This alteration consists of partial to strong replacement of silicates; it is a pervasive alteration.

Carbonatized syenite is usually grey with a locally reddish tint (Figure 1.16b). This second carbonatization event never occurs near magnetic halos; neither magnetite, nor hematite is found associated with this second carbonatization (Figure 1.7). Bourdeau et al. (2011) identified the composition of different types of carbonates; amphibole replacement consists of calcite, whereas the second carbonatization is dominated by iron-carbonates, mostly ankerite and siderite. Syn-sulfidation carbonatization led to CaO, C, and K enrichment of 200%, whereas $Na_2O$ is depleted by more than 80% (Figure 1.16c). Furthermore, ore minerals including As, Au, Mo, W, S, and Hg are enriched significantly in comparison to the least altered rock.

Hematization is the second largest alteration type in volume. It comprises more than 62 million cubic metres of rock (Figure 1.15a) with 94% of the hematization within the syenite. Hematization is recognized both as martite (martitization phase), and as a high concentration of hematite dust resulting from the destruction of martite and the remaining magnetite. Hematized rocks usually have a reddish-wine color (Figure 1.15b), typical of oxidized rocks. Even though hematite dust occurs in rare instances in some mineralized zones, hematization is not gold-related as most elements remain immobile (Figure 1.15c).

Sericitization is a smaller but widespread alteration comprising of 10 million cubic metres of rock (Figure 1.17a). Sericitized rock displays a green-color (Figure 1.17b), and sericitization occurs only in the syenite and the in Timiskaming sediments in the south (Figure 1.2c, Figure 1.17a). Bourdeau et al. (2011) identified sericite mineral as ferro-alumino-celadonite, ($KAl(Fe^{2+},Mg)Si_4O_{10}(OH_2)$). Sericitization consists of replacements of potassic minerals, mainly K-feldspar, and is associated with a strong enrichment in Au, As, Te, S, Hg, Mo, and W (Figure 1.17c). K and Rb are both enriched by about 200%. Sericite alteration is controlled by permeability of microfracture and is thus diffuse in the Fracture zone in which green-colored syenite displays large channels of about 20 meters width. When strong sericitization happens, kaolinite is widespread but less abundant than sericite (Figure 1.19a).

Silicification is the smallest alteration in terms of volume. It comprises 4 million cubic metres of rock both in the syenite and in the volcanic and turbiditic rocks (Figure 1.18a); 80% of the apparent silicification is present in the syenite, and the remaining 20% is in the host rocks. Silicified rock consists of a grey-blue pervasive silica alteration (Figure 1.18b) implying a partial to complete replacement of the host rock. High-grade mineralization is strongly associated with silicification in the Beattie deposit. Furthermore, silica alteration is associated with the strongest enrichment of elements among all alterations in comparison to the least altered rock (Figure 1.18c): $SiO_2$ increase of 130%; Au, Ag, As, Hg, Sb, Te, Mo, Se and S enrich from 250% to several thousand percent. Silica alteration is strongly controlled by structural features: breccia, veins, and faults. Unlike sericite alteration, silicification forms generally narrow volumes with sharp contacts. Field evidence of brecciated sericitised syenite fragments in silica corridors indicate sericitization pre-date silicification (Figure 1.19b).

Based on microscopic observations and field evidence, a relative chronology of alteration can be established : (1) Fe-Ti assemblage-related Ca-carbonatization, (2) hematization, (3) syn-sulfidation Fe-carbonatization, (4) sericitization, and (5) silicification.

### 1.4.5 Late-faulting

Major conjugated strike-slip faults with an oblique component crosscut the deposit: NW-SE dextral movement and NNE-SSW sinistral movements (Figure 1.1b, Figure 1.20). Within the syenite, several minor faults with two main fault dip orientations, S and W, are present (Figure 1.21b). However, fault orientation is not always homogenous. Dipping is usually steep, ranging from 60° to vertical. Oblique-slip is the dominant fault type. Most faults contain slickenlines generations with an average dip of about 50° (Figure 1.21b). Slickenlines are conserved locally in crystal fiber lineations of chlorite, tourmaline, or calcite. Fault breccia, with angular fragments cm-size and chlorite in matrix, occurs locally associated with important net slip of several meters (Figure 1.22h). Field evidence indicates ENE cherty veins and ESE flat extension veins have been affected by the late-faulting. No direct relation between ENE cherty and ESE flat extension veins has been observed; however, the different stress regimes required for their formation highlight that they could not have formed at the same time.

Stress tensor reconstruction applied on minor faults, using T-TECTO® (Appendice E), indicates a relative chronology of two main compressive regimes (Figure 1.21c): (1) NNW-SSE stress with σ1 plunging 35° to SSE. This stress episode could be the source of NW-SE and NNE-SSW trending strike-slip faults. Furthermore, this brittle compressive period matches with the NNW-SSE trending tension quartz veins considering their stress orientation. (2) ENE-WSW axis with σ1 plunging 35° to ENE. Sinistral movement observed on NNW-SSE trending tension quartz veins (Figure 1.22g) in the Fracture zone could be related to the ENE-WSW compressive event.

### 1.4.6 Stable isotopes

The oxygen and hydrogen stable isotope data for fluids in quartz veins in the Beattie deposit are reported in Table 1.6 (Appendice A). ENE cherty veins $\delta^{18}O$ values range from 12.2 to 16.1‰, with one anomalous value of 6.9‰ (n=6). Assuming a temperature of 350°C (cf. arsenopyrite geothermometer 1.5.1.2) for quartz precipitation, the oxygen isotope composition for hydrothermal fluids calculated for quartz analyses have a restricted range from 6.2 to 10.1‰ with an average value of 7.67‰ excluding the anomalous value of 0.9‰. The δD values vary from -53 to -83‰ (n=6). ESE veins $\delta^{18}O$ values range from 11.7 to 14.9‰ (n=4). The same calculation for the oxygen isotope composition for hydrothermal fluids gives a range from 5.7 to 8.9‰, with an average value of 7.95‰. The δD are homogeneous, varying from -26 to -36‰ (n=4). NNW tension veins $\delta^{18}O$ values range from 13.1 to 14.5‰ (n=4). The same calculation for the oxygen isotope composition for hydrothermal fluids returns a range from 7.1 to 9.5‰, with an average value of 8.25‰. The δD values range from -47 to -69‰ (n=4).

## 1.5 Discussion

Robert (2001) proposed a distinct classification of some syenitic gold deposits in the Abitibi belt, including Beattie, Canadian-Malartic, Holt-McDermott, Young-Davidson, and Douay. In this model, these deposits represent different components of a large magmatic-hydrothermal system centered on composite syenitic stocks. New mineralogical studies coupled with geochemical, structural, and 3D modeling data provide a better understanding of the Beattie deposit, from the precipitation and the evolution of gold, to the genetic model.

### 1.5.1 Precipitation and evolution of gold in the Beattie deposit

A bimodal distribution of gold has been recognized in the Beattie deposit: either invisible gold in arsenian-pyrite and arsenopyrite in the Beattie syenite, or visible gold in microfractures of brecciated pyrite in the Beattie and Donchester fault zones and the Fracture zone.

#### 1.5.1.1 Early invisible gold

The paragenetic sequence (Figure 1.7) indicates that invisible gold is the only gold appearance in the initial stage of sulfidation. It is related to the As-rich event (Figure 1.13a). Mesothermal vein, epithermal vein, sediment-hosted (Carlin-type), and gold-bearing volcanic-hosted massive sulphide deposits commonly contain invisible gold in arsenopyrite and arsenian-pyrite (Cabri et al., 1989; Cathelineau et al., 1989; Cook and Chryssoulis, 1990; Fleet et al., 1993; Mumin et al., 1994; Palenik et al., 2004; Reich et al., 2005; Cepedal et al., 2008; Martin-Izard and Rodríguez-Terente, 2009; Sung et al., 2009). Arsenopyrite and arsenian-pyrite are the favoured host for invisible gold (Ashley et al., 2000). Fleet et al. (1993) reported concentration up to 1.4 wt% of gold in arsenian-pyrite, whereas Kovalev et al. (2011) described gold value up to 5.36 wt% in fine acicular-prismatic arsenopyrite. However, Cook et al. (2009) concluded that As is not essential for Au to enter in the pyrite structure, but textural criteria including areas of clustered tellurides inclusions, microsheared and brecciated pyrite, as well as pyrite recrystallization would be good factors for high gold values.

The role of arsenian-pyrite and arsenopyrite in scavenging gold has been long recognized, but the scavenging mechanism remains controversial. The most common mechanism is the substitution of elements. Cook and Chryssoulis (1990) proposed that As substitution in pyrite leads to $(AsS)_3$ anion pairs. Charge could be balanced by substitution of $Fe^{2+}$ by $Au^{3+}$, $As^{3+}$ or $Sb^{3+}$. Fleet et al. (1993) reported that gold is incorporated in arsenian-pyrite as metastable solid solution via As-rich growth surfaces. Cepedal et al. (2008) proposed a mechanism in which gold is removed from ore fluids by chemisorption at As-rich, Fe-deficient surface sites and incorporated into the sulfides as solid solution. Reich et al. (2005) and Martin-Izard and Rodriguez-Terente (2009) argued that Au values below the solubility limit represents structurally bound Au occurring as solid solution ($Au^{+}$), whereas high Au values above the solubility limit correspond to nanoparticles of native gold ($Au^{0}$). Nanoparticles are usually about 2nm in size (Genkin et al., 1998). Kovalev et al. (2011) suggested the Au-enrichment in arsenopyrite would result of the high defectiveness of its structure, determined by Fe, As, S proportions. Regardless of arsenic, Sung et al. (2009) and Bi et al. (2011) concluded that a positive correlation between Au and Te indicates that gold occurs as submicroscopic Au-bearing telluride inclusions in the host mineral. In the Beattie deposit, there does not appear to be any evidence that associate gold with telluride when gold is invisible. In addition, using TEM data in the gold-bearing arsenian pyrites (Figure 1.12a, b), no gold nanoparticles have been found. However, microprobe assays indicate significant gold values in these pyrites. Hence, the gold speciation for invisible gold in the Beattie deposit is believed to be in solid solution ($Au^{+}$) resulting from substitution processes.

In the Beattie deposit, gold-bearing G1 pyrite is characterized by textural characteristics such as high porosity and the local presence of a significant number of micro-inclusions (Figure 1.10a, b, c, d, f). These features indicate that the pyrite has been affected by a new hydrothermal event. The original G1 pyrite would have been transformed into an Au-bearing arsenian-pyrite with spongy areas and metallic inclusions of arsenopyrite, galena, and sphalerite. This stage would mark the enrichment in Au and As. The fluid circulation would thus have been enriched in Au and As compared to the fluid which led to original G1 pyrite crystallization. These features suggest a coupled dissolution-reprecipitation process (Putnis, 2002) in which areas of original G1 pyrite and/or original metallic inclusions are dissolved, followed by reprecipitation. High porosity appears to be an efficient trap for the accumulation of metallic particles. Similar crystal textures are recognized in other deposits (Mumin et al., 1994; Cepedal et al., 2008; Cook et al., 2009; Sung et al., 2009; Linnen, 2012).

Sung et al. (2009) argued this dissolution-reprecipitation process may have been important in upgrading the ore grade by scavenging gold from the hydrothermal fluid.

Several factors including T, $f_{O2}$, $f_{S2}$, pH, Eh, and fluid composition control the ability of fluids to transport and deposit Au and As (Cathelineau et al., 1989). In the Beattie deposit Au-rich arsenopyrite and arsenian-pyrite crystallize together (Figure 1.7). Atomic proportions indicate arsenopyrite in G1 pyrite is about 27% As (33 atomic % is the regular stoichiometric value for arsenopyrite), which is common for invisible gold-bearing arsenopyrite (Genkin et al., 1998; Vaughan and Kyin, 2004). Using an arsenopyrite geothermometer (Barton, 1969; Kretschmar and Scott, 1976; Sharp et al., 1985), temperature and $f_{S2}$ are unquantifiable due to probable disequilibrium crystallization conditions (Figure 1.24). However, Kretschmar and Scott (1976) and Sharp et al. (1985) considered that gold-bearing pyrite and arsenopyrite crystallization is favoured at temperatures inferior to 410°C. The pyrite-arsenopyrite association gives an indication of the conditions of invisible gold deposition with regard to the oxygen and sulfur composition, and the pH (Figure 1.23a, b). The environment would be reduced (Log $a\sum S$ ranging from -2 to 0, and Log $f(O_2)$ ranging from -28.8 to -31) with a slightly lower pH compared to initial stages probably caused by the arrival of reduced fluids in the system. Many investigators have shown that Au is abundantly carried as bisulphide complexes (e.g., $Au(HS)_2^-$) in hydrothermal solutions (Cathelineau et al., 1989; Brown et al., 2003; Cepedal et al., 2008). Desulfidation of the hydrothermal phase caused by fluid-rock interaction, as well as redox variations coupled with a decrease of the oxygen fugacity and pH would result in the destabilization of the Au-bisulfide complexes and the Au deposition. Alternatively, since gold and arsenic could be transported as thioarsenide complexes ($AuAsS_2$), changes in the oxidation-state, pH increase, and/or decrease of $f_{S2}$ could cause the simultaneous precipitation of gold and arsenic (Romberger, 1986). Whereas Cameron and Hattori (1987) suggested magmatic oxidized fluid would be the best carrier of gold, Mikucki (1998) considered that reducing conditions are expected to decrease Au solubility and favor the coprecipitation of Au with the newly crystallized pyrite and arsenopyrite. A new model proposes that chalcophile melts (i.e., Bi-rich melts) would act as a gold scavenger from hydrothermal fluid (Ciobanu et al., 2006; Tooth et al., 2011). This could explain the geochemical affinity between gold and low-melting point chalcophile elements (e.g., Bi at 271°C) recognized in several gold deposits. However, the Bi content in the Beattie deposit is low (usually <2ppm). Consequently, the hypothesis of gold precipitation due to a scavenging from Bi-rich melts does not seem realistic in the Beattie deposit. In fact, the intimate relationship between Au and As in G1 pyrite and arsenopyrite suggests that a thioarsenide complexes ($AuAsS_2$) would be the most likely gold carrier, as oppose to a bisulphide complexes ($Au(HS)_2^-$).

### 1.5.1.2 Late fracture control of gold mineralization

After the crystallization of the invisible gold in arsenian-pyrite and arsenopyrite, an intense silica-rich magmatic-hydrothermal phase led to sulfide redistribution in the Beattie and Donchester fault zones and the Fracture zone. This redistribution is indicative of the progressive increase of gold concentration in the main faults zones. Minor recrystallizations of pyrite and arsenopyrite have been described in association with this hydrothermal stage (Figure 1.7), however they are gold-free. The process of gold remobilization is presented in Figure 1.25. Gold in solid solution migrated into microfractures of the brecciated pyrite, and ultimately into the groundmass, where it reprecipitated with silver to form electrum (Figure 1.11a, f). Only minor to insignificant values of invisible gold remain in the arsenian-pyrite and arsenopyrite (Table 1.3). Contrary to the invisible gold, visible gold is not correlated to high As values, but Au content appears to coincide with Ag (Figure 1.13a, b). The expulsion mechanism of invisible gold from the lattice bound of arsenian-pyrite and arsenopyrite and its redeposition as visible gold has been recognized by previous investigators (Bonnemaison and Marcoux, 1990; Mumin et al., 1994; Morey et al., 2008; Cook et al., 2009). The most common phenomena for the mechanism of expulsion could have been the combined action of deformation and hydrothermal circulation, the increase grade of metamorphism, the decrease of refractory properties of host minerals, the decrease in grain size, the increase of fluid temperature and $f_{S2}$, and the increase recrystallization of host minerals and their fracturing/brecciation. In the Beattie deposit, two end-models are highlighted: either open system changes or closed system changes. The open system changes are seen as circulation of external fluids which bring new elements, whereas closed system changes are recognized as mineral transformations only. In the Beattie deposit, post depositional processes associated with strong hydrothermal alteration and crystallization of new minerals indicate that predominant open system changes affected significantly the speciation of gold.

The hydrothermal conditions of T, $f_{O2}$, $f_{S2}$, pH, Eh and fluid type can be determined using phase diagrams. The new arsenopyrite is still As deficient with atomic proportions that indicate 28 to 30.5% As. Hence, using an arsenopyrite geothermometer (Barton, 1969; Kretschmar and Scott, 1976; Sharp et al., 1985), temperature of recrystallization is thought to be $\leq$ 350°C (Figure 1.24). In addition, the silica alteration, as well as low $f_{S2}$ (<-8.5), sulfate crystallization (e.g., barite) and late-hydroxidation (e.g., goethite) indicate the oxidizing of hydrothermal conditions at low pH (Figure 1.23a, b).

The silica-rich magmatic-hydrothermal phase has carried and deposited new elements along the Beattie and Donchester fault zones, and the Fracture zone (Figure 1.25). These elements include Hg, Te, Mo, Ag, Sb, As. Pyrite is brecciated and clustered with local alteration zones at its margins. Similar to the dissolution-reprecipitation process which occured in G1 pyrite for the invisible gold, microfractures and remaining porosity acted as traps for new metallic minerals such as enargite, coloradoite, tennantite-tetrahedrite, hessite, and electrum (Figure 1.11a, c, d, e, g).

### 1.5.2 Proposed genetic model

Based on field evidence, mineralogical and geochemical studies, new conclusions can be drawn on the evolution of the Beattie deposit with regards to the timing of gold deposition with deformation and alteration.

(1) Folding and tilting of the Kinojevis volcanic layers ($D_1$) was followed by the Timiskaming event, a period of basin formation and sediment deposition which was contemporaneous to the emplacement of alkaline intrusions. The Beattie syenite was emplaced during the last stage of this first deformation period (Mueller et al., 1996; Legault et al., 2005). Mineralogical data suggest that initial syenitic stages were uniformly oxidized (e.g., magnetite, sulfates). Liquid immiscibility remains a possible explanation for entrapment of apatite as inclusion in silicates. Then, an excess of Ba and S in the immiscible $PO_4$ liquid (Panina and Motorina, 2008) would have formed barite inclusions in the apatite. The

evolution of the system consists of an in-situ oxidation, the hematization that was not metasomatism-related as the element concentration is similar to the initial phase. At this stage, no gold mineralization was present.

(2) The subsequent step was dominated by $CO_2$-rich reduced fluids compared to the initial stages (Figure 1.23b). Destabilization of previous Fe and Ca–rich minerals (e.g., magnetite, hematite, and titanite) would have been in part the source of elements for iron-carbonate crystallization. A more reduced and S-rich fluid would have produced pyrite, arsenopyrite, galena, and sphalerite. Invisible gold-bearing arsenian pyrite and arsenopyrite are the key minerals of this stage. Consistent with field evidence which indicates that the sediments unconformably truncate mineralized stockworks in the Beattie syenite (Robert, 2001), and which does not display any invisible gold mineralization in the Duparquet formation sediments, the invisible gold must have been deposited before the Timiskaming sediment deposition (pre-D2). This mineralization step was slightly Bi-rich in comparison to the remainder of the paragenetic sequence (Figure 1.14). This highlights the dominance of magmatic fluids (Baker et al., 2005). The source of arsenic in the Beattie deposit is still controversial, however, regional studies (Dinel et al., 2005; *J.Goutier, pers. comm.*) indicate that the sediments of the Porcupine group would be As-rich. This could be the source for As in the As-rich gold deposits near this sedimentary unit such as the Beattie deposit. Therefore, contrary to well-known gold deposits in alkaline rocks where metals originate from magmatic fluids only (Mutschler, 1985), the concentration of gold and arsenic in the Beattie deposit would have resulted from mixing between external fluids and magmatic fluids. It was an open system regime in which this mixed Au-As-rich fluid would have resulted in the sulfidation stage, at which point precipitation occurred. Hence, the early gold-bearing fluids, that were responsible for the crystallization of the invisible gold in the lithologically-controlled mineralization, are interpreted as mixed magmatic and external fluids having circulated during the pre-major shortening event (D2).

(3) The remaining stages in the genetic model happened during the transition D2-D3 at a period that reached the metamorphic peak. Both the silica-rich magmatic-hydrothermal fluid circulation and the movement along the Beattie and Donchester fault and the Fracture zone were very intense. The sulfides were redistributed within the faults zones and gold was

remobilized in microfractures of the brecciated pyrite. The breccia in the Beattie deposit can be classified by the propagation and the mobility processes (Appendice C; Jébrak, 1997): A primary breccia mechanism comprised a hydraulic propagation which was associated with an insignificant mobility process considering that the motion is in-situ. A subsequent breccia formed through tectonic propagation coupled with grinding/milling mobility. This second breccia process is commonly observed in the deposit along the faults zones. It led to a decrease of the fragment size, and an increase in the motion of the fragments. These hydrothermal and tectonic processes favoured the expulsion of the invisible gold from lattice bounds of arsenian sulfides, and its precipitation as visible gold in the microfractures of brecciated pyrite. The NNW-SSE tension veins, which post-date mineralized breccia and ENE cherty veins, coincided with the late north-south shortening in Abitibi (Late-D3). Hence, the silica and metallic-rich magmatic-hydrothermal event, which caused the sulfide redistribution within the faults zones and the gold remobilization, happened between D2-D3 transition and possibly until late D3 deformation.

Based on 3D modeling data and chemical characteristics of sericitized rock at 300°c, 313.4 million cubic metres of fluid is required to alter 9.9 million cubic metres of rock (Appendice F). The required volume proportion of fluid is roughly the same as the Butte deposit, where 100 billion cubic metres of magmatic fluid are required to alter 4.5 billion cubic metres of rock (Cathles and Shannon, 2007). Therefore, the sericite alteration in the Beattie deposit is similar to a closed system dominated by magmatic fluids in a porphyry deposit. Also, it is believed that a portion of the potassium came from the alteration of pre-existing feldspars. The timing of sericite crystallization is thought to be early during the transition D2-D3. Unlike the sericitization, the silicification is clearly an open system as the strong increase in silica (enrichment of 17.74% in silica) could not come from the magmatic system. Based on 3D modeling data and chemical characteristics of silicified rock at 300°c, 388 million cubic metres of fluid are required to silicify 4 million cubic metres of rock. Silicification is most likely occurred during peak metamorphism, when the hydrothermal circulation in the plumbing was most intense.

The veins clearly formed before (e.g., ENE cherty veins, ESE flat extension veins) or during (e.g., NNW tension veins) the late-D3 deformation (Table 1.5). Regardless of the type of vein stable isotope signature of $\delta^{18}O$ (>5.7 and <10.1‰) is roughly similar, whereas the $\delta D$ value is more discriminating (Table 1.6; ENE cherty veins average -66, ESE flat extension veins < -36, NNW tension veins average -60). McCuaig and Kerrich (1998) considered that $\delta^{18}O$ values greater than +8‰ cannot be magmatic fluids alone. Hence, data for ENE cherty veins suggests that magmatic fluids could be the dominant source for the fluids (Figure 1.26); however, a metamorphic component is likely to be present too. NNW tension veins share both magmatic and metamorphic characteristics, whereas ESE flat extension veins only have metamorphic fluids signature (Figure 1.26). Age constraints on the field and isotope data highlight the metamorphic feature of the ESE flat extension veins. They appear similar to the gold-bearing veins of the Sigma deposit (Robert, 1994) as they emplaced during metamorphic peak. However, the flat extension veins are not mineralized at the Beattie deposit. McCuaig and Kerrich (1998) argued that the range in $\delta D$ values may be due to the presence of heterogeneous fluids or the nature of the fluids inclusion (primary vs. secondary). The calculated oxygen and hydrogen isotope for fluids in Archean lode gold deposit was restricted to 6 to 11‰ $\delta^{18}O$, and -30 to -80‰ $\delta D$ (McCuaig and Kerrich, 1998; Neumayr, 2007). In addition, Legault et al. (2005) identified $\delta^{18}O$ between 13.2 and 14.7‰ for deposits similar to the Beattie deposit along PDFZ. These values are consistent with those from the Archean quartz veins in the Beattie deposit.

The obliquity of the two stress tensor ($\sigma 1$ plunging 35°; Appendice E; Figure 1.21c) suggests ESE tilting of the mineralized syenite after the late-faulting event. Tilting hypothesis is supported by 3D modeling in which the 35° plunging of the units is visible (Appendice B; Figure 1.27); the plunging was observed in the Beattie underground mine as well (Davidson and Banfield, 1944). The gold mineralization is still present at the base of the model (Figure 1.27), that supposes the mineralization continue in depth. Hence, the tilting could have had a significant part in the preservation of the deposit.

### 1.5.3 Comparison

The classification of the Beattie deposit is not unequivocal. Davidson and Banfield (1944) argued that the Beattie deposit should be classified as mesothermal or epithermal, whereas Robert (2001) and Legault et al. (2005) classified the Beattie deposit as an intrusion-related gold deposit.

According to this study, the Beattie deposit shares characteristics with several types of deposit. Regarding the felsic host rock of the mineralization, the dominance of lithologically-controlled facies in which mineralization is disseminated and in stockworks, the relatively low-grade bulk-tonnage mineralization related to sulfides, the As-rich assemblage, and the sericite and carbonate alteration, the Beattie deposit looks like an intrusion-related gold deposit in accordance with Lang and Baker (2001), and Hart (2005, 2007). However, some features are atypical of intrusion-related gold deposits, particularly the oxidizing environment, the pervasive alteration, and the characteristics of the structurally-controlled facies. The mineralization in the structurally-controlled facies is significantly different. The very low Au/Ag ratio ≈0.8, the strong enrichment in Hg, Mo, Te, Ag, As, and Sb, the metallic mineralogy (e.g., enargite, tennanthite-tetrahedrite, coloradoite, hessite, electrum), the breccia ore and mineralized veins, the strong silicification, sericitization, and local kaolinization, the trachytic and pseudo-colloform textures, and the clear control of faults suggest that the Beattie deposit finds analogies with low to intermediate sulfidation epithermal deposits, according to Sillitoe and Hedenquist (2003) and Corbett (2009). However, some of these features are also typical of the apical part of mesothermal deposit (Groves et al., 1998). The coexistence of intrusion-related gold deposit signatures, epithermal deposit features, and mesothermal deposit characteristics in a same environment would be the result of an evolution from a magmatic dominant system to a shallow hydrothermal dominant system. Two cases are possible: (1) The mineralized intrusion (lithologically-controlled facies) would have been overprinted by mesothermal shear zones (structurally-controlled facies) as a result of the D2-D3 metamorphic event. (2) In a large magmatic environment, the porphyry system (lithologically-controlled facies) would have been overprinted by an epithermal system (structurally-controlled facies) within shear and faults zones during the D2-D3 contractional event. This transition from porphyry to epithermal has already been recognized (Barron, 1998; Richards, 1992; Müller et al., 2002; Williams-Jones and Heinrich, 2005; Sillitoe, 2010; Cooke et al., 2011), and can provide important metal remobilization and reprecipitation events. This latter case appears the most probable for the Beattie deposit.

Based on the geometry of the deposit and the mineral association and occurrences, some Archean Canadian gold deposits share analogous characteristics with the Beattie deposit. Two examples in the Abitibi belt include the Douay deposit and the Young-Davidson deposit, along the major Casa-Berardi-Douay-Cameron fault zone in the Joutel gold district and along the Larder-Lake-Cadillac fault zone in the Matachewan gold district, respectively. The Douay deposit appears to be the most similar deposit to the Beattie deposit. It is an oxidized porphyritic syenite-hosted gold deposit in which gold-mineralization is pyrite related and associated with silicification, carbonatization, albitization, and sericitization. Ore bodies consist of disseminated low-grade material set both in the syenite and along the sheared lithological contacts (Dupéré and Duplessis, 2007). The mineral paragenesis consists of early magnetite and hematite which evolved in gold-bearing pyrite, followed by a cataclasic event which led to liberation of gold (Gauthier and Harnois, 1994). The Young-Davidson deposit is an oxidized syenite-hosted gold deposit which intruded the Timiskaming sediments. Mineralization is structurally-controlled as veins. Several generations of pyrite are recognized and some are gold-bearing. The first generation displays a spongy core with a myriad of metallic inclusions. Gold occurs as visible both as inclusion and in the fractures of the pyrite (Linnen, 2012). The Archean Beattie deposit also shares analogous features with more recent deposits, more particularly the Mesozoic and Cenozoic gold deposits associated with the alkaline magmatism in the American cordillera (Mutschler, 1985), or even with the Oligocene Cripple Creek deposit in Colorado (Thompson et al., 1985).

## 1.6 Conclusion

The ore assemblage from the Beattie deposit is dominated by disseminated pyrite, both As-rich and As-free, and arsenopyrite. Gold appears as both invisible and visible. Invisible gold occurs in solid-solution in the spongy As-rich pyrite (G1) and arsenopyrite within the strongly iron-carbonatized Beattie syenite. This mineralization facies is lithologically-controlled. Visible gold is associated with a later-stage alteration event, dominated by silicification, which produced sulfide redistribution within the faults zones (e.g., the Beattie fault, the Donchester fault, the Fracture zone) and the veins (e.g., ENE-WSW cherty), and gold remobilization in microfractures of brecciated pyrite. Gold crystallized as electrum, and arsenic is not positively correlated to gold in this case. This mineralization facies is structurally-controlled, and related to significant enrichment in Hg, Te, Mo, Ag, Sb, As, and Se.

The deposit evolved from oxidizing (e.g., magnetite, sulfates, hematite) to reducing (e.g., pyrite, arsenopyrite) conditions. In addition, the hydrothermal system progressed from a $CO_2$-rich magmatic fluid widely present in the deposit, to Si-rich magmatic-hydrothermal fluids limited to the fault zones. These differences in distribution of alteration highlight a progressive reorganization of the hydrothermal system. Maturity of an evolving fluid, marked by changes of redox condition, pH, $f_{S2}$, and a fluid mixing would have caused the decrease of the gold solubility in the fluid and then its precipitation as invisible state in the As-rich sulfides within the Beattie syenite. One unique magmatic gold event occurred in the deposit, and is associated with the first crystallization of pyrite and arsenopyrite. Subsequent physico-chemical modifications (e.g., increase in temperature and $f_{S2}$, brecciated textures), in an active tectonic and hydrothermal environment during metamorphic peak, would have caused the expulsion of about 15% of the overall gold from lattice bounds, and their redeposition as visible gold within the E-W fault zones. The speciation of gold in the Beattie deposit is a consequence of the dominance of open system regimes, both for the incorporation of arsenic that control early gold deposition, and for the circulation of hydrothermal silica-rich fluids which dominated the late fracture-control gold mineralization.

This study has provided a greater understanding of the metallogeny of the Beattie deposit. However, several aspects need to be clarified, particularly the precise structural setting of the deposit, the exact age of the gold event (Re-Os dating on pyrite) as well as nature of the gold-bearing pyrite ($\delta^{34}S$), or even the possible link with the lamprophyres.

**Aknowledgments**

The authors thank Osisko Mining Corporation, NSERC, and FQRNT for funding this study, which is part of a M.Sc. project by LB. We specially thank the staff of Osisko exploration for their inspiring discussions, particularly Carl Corriveau. Claude Gagnier, Olivier Nadeau, Julie Bourdeau, André Lalonde, Jean Goutier, Silvain Rafini, and Stéphane Faure are acknowledged for their constructive comments that greatly improved the quality of the paper. Robert Wares (Osisko) and Michel Gauthier (UQAM) are thanked for the review of the document. We also thank Raynald Lapointe, Dirk Schuman, and Lang Shi for their assistance with acquiring respectively SEM, TEM, and Microprobe data. We can't forget Michelle Laithier for the excellent artwork.

## References

Ashley, P. M. , C. J. Creagh, et C. G. Ryan. 2000. «Invisible gold in ore and mineral concentrates from the Hillgrove gold-antimony deposits, NSW, Australia». *Mineralium Deposita*, vol. 35, p. 285-301.

Ayer, J. A., P. C. Thurston, R. Bateman, B. Dube, H. L. Gibson, M. A. Hamilton, B. Hathway, S. M. Hocker, M. G. Houle, G. Hudak, V. O. Ispolatov, B. Lafrance, C. M. Lesher, P. J. MacDonald, A. S. Peloquin, S. J. Piercey, L. E. Reed, et P. H. Thompson (2005). Overview of results from the Greenstone Architecture Project; Discover Abitibi Initiative. Open File Report - Ontario Geological Survey. Canada, Ontario Geological Survey : Toronto, ON, Canada.

Ayer, J., Y. Amelin, F. Corfu, S. Kamo, J. Ketchum, K. Kwok, et N. Trowell. 2002. «Evolution of the southern Abitibi greenstone belt based on U–Pb geochronology: autochthonous volcanic construction followed by plutonism, regional deformation and sedimentation». *Precambrian Research*, vol. 115, p. 63-95.

Baker, T., P. J. Pollard, R. Mustard, G. Mark, et J. L. Graham. 2005. «A comparison of granite-related tin, tungsten, and gold-bismuth deposits; implications for exploration». *SEG Newsletter*, vol. 61, p. 5.

Barron, K.M. 1998. «The Petrological and Metallogenic Signifiance of the Alkaline Igneous Centre at the Springpole Gold Prospect, Northwestern Ontario». Ph.D. Thesis, Department of Earth Sciences, Univerity of Western Ontario, London, Ontario.

Barton, P.B.Jr. 1969. «Thermochemical study of the system Fe-As-S». *Geochimica et Cosmochimica Acta*, vol. 33, no 7, p. 841-857.

Bedart, J.H., L. B. Harris, et P. Thurston. 2012. «The hunting of the snARC». *Precambrian Research.*

Benn, K., et A. Peschler. 2005. «A detachment fold model for fault zones in the Late Archean Abitibi greenstone belt». *Tectonophysics*, vol. 400, no 1-4, p. 85-104.

Bevan, P.A. (2009). Technical Report on Beattie-Donchester Gold Mine Property, Duparquet, Quebec. NI 43-101 Report: 42 p.

Bi, S. J., J. W. Li, M. F. Zhou, et Z. K. Li. 2011. «Gold distribution in As-deficient pyrite and telluride mineralogy of the Yangzhaiyu gold deposit, Xiaoqinling district, southern North China craton». *Mineralium Deposita*, vol. 46, no 8, p. 1-17.

Bleeker, W., et R.R. Parrish. 1996. «Stratigraphy and U - Pb zircon geochronology of Kidd Creek: implications for the formation of giant volcanogenic massive sulphide deposits and the tectonic history of the Abitibi greenstone belt». *Canadian Journal of earth Sciences*, vol. 33, p. 1213-1231.

Boivin, P. 1974. «Pétrographie, stratigraphie et structure de la ceinture de schistes verts de Noranda, dans les cantons de Hébécourt, de Duparquet et de Destor, Québec.». Clermont-Ferrand, Université de Clermont-Ferrand, France, 133 p.

Bonnemaison, M., et E. Marcoux. 1990. «Auriferous mineralization in some shear-zones: A three-stage model of metallogenesis». *Mineralium Deposita*, vol. 25, no 2, p. 96-104.

Bourdeau, J., A.E. Lalonde, et J. Goutier. 2011. «Petrology, mineralogy, and geochemistry of the Beattie syenite, Porcupine-Destor fault zone, Abitibi Subprovince, Québec». *Association géologique du Canada - Association minéralogique du Canada*, vol. 34, p. 24.

Brown, S. M., C.A. Johnson, R.J. Watling, et W. R. Premo. 2003. «Constraints on the composition of ore fluids and implications for mineralising events at the Cleo gold deposit, Eastern Goldfields Province, Western Australia». *Australian Journal of Earth Sciences*, vol. 50, no 1, p. 19-38.

Cabri, L.J., S.L. Chryssoulis, J.P.R. De Villiers, J.H. Gilles Laflamme, et Peter R. Buseck. 1989. «The Nature of "Invisible" Gold in Arsenopyrite». *The Canadian Mineralogist*, vol. 27, p. 353-362.

Cameron, E.M., et K. Hattori. 1987. «Archean gold mineralization and oxidized hydrothermal fluids». *Economic Geology and the Bulletin of the Society of Economic Geologists*, vol. 82, no 5, p. 1177-1191.

Cathelineau, M., M.C. Boiron, P. Holliger, P. Marion, et M. Denis. 1989. «Gold in Arsenopyrites : Crystal Chemistry, Location and State, Physical and Chemical Conditions of Deposition». *Economic Geology Monography*, vol. 6, p. 328–341.

Cathles, L. M., et R. Shannon. 2007. «How potassium silicate alteration suggests the formation of porphyry ore deposits begins with the nearly explosive but barren expulsion of large volumes of magmatic water». *Earth and Planetary Science Letters*, vol. 262, no 1-2, p. 92-108.

Cepedal, A., M. Fuertes-Fuente, A. Martin-Izard, S. Gonzalez-Nistal, et M. Barrero. 2008. «Gold-bearing As-rich pyrite and arsenopyrite from the El Valle gold deposit, Asturias, northwestern Spain». *The Canadian Mineralogist*, vol. 46, p. 233-247.

Chown, E.H. 1992. «Tectonic evolution of the Northern Volcanic Zone, Abitibi Belt, Quebec». *Canadian Journal of Earth Sciences = Revue Canadienne des Sciences de la Terre*, vol. 29, no 10, p. 2211-2225.

Ciobanu, C. L., N.J. Cook, F. Damian, et G. Damian. 2006. «Gold scavenged by bismuth melts; an example from Alpine shear-remobilizates in the Highis Massif, Romania». *Mineralogy and Petrology*, vol. 87, no 3-4, p. 351-384.

Colvine, A.C. 1989. «An empirical model for the formation of Archean gold deposits: products of final cratonization of the Superior province, Canada». *In:*, vol. Keays RR, Ramsay WRH, Groves DI (eds). The geology of gold deposits: the perspective in 1988. Economic Geology Monography 6, p. 37-53.

Cook, N. J., C. L. Ciobanu, et J. Mao. 2009. «Textural control on gold distribution in As-free pyrite from the Dongping, Huangtuliang and Hougou gold deposits, North China Craton (Hebei Province, China)». *Chemical Geology*, vol. 264, no 1-4, p. 101-121.

Cook, N.J., et S.L. Chryssoulis. 1990. «Concentration of "Invisible Gold" in the common sulfides». *The Canadian Mineralogist*, vol. 28, p. 1-16.

Cooke, D.R., C.L. Deyell, P.J. Waters, R.I. Gonzales, et K. Zaw. 2011. «Evidence for magmatic-hydrothermal fluids and ore-forming processes in epithermal and porphyry deposits of the Baguio District, Philippines». *Economic Geology and the Bulletin of the Society of Economic Geologists*, vol. 106, no 8, p. 1399-1424.

Corbett, G. 2009. «Anatomy of porphyry-related Au-Cu-Ag-Mo mineralised systems: Some exploration implications». In *Australian Institute of Geoscientists North Queensland Exploration*, p. 13.

Daigneault, R., W.U. Mueller, et E.H. Chown. 2002. «Oblique Archean subduction: accretion and exhumation ofan oceanic arc during dextral transpression, Southern Volcanic Zone, Abitibi Subprovince Canada». *Precambrian Research*, vol. 115, p. 261–290.

David, J., C. Dion, J. Goutier, P. Roy, D. Bandyayera, M. Legault, et P. Rhéaume (2006). Datations U-Pb effectuées dans la Sous-province de l'Abitibi à la suite des travaux de 2004-2005, Ministère des Ressources Naturelles et Faune; RP 2006-04: 22 p.

Davidson, S., et A. F. Banfield. 1944. «Geology of the Beattie Gold Mine, Duparquet, Quebec». *Economic Geology*, vol. 39, p. 535-556.

Dimroth, E. 1982. «Evolution of the south-central part of the Archean Abitibi Belt, Quebec; Part I, Stratigraphy and paleogeographic model». *Canadian Journal of Earth Sciences = Revue Canadienne des Sciences de la Terre*, vol. 19, no 9, p. 1729-1758.

Dinel, E., A.D. Fowler, J. Ayer, A. Still, K. Tylee, et E. Barr. 2008. «Lithogeochemical and Stratigraphic Controls on Gold Mineralization within the Metavolcanic Rocks of the Hoyle Pond Mine, Timmins, Ontario». *Economic Geology*, vol. 103, no 6, p. 1341-1363.

Dolejs, D., et C. E. Manning. 2010. «Thermodynamic model for mineral solubility in aqueous fluids; theory, calibration and application to model fluid flow systems». *Geofluids [Oxford]*, vol. 10, no 1-2, p. 20-40.

Doucet, P., J. Goutier, M. Melaçon, et L. Ste-Croix (2000). L'Abitibi: Un centenaire d'exploration et de succès minier, Ministère des Ressources naturelles, faune et parcs, Québec. DV 2000-03: 44 p.

Dupéré, M., et C. Duplessis (2007). Technical Report - Resource Evaluation on the Douay Project for SEM Vior Inc.: 188 p.

Dupéré, M., C. Duplessis, et J. Gagné (2011). NI 43-101 Technical Report Mineral Resource Estimation Duparquet – Beattie Property For Osisko Mining Corporation and Clifton Star Resources Inc.: 125 p.

Duuring, P., K. Cassidy, et S. Hagemann. 2007. «Granitoid-associated orogenic, intrusion-related, and porphyry style metal deposits in the Archean Yilgarn Craton, Western Australia». *Ore Geology Reviews*, vol. 32, no 1-2, p. 157-186.

Fleet, M. E., S. L. Chryssoulis, R. Davidson, C. G. Weisener, et P. J. Maclean. 1993. «Arsenian pyrite from gold deposits: Au and As distribution investigated by SIMS and EMP, and color staining and surface oxidation by XPS and LIMS». *Canadian Mineralogist*, vol. 31, no 1, p. 1-17.

Gauthier, M., et L. Harnois (1994). Étude sommaire des protolithes, des patrons d'altération et des paragenèses minérales des minéralisations aurifères du canton de Douay (Abitibi). Rapport d'étape soumis à Richard Laplante et Denis Raymond du bureau régional d'Abitibi de SOQUEM, Université du Québec à Montréal.

Genkin, A.D., N.S. Bortnikov, L.J. Cabri, F. E. Wagner, C.J. Stanley, Y.G. Safonov, G. McMahon, J. Friedl, A.L. Kerzin, et G.N. Gamyanin. 1998. «A multidisciplinary study of invisible gold in arsenopyrite from four mesothermal gold deposits in Siberia, Russian Federation». *Economic Geology and the Bulletin of the Society of Economic Geologists*, vol. 93, no 4, p. 463-487.

Goutier, J., et S. Lacroix (1992). Géologie du secteur de la faille de Porcupine-Destor dans les cantons de Destor et Duparquet, Ministère de l'Énergie et des Ressources, Québec; MB 92-06: 67 p.

Grant, J. 2005. «Isocon analysis: A brief review of the method and applications». *Physics and Chemistry of the Earth, Parts A/B/C*, vol. 30, no 17-18, p. 997-1004.

Groves, D.I., R.J. Goldfarb, M. Gebre-Mariam, S.G. Hagemann, et F. Robert. 1998. «Orogenic gold deposits: A proposed classification in the context of their crustal distribution and relationship to other gold deposit types». *Ore Geology Reviews*, vol. 13, p. 7–27.

Groves, D.I., R.J. Goldfarb, F. Robert, et C. J. R. Hart. 2003. «Gold Deposits in Metamorphic Belts: Overview of Current Understanding, Outstanding Problems, Future Research, and Exploration Significance». *Economic Geology*, vol. 98, p. 1–29.

Hart, C.J.R. 2005. «Classifying, distinguishing and exploring for intrusion-related gold systems». *Program with Abstracts - Geological Association of Canada; Mineralogical Association of Canada: Joint Annual Meeting*, vol. 30, p. 81-81.

Hart, C.J.R. (2007). Reduced Intrusion-Related Gold Systems. W.D. *in* Goodfellow, ed., Mineral deposits of Canada: A Synthesis of Major Deposit Types, District et the Evolution of Geological Provinces Metallogeny, and Exploration Methods: Geological Association of Canada, Mineral Deposits Division. Special publication No 5: 95-112 p.

Jébrak, M. 1997. «Hydrothermal breccias in vein type ore deposit : A review of mechanisms, morphology and size distribution». *Ore Geology Reviews*, vol. 12, p. 111-134.

Jébrak, M., et E. Marcoux. 2008. *Géologie des ressources minérales*, Denis L. Lefebvre, ing.: Ministère des Ressources Naturelles et de la Faune. Québec, 667 p.

Kerrich, R., A. Polat, et Q. Xie. 2008. «Geochemical systematics of 2.7 Ga Kinojevis Group (Abitibi), and Manitouwadge and Winston Lake (Wawa) Fe-rich basalt–rhyolite associations: Backarc rift oceanic crust?». *Lithos*, vol. 101, no 1-2, p. 1-23.

Kovalev, K. R., Y. Kalinin, E. A. Naumov, M. K. Kolesnikova, et V. N. Korolyuk. 2011. «Gold-bearing arsenopyrite in eastern Kazakhstan gold-sulfide deposits». *Russian Geology and Geophysics*, vol. 52, no 2, p. 178-192.

Kretschmar, U., et S. D. Scott. 1976. «Phase relations involving arsenopyrite in the system Fe-As-S and their application». *Canadian Mineralogist*, vol. 14, Part 3, p. 364-386.

Legault, M., J. Goutier, G. Baudoin, et M. Aucoin (2005). Synthese-metallogenique-de-la-faille-Destor-Porcupine, Ministère des Ressources Naturelles et de la Faune, Québec; ET 2005-01: 37 p.

Linnen, R. 2012. «Syenite-Hosted Gold Mineralization at the Young-Davidson Deposit». In *Short Course Intrusion Related Gold in the Abitibi : Theory and Application to Exploration* (University of Western Ontario, London, Ontario, Canada). Resource Geoscience Wester London Student Chapter. University of Western Ontario, London, Ontario, Canada.

Martin-Izard, A., et L. Rodríguez-Terente. 2009. *Invisible gold at the Salave Deposit, NW Spain*: *Proceedings of the Tenth Biennial SGA Meeting* (Townsville).

McCuaig, T. C., et R. Kerrich. 1998. «P-T-t-deformation-fluid characteristics of lode gold deposits: Evidence from alteration systematics». *Ore Geology Reviews*, vol. 12, no 6, p. 381-453.

Mexias, A.S., G. Berger, M.E.B. Gomes, M.L.L. Formoso, N. Dani, J.C. Frantz, et E.M. Bongiolo. 2005. «Geochemical modeling of gold precipitation conditions in the Bloco do Butia Mine, Lavras do Sul, Brazil». *Anais da Academia Brasileira de Ciencias*, vol. 77, no 4, p. 717-728.

Mikucki, E.J. 1998. «Hydrothermal transport and depositional processes in Archean lode-gold systems; a review». *Ore Geology Reviews*, vol. 13, no 1-5, p. 307-321.

Mikucki, E.J., et F.I. Roberts (2004). Metamorphic petrography of the Kalgoorlie region, Eastern Goldfields granite-greenstone terrane: METPET database. Geological Survey of Western Australia Record 2003/12: 40 p.

Morey, A.A., A.G. Tomkins, F.P. Bierlein, R.F. Weinberg, et G.J. Davidson. 2008. «Bimodal Distribution of Gold in Pyrite and Arsenopyrite: Examples from the Archean Boorara and Bardoc Shear Systems, Yilgarn Craton, Western Australia». *Economic Geology*, vol. 103, no 3, p. 599-614.

Müller, D., K. Kaminski, S. Uhlig, T. Graupner, P. Herzig, et S. Hunt. 2002. «The transition from porphyry- to epithermal-style gold mineralization at Ladolam, Lihir Island, Papua New Guinea: a reconnaissance study». *Mineralium Deposita*, vol. 37, no 1, p. 61-74.

Mueller, W.U., R. Daigneault, J.K. Mortensen, et E.H. Chown. 1996. «Archean terrane docking: upper crust collision tectonics, Abitibi greenstone belt, Quebec, Canada». *Tectonophysics*, vol. 265, p. 127-150.

Mumin, A.H., M.E. Fleet, et S. Chryssoulis. 1994. «Gold mineralization in As-rich mesothermal gold ores of the Bogosu-Prestea mining district of the Ashanti gold belt, Ghana; remobilization of 'invisible' gold». *Mineralium Deposita,* vol. 29, no 6, p. 445-460.

Mutschler, F.E. 1985. «Precious metal deposits related to alkaline rocks in the North American Cordillera; an interpretive review». *Verhandelinge van die Geologiese Vereniging van Suid Afrika = Transactions of the Geological Society of South Africa,* vol. 88, no 2, p. 355-377.

Neumayr, P. 2007. «Fluid chemistry and evolution of hydrothermal fluids in an Archaean transcrustal fault zone network; the case of the Cadillac tectonic zone, Abitibi greenstone belt, Canada». *Canadian Journal of earth Sciences,* vol. 44, no 6, p. 745-773.

O'Neill, J.J. (1932). La mine d'or Beattie, canton de Duparquet. Service des mines du québec, Service des Mines de Québec.

Palenik, C.S., S. Utsunomiya, M. Reich, S.E. Kesler, L. Wang, et R.C. Ewing. 2004. «"Invisible" gold revealed: Direct imaging of gold nanoparticles in a Carlin-type deposit». *American Mineralogist,* vol. 89, no 10, p. 1359-1366.

Panina, L.I., et I.V. Motorina. 2008. «Liquid Immiscibility in Deep-Seated Magmas and the Generation of Carbonatite Melts». *Geochemistry International,* vol. 46, no 5, p. 443-464.

Pelissonnier, H. 2001. *Réflexion sur la métallogénie.* Paris: Société de l'industrie minérale, 413 p.

Peschler, A. P., K. Benn, et W. R. Roest. 2006. «Gold-bearing fault zones related to Late Archean orogenic folding of upper and middle crust in the Abitibi granite-greenstone belt, Ontario». *Precambrian Research,* vol. 151, no 3-4, p. 143-159.

Piché, M., et M. Jébrak. 2004. «Normative minerals and alteration indices developed for mineral exploration». *Journal of Geochemical Exploration,* vol. 82, no 1-3, p. 59-77.

Powell, W.G., D.M. Carmichael, et C.J. Hodgson. 1995. «Conditions and timing of metamorphism in the southern Abitibi greenstone belt, Quebec». *Canadian Journal of earth Sciences,* vol. 32, p. 787-805.

Putnis, A. 2002. «Mineral replacement reactions; from macroscopic observations to microscopic mechanisms». *Mineralogical Magazine,* vol. 66, no 5, p. 689-708.

Reich, M., S. Kesler, S. Utsunomiya, C. Palenik, S. Chryssoulis, et R. Ewing. 2005. «Solubility of gold in arsenian pyrite». *Geochimica et Cosmochimica Acta,* vol. 69, no 11, p. 2781-2796.

Richards, J.P. 1992. «Magmatic-epithermal transitions in alkalic systems; Porgera gold deposit, Papua New Guinea». *Geology [Boulder],* vol. 20, no 6, p. 547-550.

Robert, F. 2001. «Syenite associated disseminated gold deposit in the Abitibi greenstone belt, Canada». *Mineralium Deposita,* vol. 36, p. 505-516.

Robert, F. (1994). Vein fields in gold districts; the example of Val d'Or, southeastern Abitibi Subprovince, Quebec. Canada, Geological Survey of Canada : Ottawa, ON, Canada: 295-302 p.

Robert, F., K.H. Poulsen, K.F. Cassidy, et C.J. Hodgson. 2005. «Gold Metallogeny of the Superior and Yilgarn Cratons». *Economic Geology,* vol. 100th Anniversary Volume, p. 1001-1033.

Romberger, S.B. 1986. «The Solution Chemistry of Gold Applied to the Origin of Hydrothermal Deposits». *Canad. Inst. Mining Special,* vol. 38, p. 168-186.

Sharp, Z.D., E.J. Essene, et W.C. Kelly. 1985. «A re-examination of the arsenopyrite geothermometer: Pressure considerations and applications to natural assemblages». *The Canadian Mineralogist,* vol. 23, p. 517–534.

Sillitoe, R. H. 2010. «Porphyry copper systems». *Economic Geology,* vol. 105, no 1, p. 3-41.

Sillitoe, R.H., et J.W. Hedenquist. 2003. «Linkages between volcanotectonic settings, ore-fluid compositions, and epithermal precious metal deposits». *Special Publication [Society of Economic Geologists [U. S.]],* vol. 10, p. 315-343.

Sung, Y. H., J. Brugger, C. L. Ciobanu, A. Pring, W. Skinner, et M. Nugus. 2009. «Invisible gold in arsenian pyrite and arsenopyrite from a multistage Archaean gold deposit: Sunrise Dam, Eastern Goldfields Province, Western Australia». *Mineralium Deposita,* vol. 44, no 7, p. 765-791.

Thompson, T.B., A.D. Tbippel, et P.C. Dwelley. 1985. «Mineralized Veins and Breccias of the Cripple Creek District, Colorado». *Economic Geology,* vol. 80, p. 1669-1688.

Tooth, B., C. L. Ciobanu, L. Green, B. O'Neill, et J. Brugger. 2011. «Bi-melt formation and gold scavenging from hydrothermal fluids: An experimental study». *Geochimica et Cosmochimica Acta,* vol. 75, no 19, p. 5423-5443.

Vaughan, J. P., et A. Kyin. 2004. «Refractory gold ores in Archaean greenstones, Western Australia; mineralogy, gold paragenesis, metallurgical characterization and classification». *Mineralogical Magazine,* vol. 68, no 2, p. 255-277.

Wares, R. 2010. «Communiqué de presse : Osisko et Clifton Star recoupent 42 mètres à une teneur moyenne de 3,38g/t Au à Duparquet ». En ligne :

http://www.osisko.com/en/press/2010/12/06/563/osisko-and-clifton-star-intersect-42-metres-averaging-3-38-g-t-au-at-duparquet.html.

Williams-Jones, A. E., et C. A. Heinrich. 2005. «100th Anniversary Special Paper: Vapor transport of metals and the formation of magmatic-hydrothermal ore deposits». *Economic Geology*, vol. 100, no 7, p. 1287-1312.

Witt, W.K. 1992. «Porphyry intrusions and albitites in the Bardoc-Kalgoorlie area, Western Australia and their role in the Archean epigenetic gold mineralization». *Canadian Journal of earth Sciences*, vol. 29, p. 1609-1622.

Zhang, P.L., N. Machado, J. Ludden, et D. Moore. 1993. «Geotectonic constraints fro U-Pb ages from the Black River Group, the Kinojévis Group and the Normétal mine area, Abitibi, Québec». *Association géologique du Canada - Association minéralogique du Canada*, vol. 18, p. A114.

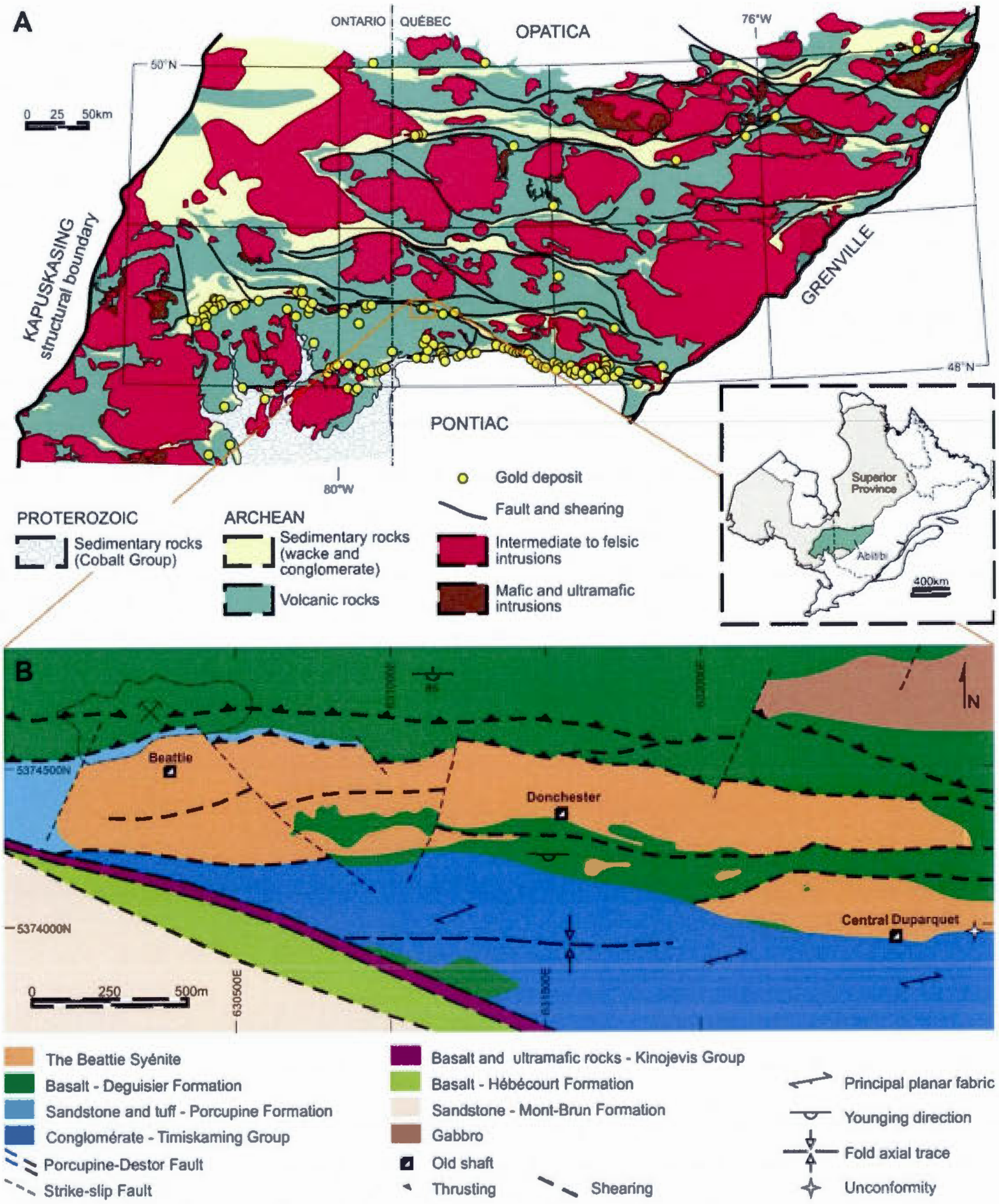


**Figure 1.1.** (a) Simplified geology of the Abitibi greenstone belt (modified from Doucet et al., 2000). (b) Geology of Duparquet property (modified from Mueller et al., 1996, and Bourdeau et al., 2011).

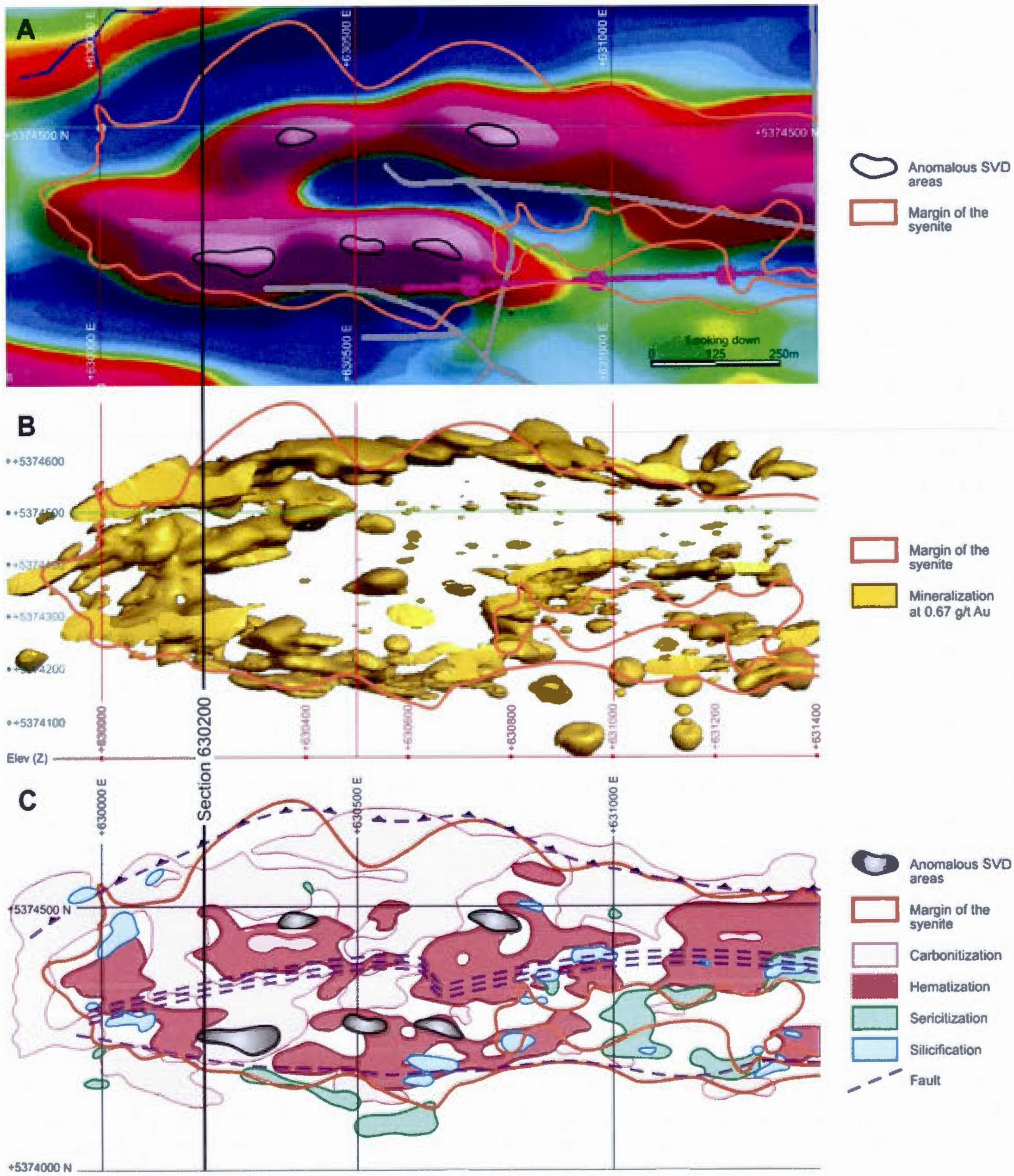


**Figure 1.2.** Comparison at the same scale: (a) Airborne Geophysics (SVD). (b) Mineralized zones in the Beattie deposit at 0.67g/t Au. (c) Alteration halos on the surface, with the Beattie fault (north), the Donchester fault (south), and the Fracture zone (center of the syenite), and with anomalous SVD areas.

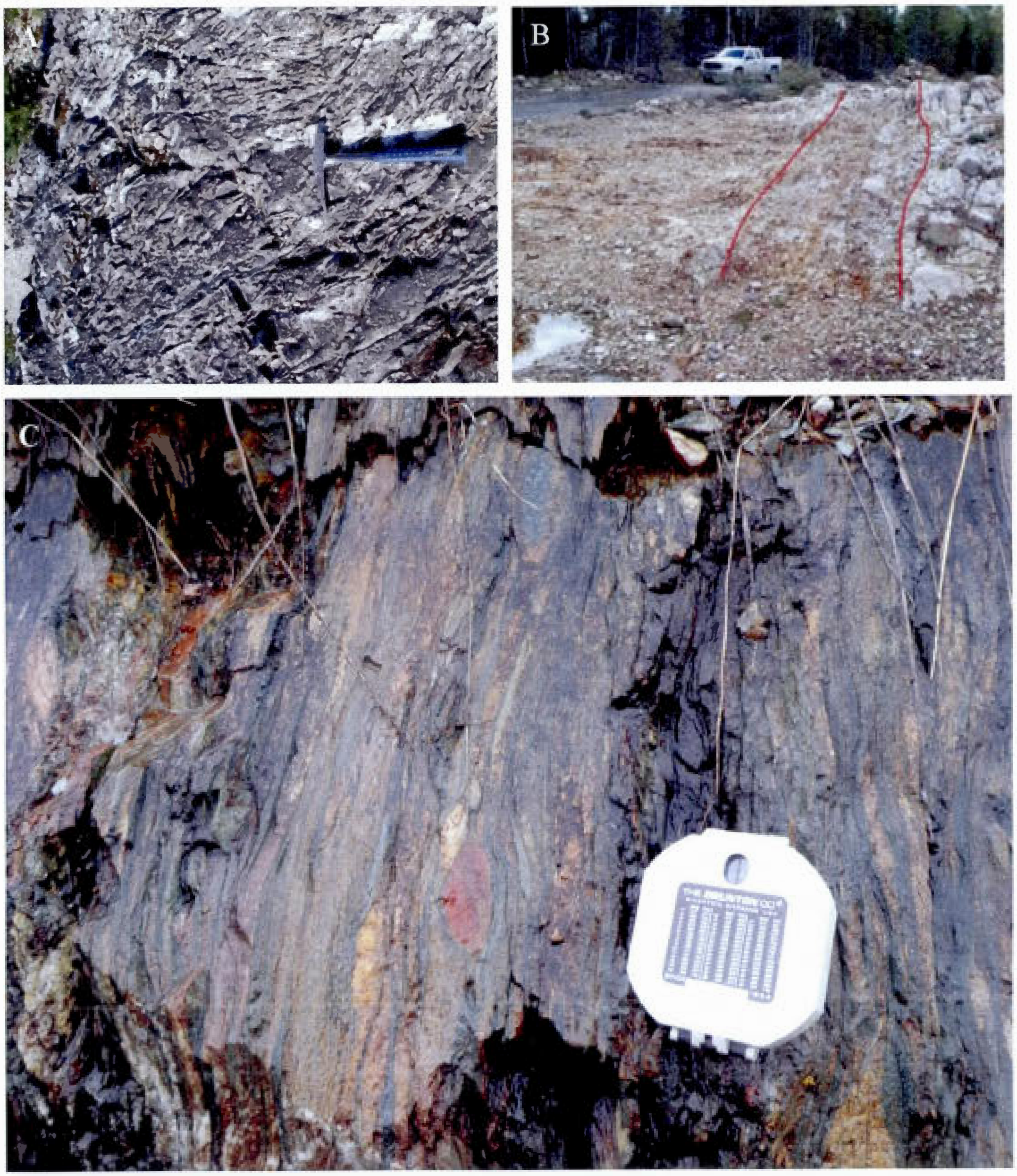


**Figure 1.3.** Photographs illustrating structural particularities of the Beattie deposit. (a) Joint network well developed. (b) The Fracture zone ENE trending. (c) E-W flattening in the Duparquet sediment formation.

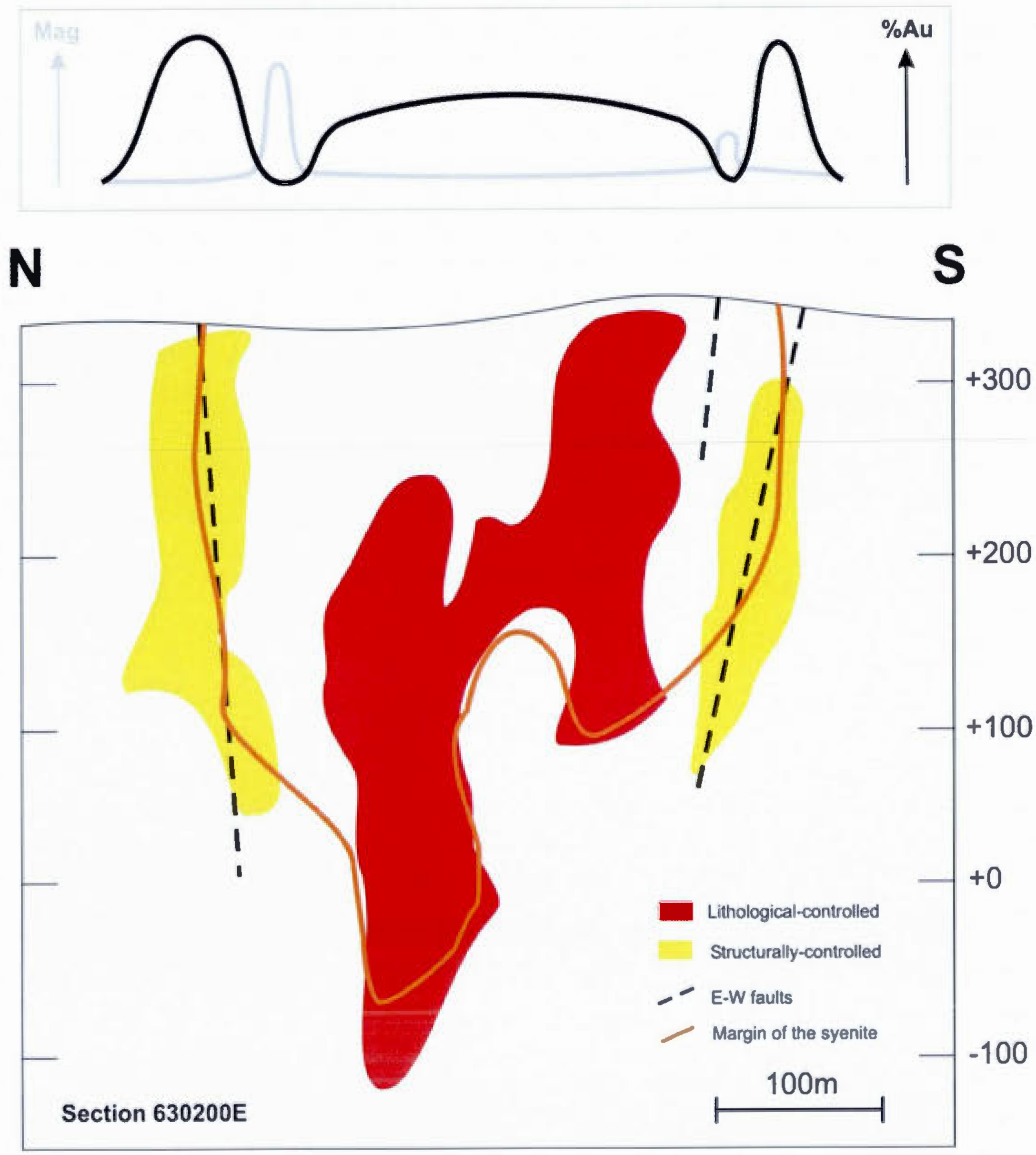

Mag
%Au
N
S
+300
+200
+100
+0
-100
Lithological-controlled
Structurally-controlled
E-W faults
Margin of the syenite
100m
Section 630200E

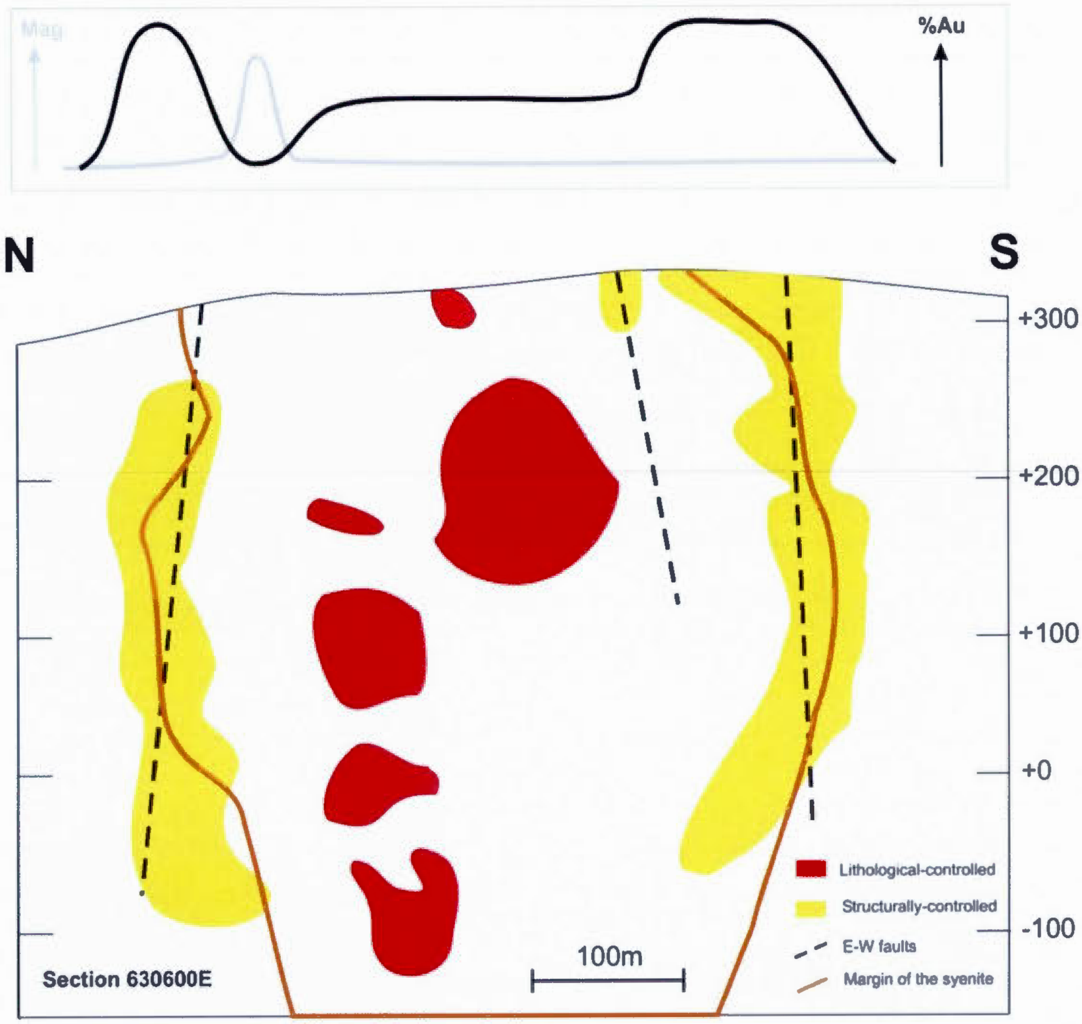


**Figure 1.4.** Two cross sections in the Beattie deposit (630200E, and 630600E) showing the control of the mineralization, lithological and structural. Cartoon based on the 2008, 2009, and 2010 drilling program.

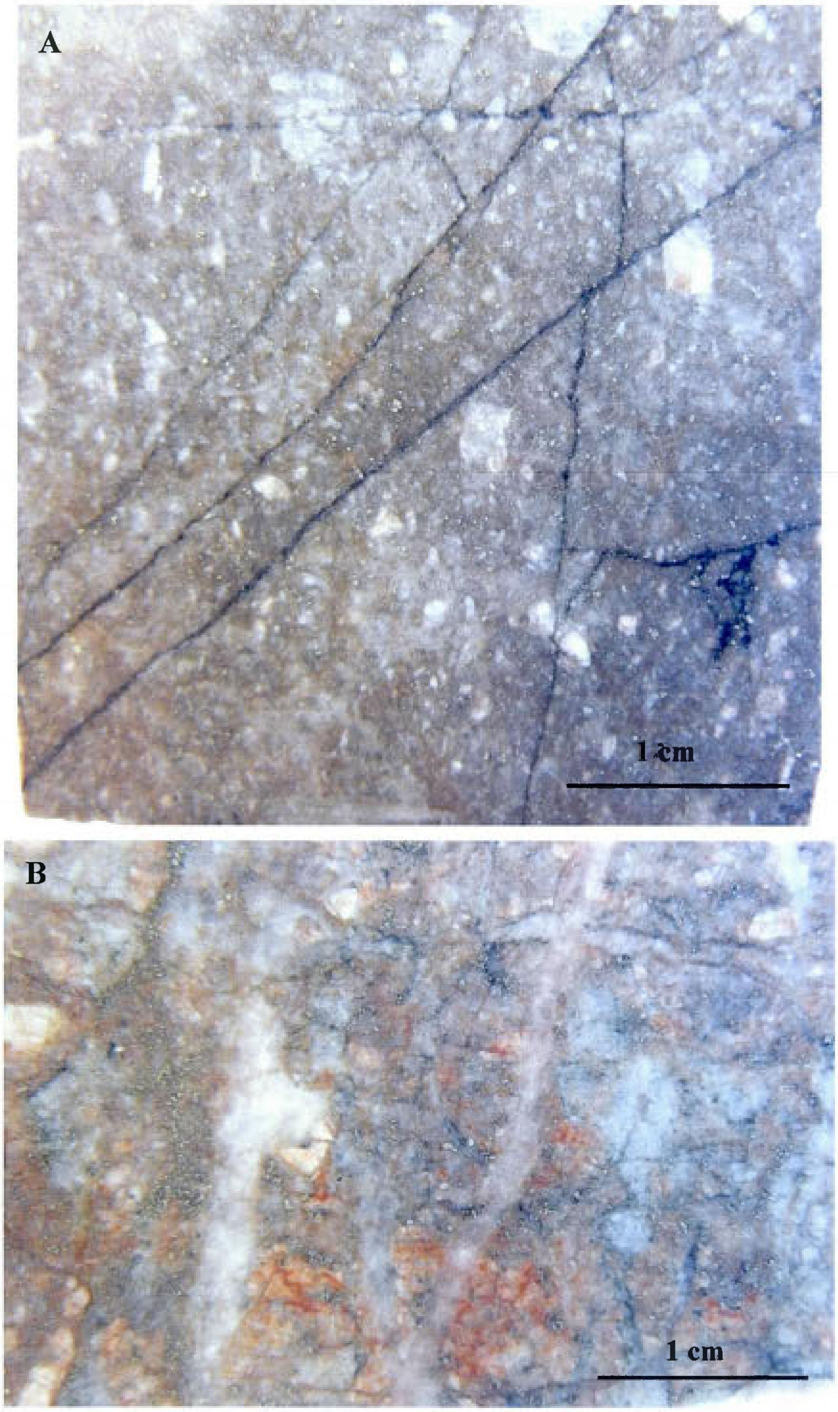


**Figure 1.5.** Photographs of the syenite illustrating the lithologically-controlled facies. (a) Grey massive syenite, carbonatized, with disseminated sulfides (1.5g/t Au). (b) Reddish syenite with disseminated sulfides, and cut by carbonate veinlets (2.4g/t Au).

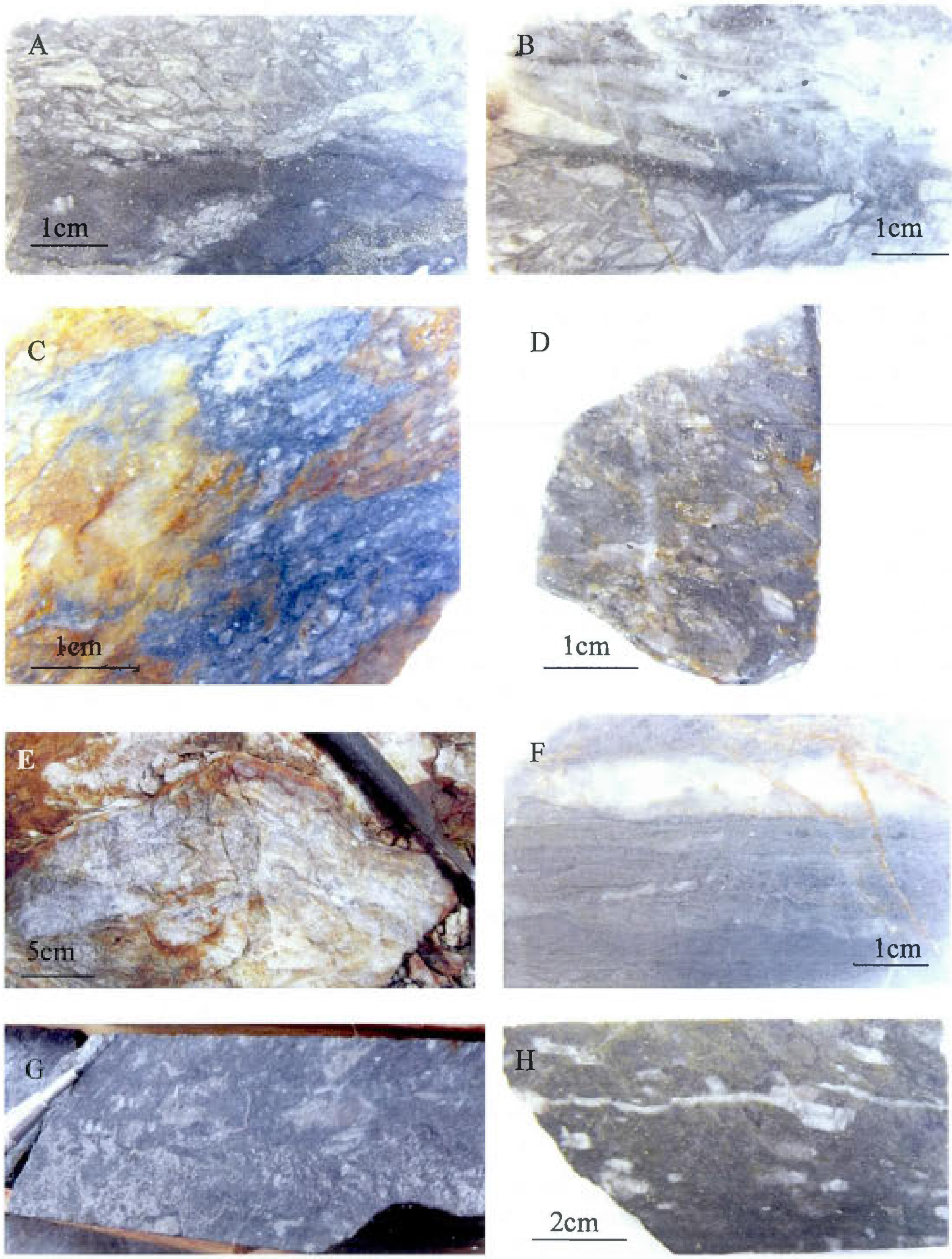


**Figure 1.6.** Photographs of rock samples illustrating the structurally-controlled facies. (a), (b), (c), and (d) Breccia ore with disseminated and small cluster of sulfides, very strong silicification (A: 21.9g/t Au; B: 17.45g/t Au; C: 9.7g/t Au; D: 18.6g/t Au). (e) and (f) Cherty quartz veins with fine sulfides (10.6g/t Au). (g) Semi-massive polymetallic high-grade vein

(120g/t Au), related to important silicification. (h) Trachytic syenite dyke with preserved phenocrysts in a carbonatized matrix (similar as the grey massive syenite – Fig.5A), and with disseminated sulfides (5.6g/t Au).

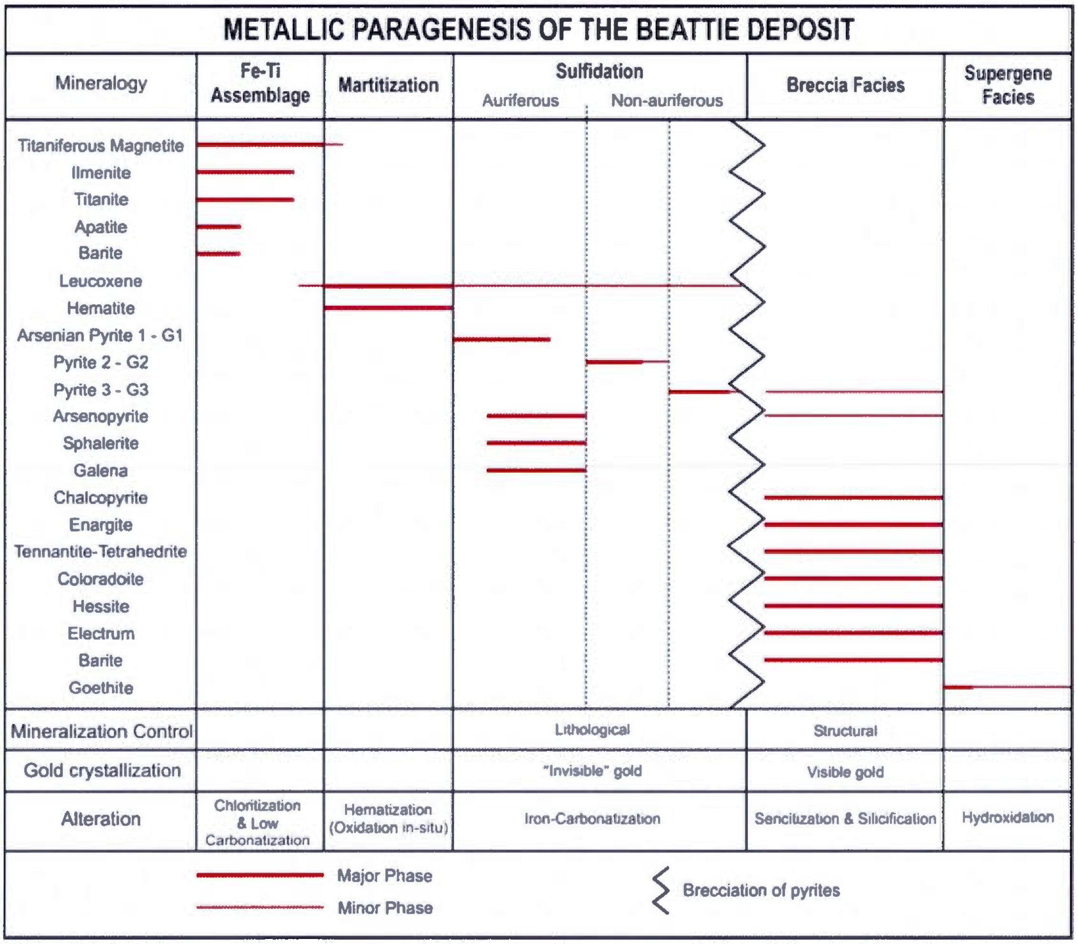


**Figure 1.7.** Metallic paragenesis of the Beattie deposit.

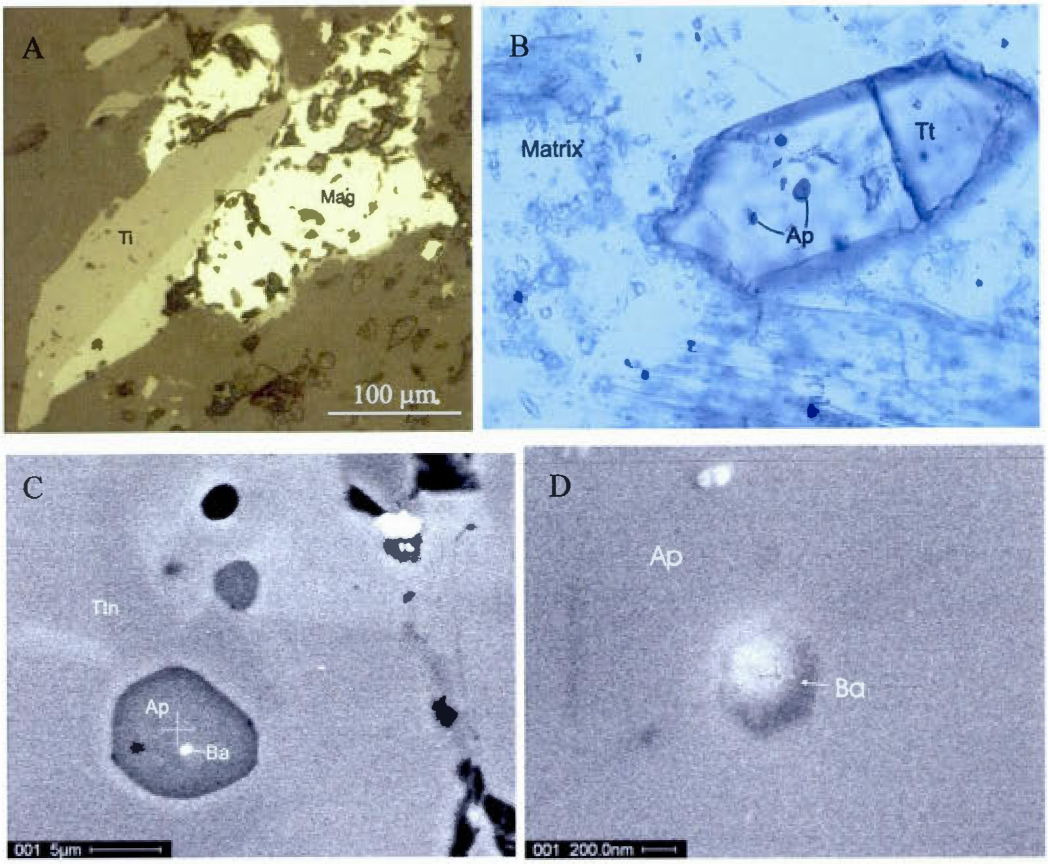


**Figure 1.8.** Microphotographs of the Fe-Ti assemblage. (a) Magnetite and titanite. (b) titanite crystal with mineral inclusions of apatite and barite. (c) and (d) Barite in inclusion within an apatite crystal included in titanite.

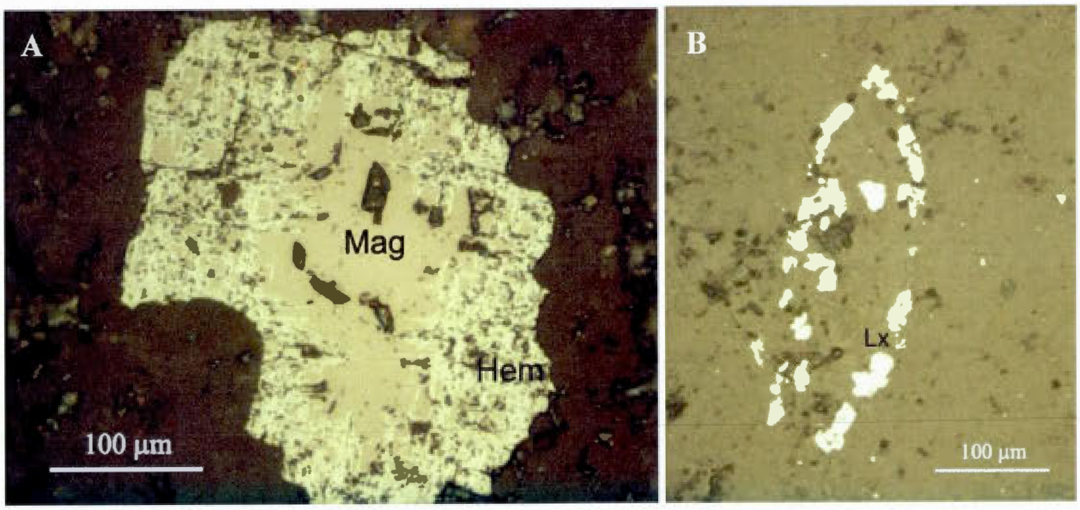


**Figure 1.9.** Microphotographs of the Martitization phase. (a) Exsolutions of hematite in a magnetite crystal. (b) Leucoxene as pseudomorph of titanite crystal.

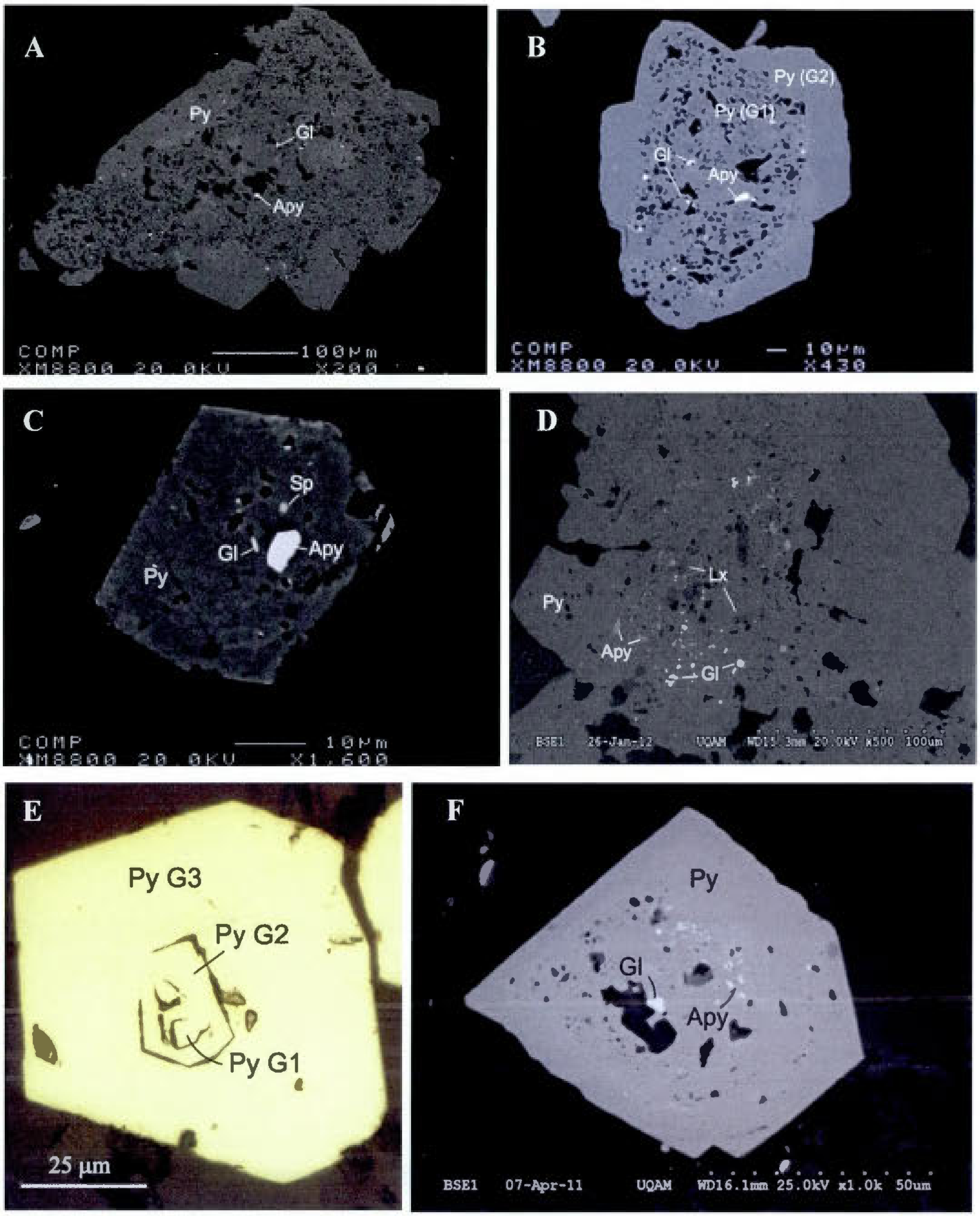


**Figure 1.10.** Microphotographs of the Sulfidation phase (lithologically-controlled facies). (a) and (b) Typical gold-bearing spongy pyrite (picture A: 200ppm Au in mineral; picture B: 180ppm Au in mineral) with metallic inclusions of arsenopyrite and galena (G1 Pyrite); G2 overgrowthing pyrite gold-free and without porosity. (c) G1 pyrite with inclusions of arsenopyrite (420ppm Au in mineral), galena, and sphalerite. (d) Pyrite's core with a myriad of inclusions of leucoxene, galena, and arsenopyriyte, in addition to porosity. (e) Three generations of pyrite. (f) Porous pyrite core (G1) with arsenopyrite and galena inclusion, and G2 clean pyrite.

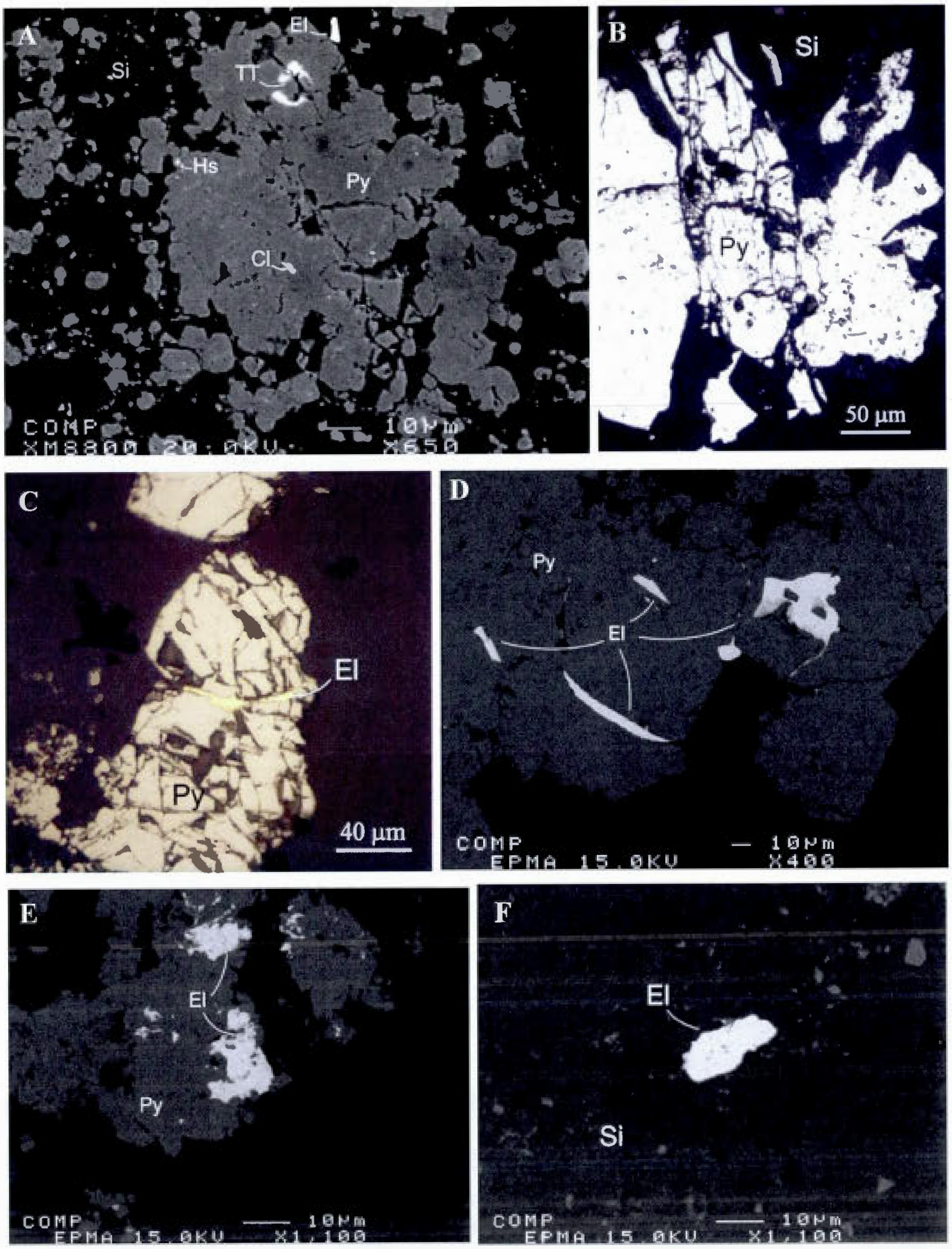
A
El
Si
TT
Hs
Py
Cl
COMP
XM8800 20.0KV
10µm
X650
B
Si
Py
50 µm
C
El
Py
40 µm
D
Py
El
COMP
EPMA 15.0KV
10µm
X400
E
El
Py
COMP
EPMA 15.0KV
10µm
X1,100
F
El
Si
COMP
EPMA 15.0KV
10µm
X1,100

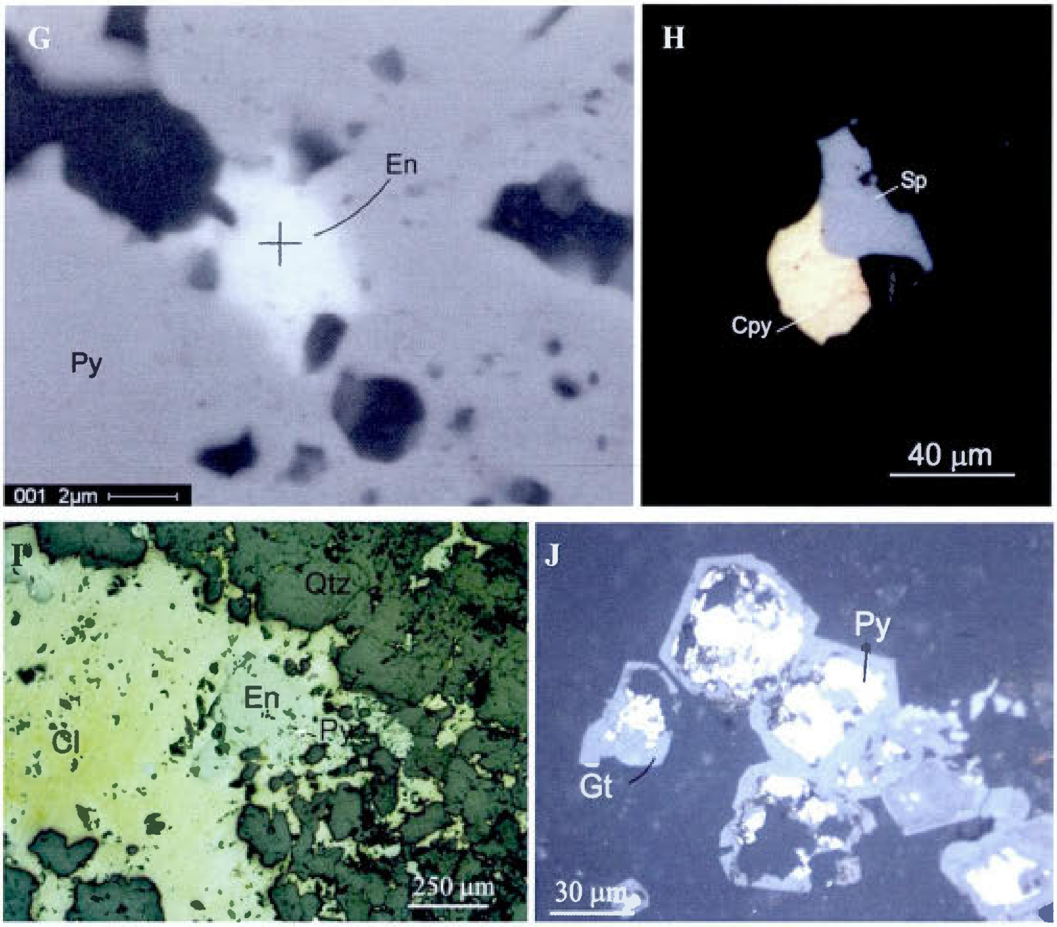


**Figure 1.11.** Microphotographs of the Breccia phase (structurally-controlled facies). (a) Brecciated pyrite with crystals of tennantite-tetrahedrite, coloradoite, and hessite in microfractures. Electrum is free in the matrix. (b) Hydraulic brecciation of pyrite in silica corridors. (c), (d), and (e) Electrum crystal in microfractures and porosity of brecciated pyrite in silica corridors. (f) Free electrum in the groundmass within silica corridors. (g) Enargite crystal trapped in porosity of pyrite. (h) Chalcopyrite and sphalerite in the matrix. (i) Enargite, coloradoite, and pyrite as semi-massive veins with high-silica content. (j) Coronitic texture of goethite around pyrite.

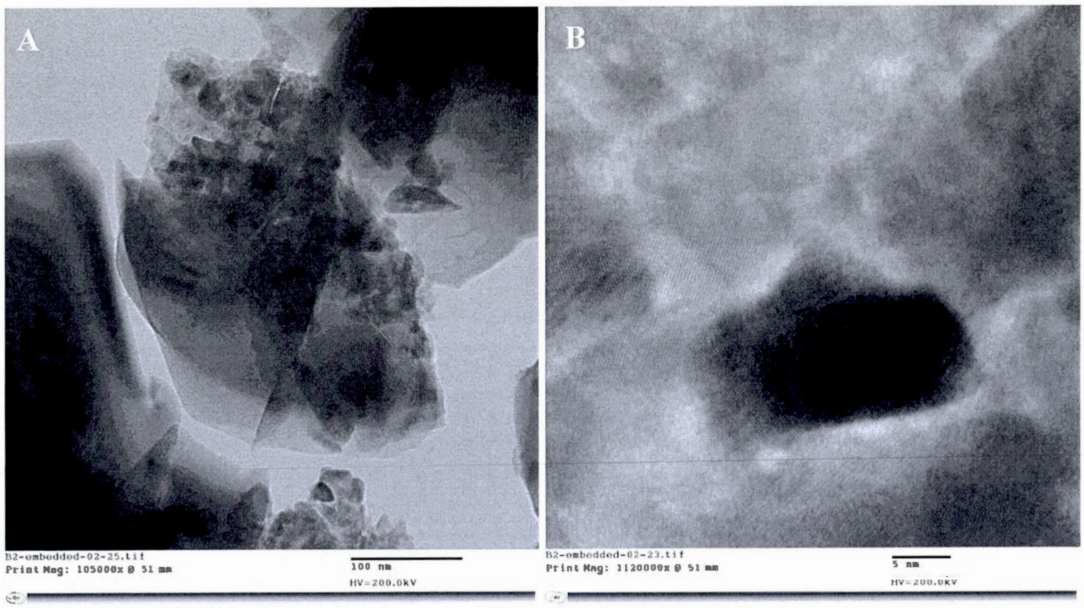


**Figure 1.12.** Microphotographs of arsenic-rich pyrite in the lithologically-controlled facies with TEM. (a) As-rich pyrites crystals. (b) Close up of (a): lattice fringes are very heterogeneous; the dark zone is an arsenic-rich portion of the pyrite.

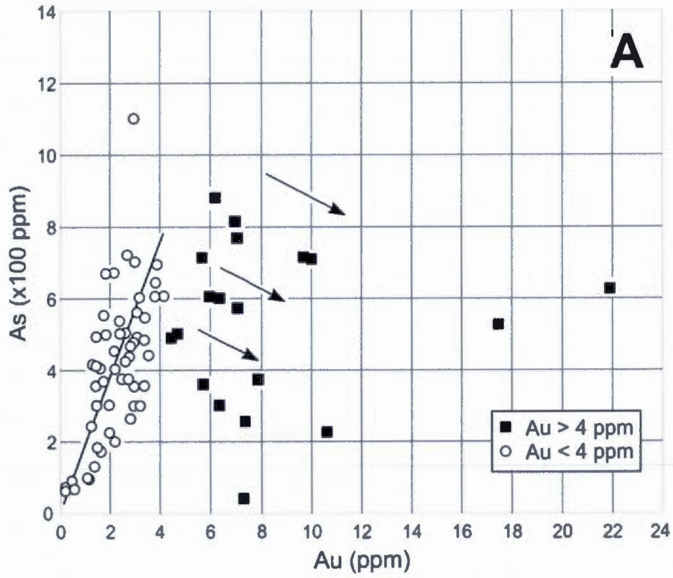


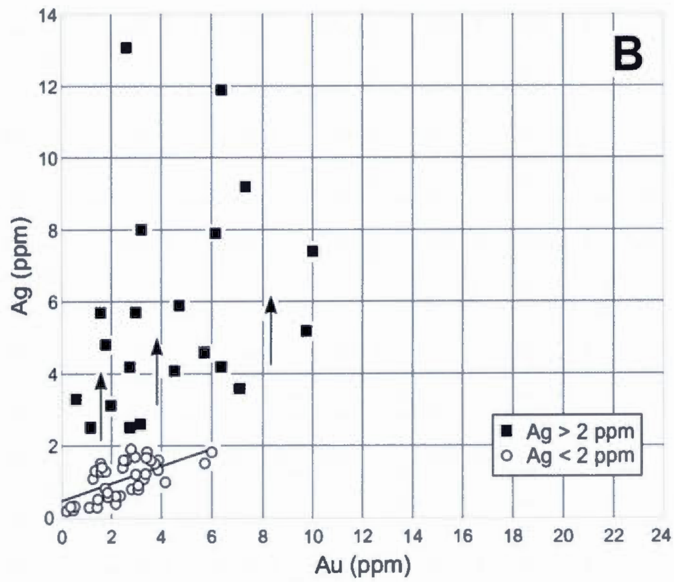


**Figure 1.13.** (a) As vs Au: two populations are distinguished with a threshold around 4ppm Au. (b) Ag vs Au: two populations are also highlighted with a threshold of 2ppm Ag. Two gold values present in the As vs Au diagram do not appear in the Ag vs Au diagram as their Ag value is above the Y-scale (for Au=10.6ppm, Ag=21ppm; for Au=17.5ppm, Ag=42ppm; for Au=21.9ppm, Ag=21.3ppm)

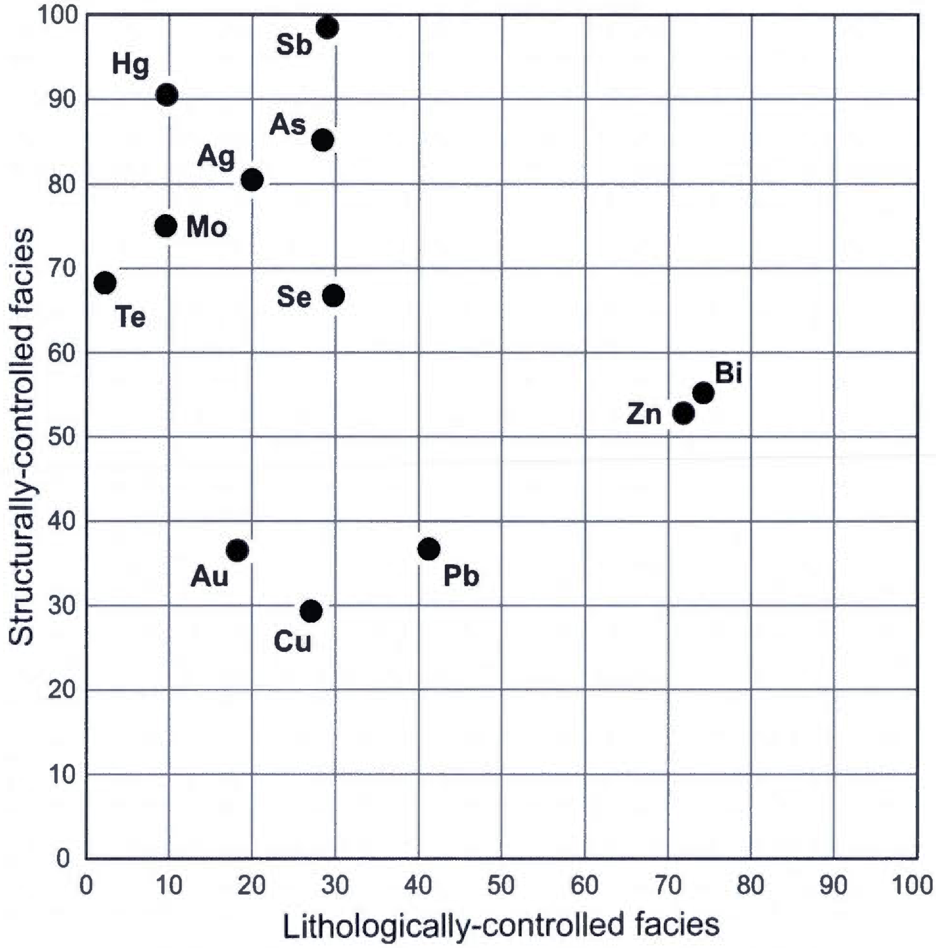


**Figure 1.14.** Comparison of the two mineralization styles in the Beattie deposit in terms of element concentration. It is an Isocon diagram (Grant, 2005). Same elements have been compared in the two mineralization styles, their ratio is plotted in the diagram. It is a quantitative estimation of changes in concentration depending on the mineralization style.

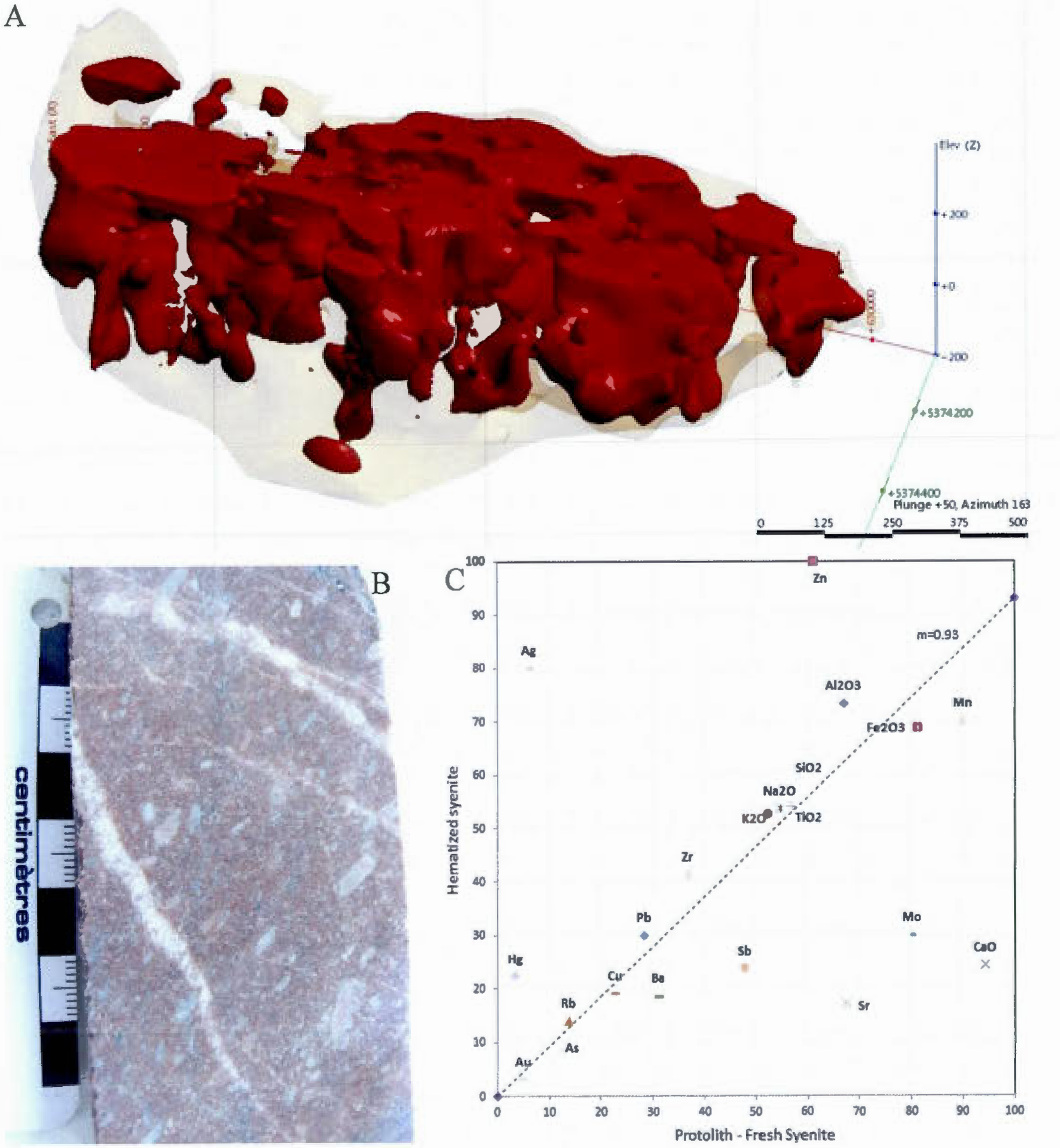


**Figure 1.15.** Hematization. (a) 3D model of hematized rocks – view plunges 50° to N163. (b) Reddish hematized syenite. (c) Isocon diagram of hematization.

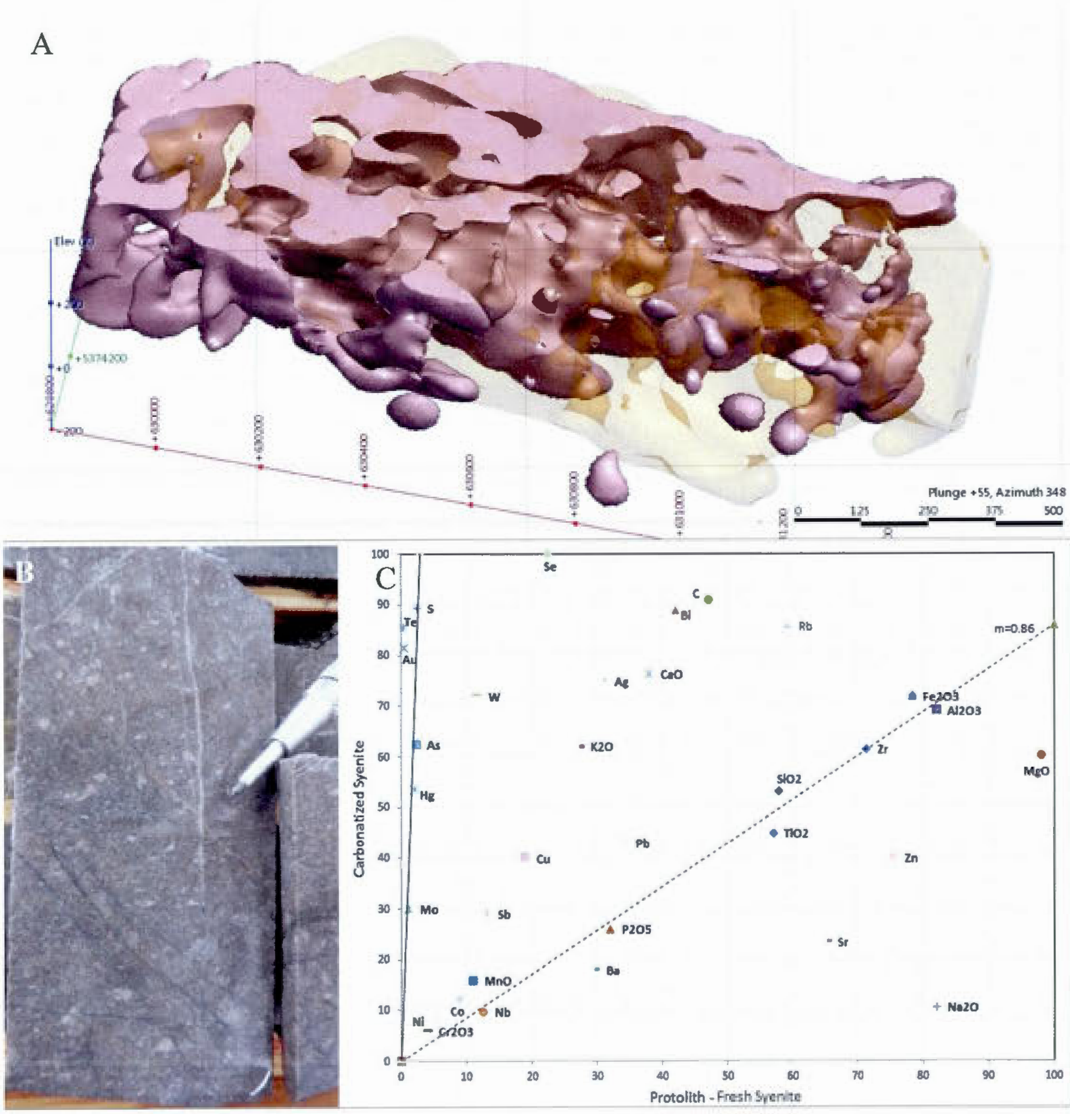


**Figure 1.16.** Carbonatization. (a) 3D model of carbonatized rocks – view plunges 55° to N348. (b) Grey carbonatized syenite. (c) Isocon diagram of carbonatization.

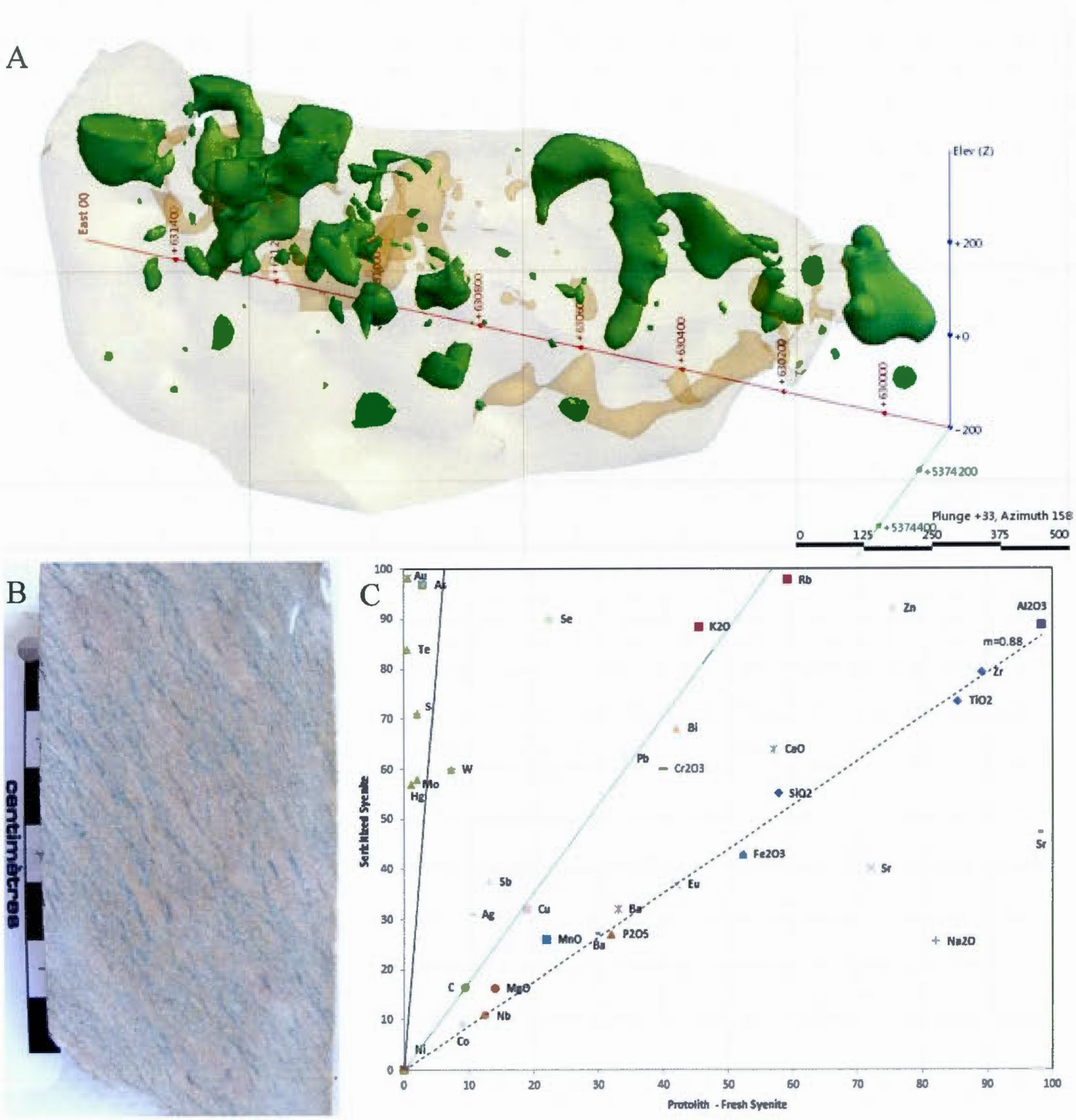


**Figure 1.17.** Sericitization. (a) 3D model of sericitized rocks – view plunges 33° to N158. (b) Green sericitized syenite. (c) Isocon diagram of sericitization.

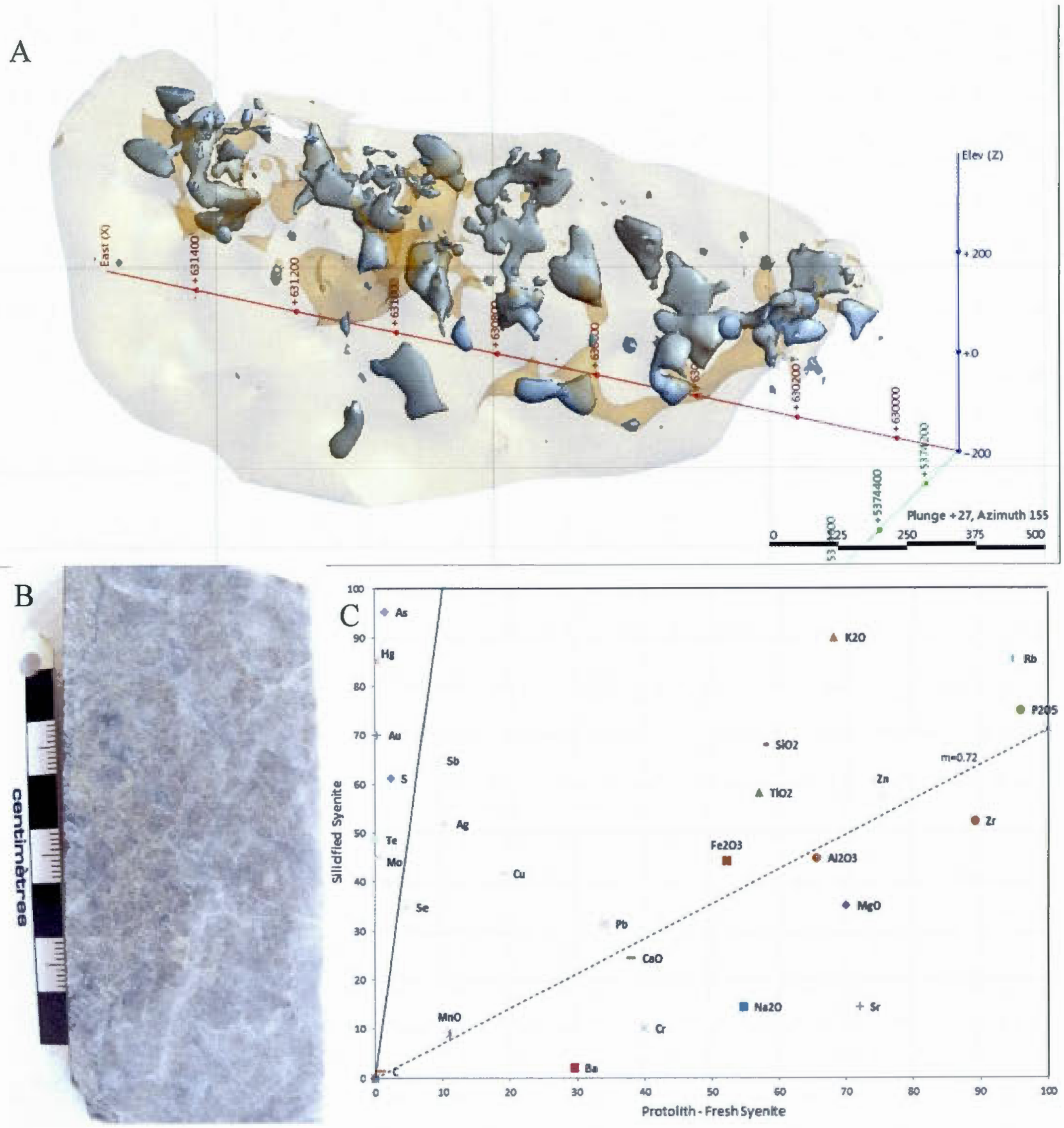


**Figure 1.18.** Silicification. (a) 3D model of silicified rocks – view plunges 27° to N155. (b) Grey silicified syenite. (c) Isocon diagram of silicification.

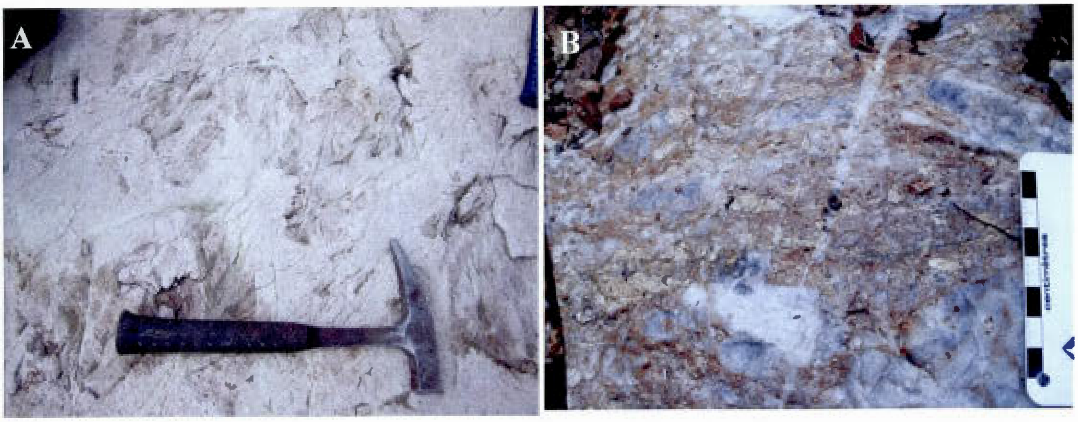


**Figure 1.19.** (a) Kaolinization, related to strong sericitization. (b) Fragments of sericitized syenite in silica corridors.

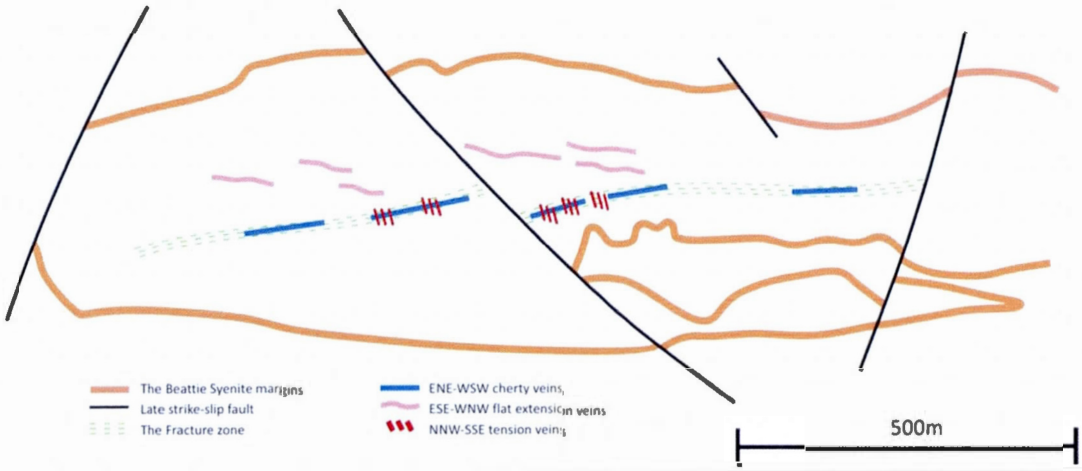


**Figure 1.20.** Cartoon of the different styles of veins and their location in the Beattie deposit.

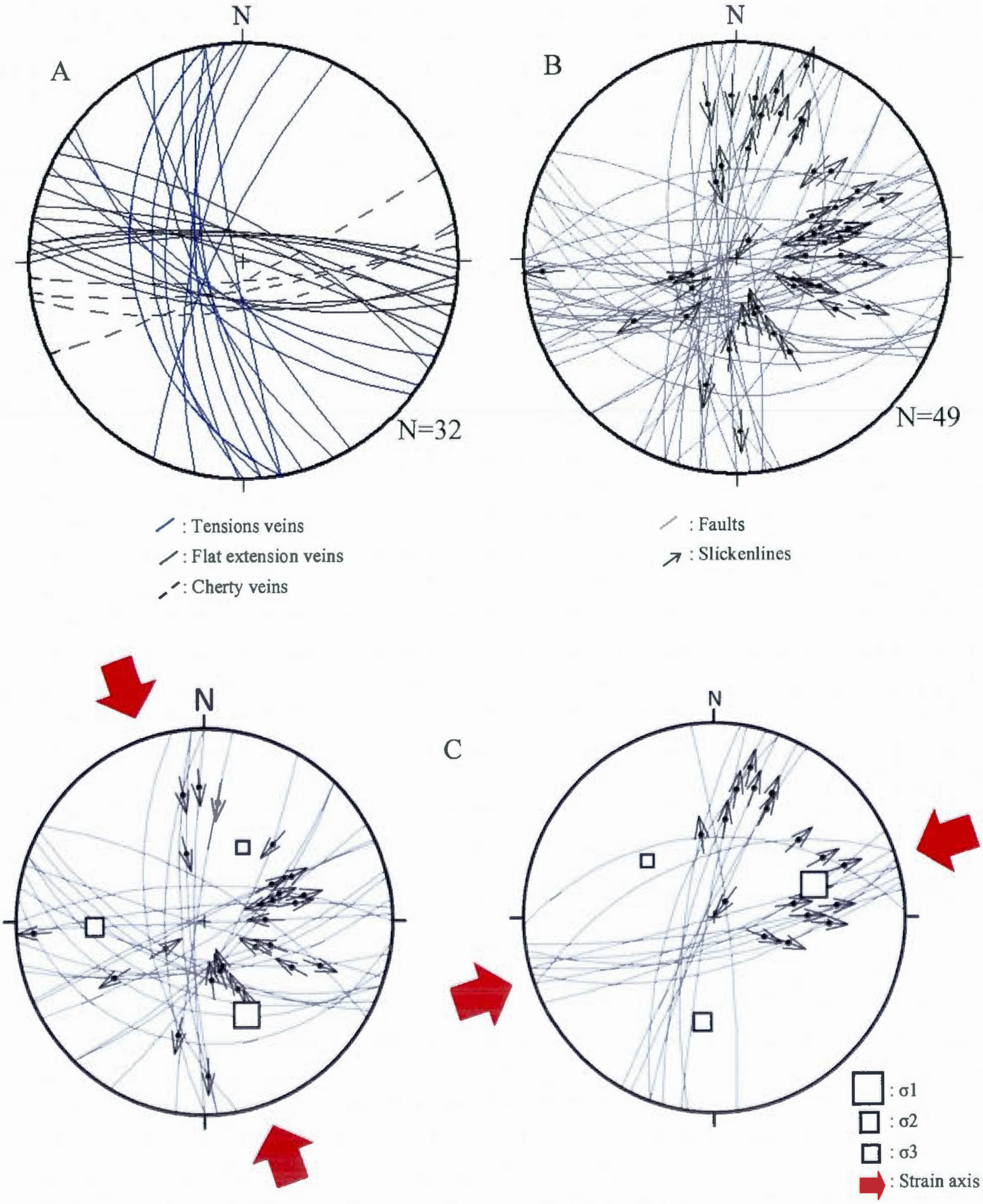


**Figure 1.21.** Structural analysis in the Beattie deposit. (a) Stereonet of veins. (b) Stereonet of minor late faults with slickenlines orientation. (c) Paleostress reconstruction using T-Tecto ®: phase 1, strain axis NNW-SSE with σ1 plunging 35° to SSE; phase 2, strain axis ENE-WSW with σ1 plunging 35° to ENE.

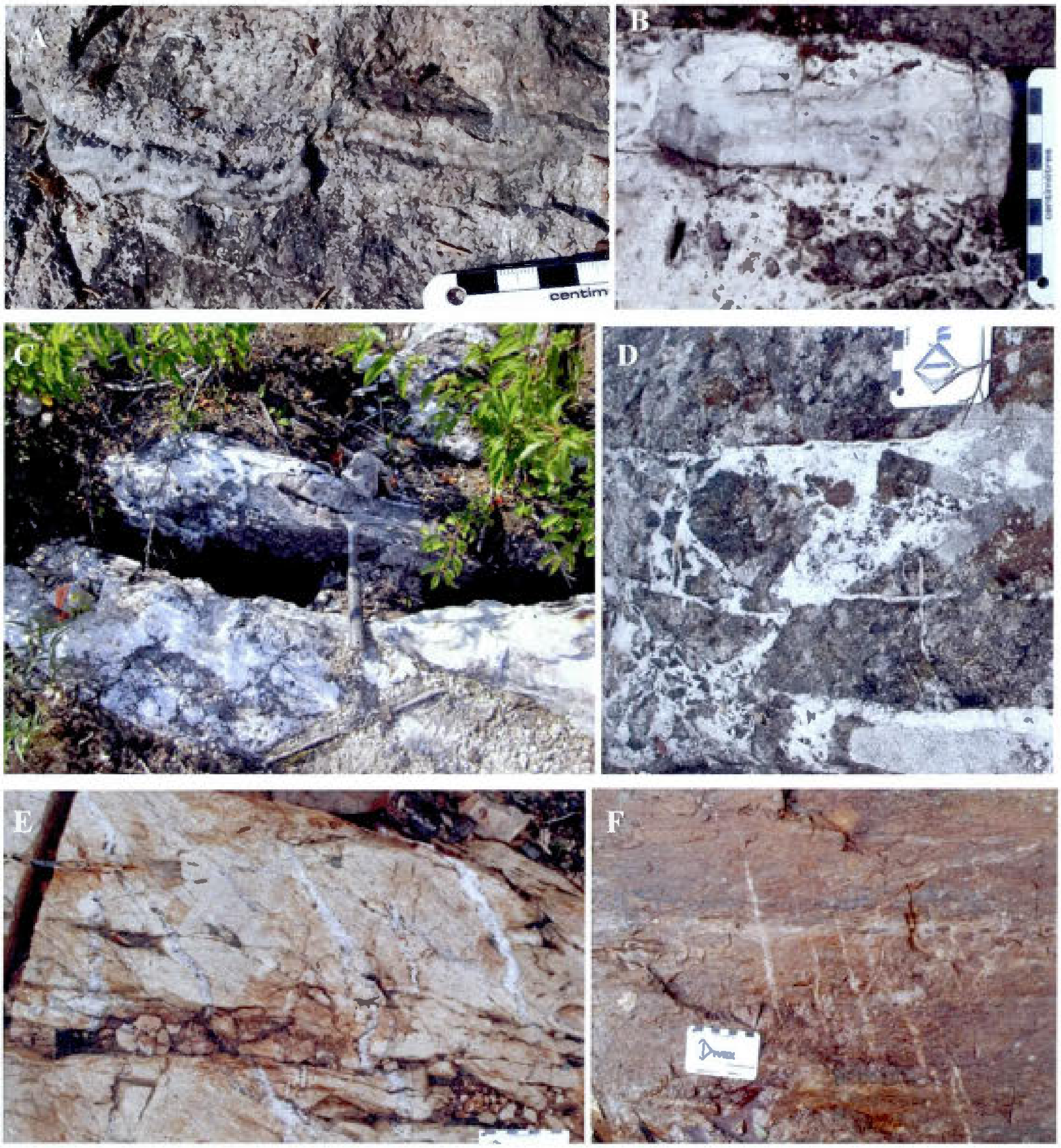
A
B
C
D
E
F

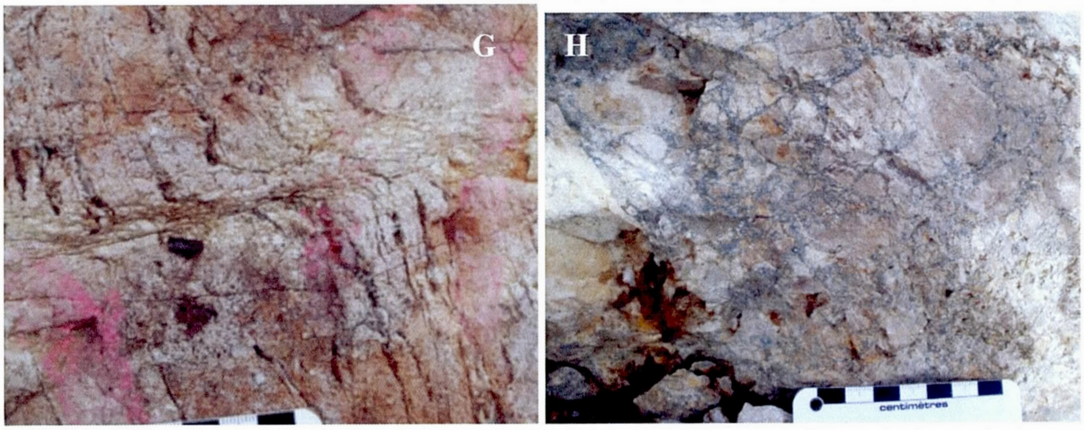


**Figure 1.22.** Photographs illustrating some of the vein styles. (a) ESE-WNW veins with open space crystallization. (b) ESE-WNW veins with pseudo-colloform texture. (c) ESE-WNW veins with a strong carbonate dissolution. (d) ESE-WNW vein with hydraulic breccia. (e) NNW-SSE tension veins near the Fracture zone. (f) NNE-SSE tension veins which cut ENE-WSW cherty veins. (g) NNW-SSE tension veins associated with carbonate dissolution, and cut by ENE-WSW shear. (h) Breccia fault related to an important net-slip on the NNE-SSW sinistral fault.

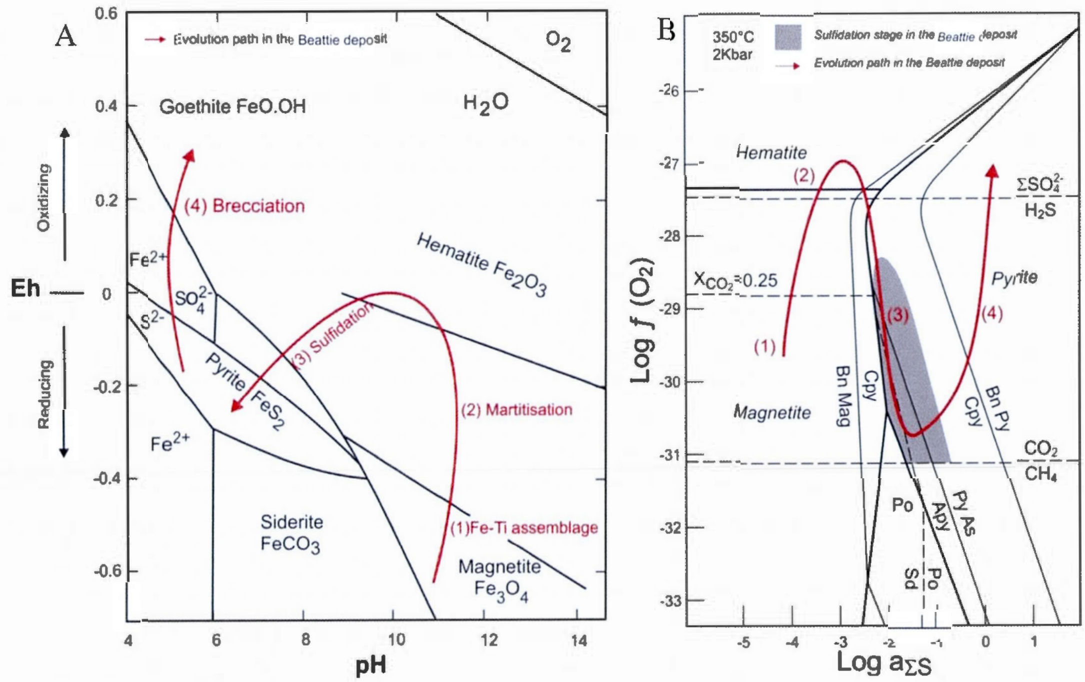


**Figure 1.23.** Evolution of the chemical conditions in the Beattie deposit. (a) Eh vs pH stability diagram, modified from Pélissonier (2001). (b) $f(O_2)$ vs Log $a_{\Sigma S}$ stability diagram, modified from Mikucki and Roberts (2004).

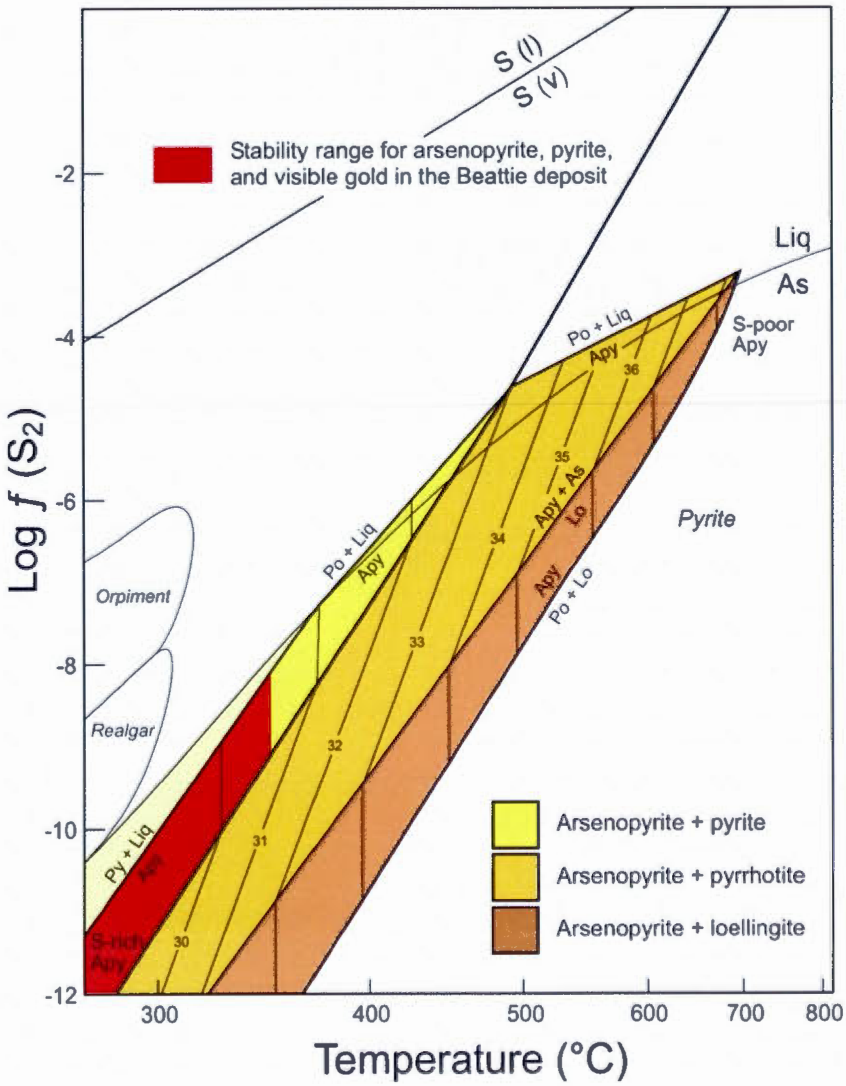


**Figure 1.24.** The average composition of magmatic-hydrothermal arsenopyrite of the breccia stage is plotted. Phase diagram redrawn from Barton (1969), Kretschmar and Scott (1976), and Sharp et al. (1985). Apy: arsenopyrite, Py: pyrite, Lo: loellingite. Atomic proportions of Arsenopyrite are indicated.

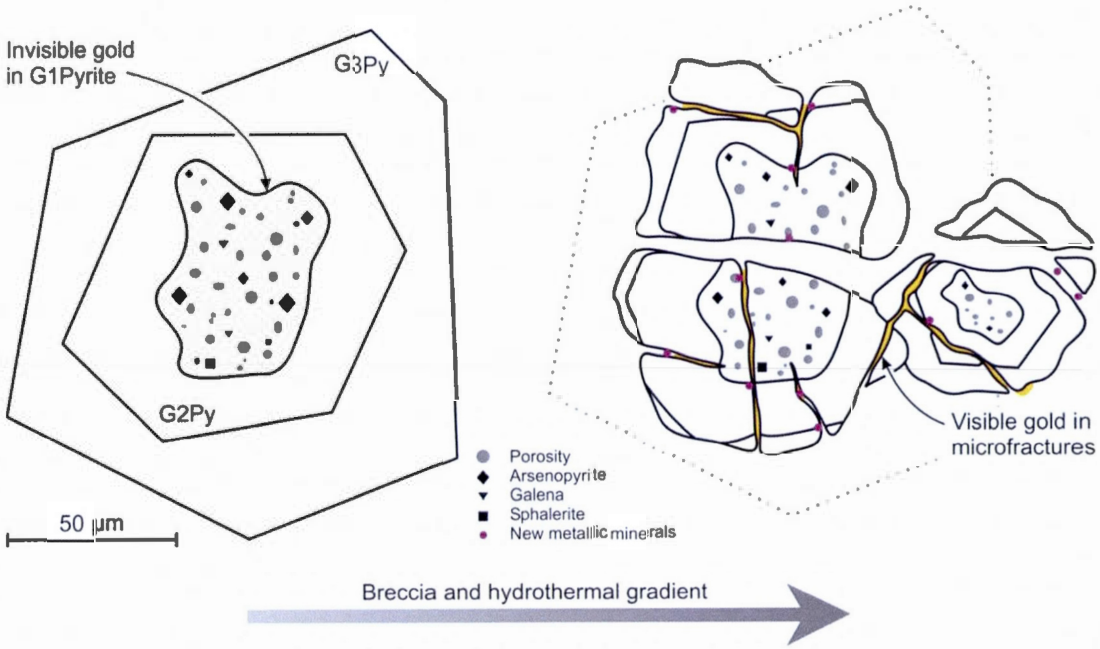


**Figure 1.25.** Cartoon of gold evolution in the Beattie deposit. Left: insivible gold in arsenian pyrite (G1) and arsenopyrite. Gold is in solid solution (yellow grid) in lattice bounds. Right: brecciated pyrite with several microfractures and new-porosity. Gold (yellow stripes) is remobilized and redeposited as visible in microfractures. New metallic minerals (Tennantite-tetrahedrite, enargite, hessite, coloradoite, chalcopyrite, barite) crystallize in the microfractures. There are two brecciated pyrites instead of only one in the left cartoon, it illustrates the increase of concentration of pyrite (two times more abundant).

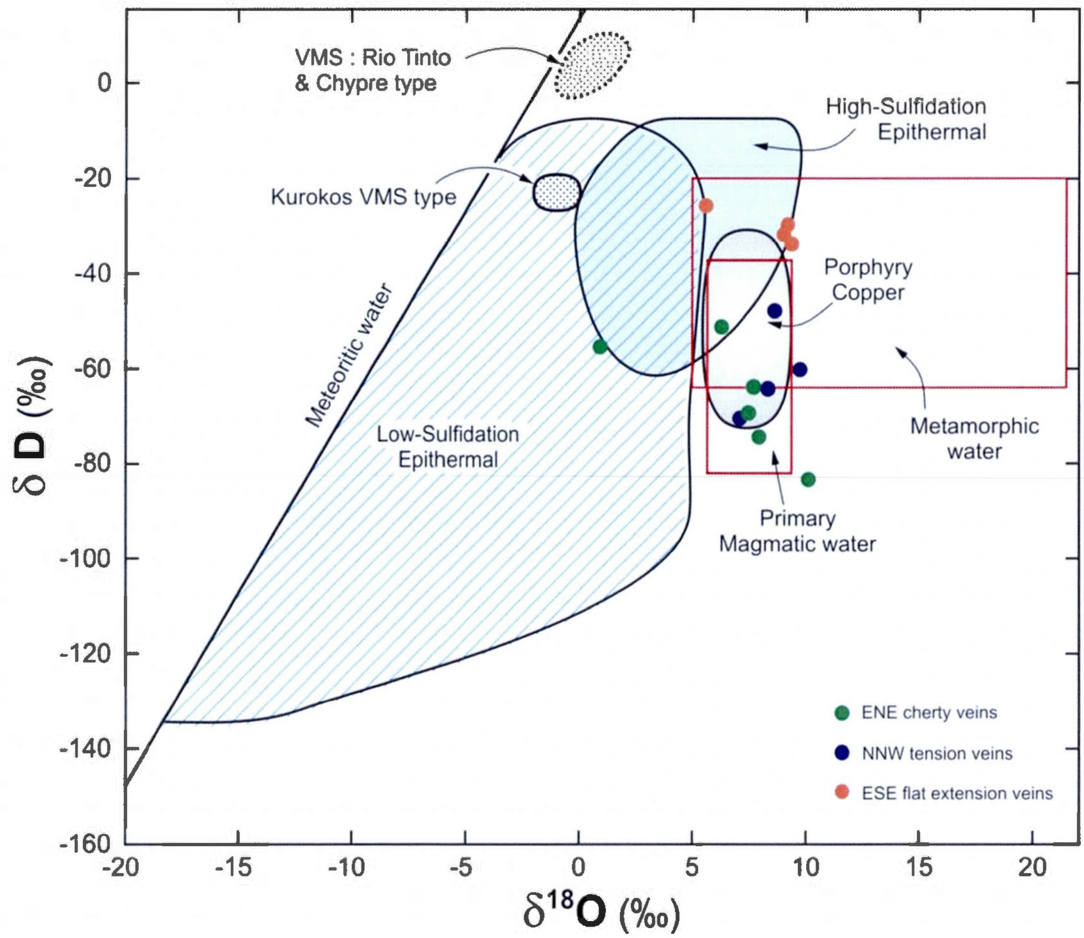


**Figure 1.26.** Calculated isotopic composition for fluids in the Beattie deposit (colored spots) in comparison to other types of deposit. Modified from Jébrak and Marcoux (2008).

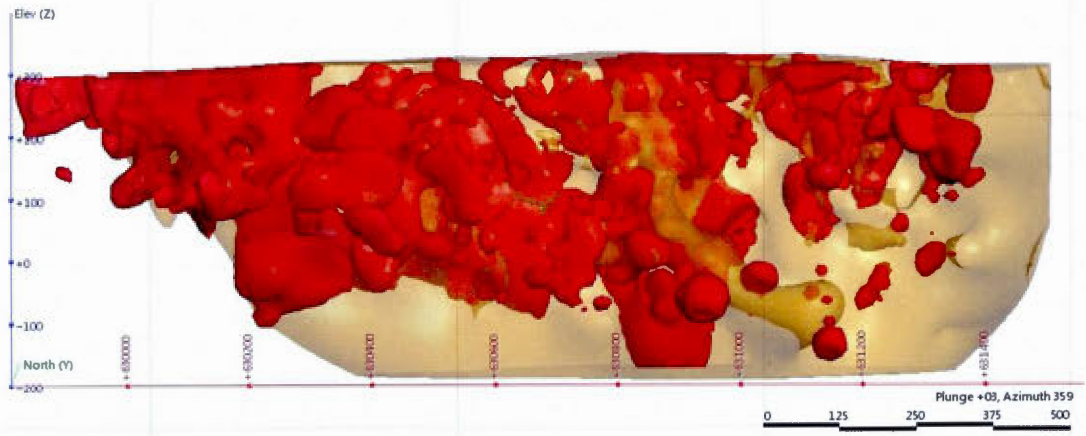


**Figure 1.27.** View to the north of ore bodies at 0.67 g/t Au (red) and the syenite (light brown). Evidence of plunging about 35° to ESE.

**Table 1.1.** Main characteristics of the two mineralization styles in the Beattie deposit.

| | **Lithologically-controlled facies** | **Structurally-controlled facies** |
|---|---|---|
| **Nature of the Mineralization** | disseminated sulfides | disseminated sulfides, small clusters of sulfides |
| **Structure** | massive, stockwork | replacement, breccia, veins, dyke, silica corridors |
| **Settings of the Mineralization** | limited to the Beattie syenite | in second order breaks and shear zones adjacent and within the Beattie syenite |
| **Alteration** | iron-carbonatization | silicification, sericitization |
| **Metallic Mineralogy** | PY, APY, GL, SP | PY, APY, GL, SP, CP, EN, TT, CL, HS, EL |
| **Elemental Association (+Au)** | As, Zn, Pb, Ag | As, Zn, Pb, Ag, Te, Hg, Mo, Cu, Sb, Se |
| **Gold Occurrence** | invisible gold included in lattice bounds of arsenian pyrite and arsenopyrite | electrum in microfractures and porosity of brecciated pyrite |
| **Au Grades** | <2.5g/t Au | >2.5g/t Au ; regularly higher than 5g/t Au |
| **Sulfide Contents** | 5 to 8% | 10 to 20% |
| **Au/Ag** | 1.2 | 0.8 |
| **Process** | Magmatic stage : syn-sulfidation | Magmatic-Hydrothermal stage : breccia facies |

**Abbreviations** PY:Pyrite; APY:Arsenopyrite; GL:Galena; SP:Sphalerite; CP:Chalcopyrite; EN:Enargite; TT:Tennantite-Tetrahedrite; CL:Coloradoite; HS:Hessite; EL:Electrum

**Table 1.2.** Microprobe assays on pyrite in the lithologically-controlled facies (EMP wt %)

| **Sample ID** | Ag % | Se % | Fe % | S % | As % | Hg % | Te % | Au % | Cu % | Total % |
|---|---|---|---|---|---|---|---|---|---|---|
| 1A-2 | 0.016 | 0.018 | 45.5 | 50.8 | 3.80 | 0.020 | 0.000 | 0.027 | 0.049 | 100.26 |
| 1A-3 | 0.000 | 0.012 | 46.3 | 53.3 | 1.02 | 0.000 | 0.000 | 0.009 | 0.001 | 100.65 |
| A1-1 | 0.004 | 0.009 | 45.4 | 52.1 | 1.69 | 0.035 | 0.000 | 0.012 | 0.280 | 99.45 |
| A1-2 | 0.000 | 0.015 | 45.7 | 50.4 | 4.40 | 0.022 | 0.005 | 0.013 | 0.028 | 100.61 |
| A1-3 | 0.000 | 0.017 | 46.7 | 53.4 | 0.381 | 0.040 | 0.015 | B.D.L | 0.036 | 100.60 |
| B2-1 | 0.009 | 0.015 | 47.1 | 53.6 | 0.014 | 0.003 | 0.008 | B.D.L | 0.000 | 100.74 |
| B2-2 | 0.008 | 0.023 | 46.1 | 51.4 | 2.57 | 0.002 | 0.000 | 0.020 | 0.006 | 100.10 |
| B2-3 | 0.022 | 0.015 | 46.2 | 52.2 | 1.35 | 0.008 | 0.000 | 0.015 | 0.011 | 99.83 |
| B2-4 | 0.000 | 0.004 | 46.7 | 52.6 | 0.439 | 0.000 | 0.015 | B.D.L | 0.000 | 99.69 |
| A4-2 | 0.002 | 0.013 | 45.6 | 50.0 | 4.71 | 0.019 | 0.006 | 0.018 | 0.173 | 100.46 |
| A4-3 | 0.000 | 0.008 | 47.0 | 53.3 | 0.058 | 0.011 | 0.012 | B.D.L | 0.007 | 100.38 |
| 11-APY | 0.000 | 0.210 | 35.2 | 20.6 | 37.8 | 0.008 | 0.009 | 0.042 | 0.008 | 93.96 |
| 6-1 | 0.011 | 0.007 | 46.1 | 51.2 | 2.87 | 0.029 | 0.000 | 0.008 | 0.023 | 100.21 |
| 6-2 | 0.000 | 0.017 | 46.2 | 52.0 | 1.95 | 0.004 | 0.002 | 0.008 | 0.015 | 100.15 |
| 6-3 | 0.000 | 0.004 | 46.8 | 53.3 | 0.020 | 0.000 | 0.000 | B.D.L | 0.000 | 100.12 |
| 11-1 | 0.001 | 0.011 | 46.1 | 53.4 | 0.162 | 0.022 | 0.000 | B.D.L | 0.000 | 99.74 |
| 11-2 | 0.004 | 0.009 | 45.7 | 51.9 | 1.92 | 0.000 | 0.000 | 0.011 | 0.004 | 99.58 |

**Table 1.3.** Microprobe assays on pyrite in the structurally-controlled facies (EMP wt %)

| **Sample ID** | Ag % | Se % | Fe % | S % | As % | Hg % | Te % | Au % | Cu % | Total % |
|---|---|---|---|---|---|---|---|---|---|---|
| 1-1 | 0.000 | 0.131 | 35.9 | 21.4 | 42.5 | 0.061 | 0.019 | B.D.L | 0.000 | 100.08 |
| 1-2 | 0.008 | 0.138 | 34.9 | 21.5 | 42.4 | 0.061 | 0.032 | 0.007 | 0.000 | 99.02 |
| 62-1 | 0.037 | 0.014 | 46.0 | 52.8 | 0.551 | 0.000 | 0.000 | B.D.L | 0.362 | 99.80 |
| 62-2 | 0.022 | 0.007 | 45.4 | 51.5 | 2.45 | 0.005 | 0.000 | B.D.L | 0.909 | 100.24 |
| 62-3 | 0.000 | 0.008 | 46.5 | 53.0 | 0.498 | 0.027 | 0.000 | B.D.L | 0.001 | 100.01 |
| 86-2 | 0.025 | 0.088 | 46.9 | 52.9 | 0.485 | 0.017 | 0.000 | B.D.L | 0.004 | 100.36 |
| 62-1 | 0.002 | 0.011 | 46.0 | 52.2 | 1.75 | 0.008 | 0.000 | B.D.L | 0.050 | 100.03 |
| 62-2 | 0.008 | 0.010 | 41.5 | 47.6 | 1.64 | 0.000 | 0.011 | B.D.L | 0.024 | 91.07 |

**Table 1.4.** Microprobe assays on electrum in the structurally-controlled facies (EMP wt %)

| **Sample ID** | Au % | Ag % | Total % |
|---|---|---|---|
| El-1 | 85.71 | 15.23 | 100.940 |
| El-2 | 84.75 | 15.24 | 99.990 |
| El-3 | 87.30 | 12.68 | 99.980 |
| El-4 | 90.44 | 9.000 | 99.440 |
| El-5 | 85.22 | 15.10 | 100.320 |
| El-6 | 85.19 | 14.96 | 100.150 |
| El-7 | 83.35 | 15.80 | 99.150 |
| El-8 | 83.87 | 14.52 | 98.390 |
| El-9 | 83.39 | 16.06 | 99.450 |
| El-10 | 85.19 | 15.25 | 100.440 |
| El-11 | 85.05 | 15.53 | 100.580 |
| El-12 | 83.50 | 14.50 | 98.710 |

**Table 1.5.** Main characteristics of the three veins style in the Beattie deposit

| | ENE-WSW | ESE-WNW | NNW-SSE |
|---|---|---|---|
| **Location** | In the Fracture zone | Out of the Fracture zone | In the Fracture zone |
| **Dip** | steep to the south | shallow to the north | medium to steep to the west |
| **Structure** | massive | flat extension, open-space, pseudo-colloform | tension veins, periodic |
| **Morphology** | straight, narrow, irregular | sinuous, occasionnaly large | thin, occasionnaly folded and sheared |
| **Composition** | cherty quartz, few sericite | quartz, carbonate (calcite to ankerite), few sericite | quartz, carbonate (brown ankerite) |
| **Carbonate Dissolution** | none | yes, locally total | yes, partial |
| **Gold Occurrence** | fine disseminated in sulfides, >10 g/t Au | none | none |
| **Breccia-related** | breccia ore spatially related | hydraulic breccia | none |
| **Relative Chronology** | early | early (different from ENE veins) | late |

**Table 1.6.** Isotopic results for quartz veins in the Beattie deposit.

| **Sample** | Vein type | δO18 (‰ VSMOW) | δO18 fluid at 350°c (‰ VSMOW) | δD (‰ VSMOW) |
|---|---|---|---|---|
| 6-A | ENE-WSW cherty | 13.35 | 7.30 | -67 |
| 4-B | ENE-WSW cherty | 13.71 | 7.67 | -74 |
| Iso2 | ENE-WSW cherty | 13.2 | 7.2 | -63 |
| Iso4 | ENE-WSW cherty | 12.2 | 6.2 | -53 |
| Iso8 | ENE-WSW cherty | 16.1 | 10.1 | -83 |
| Iso10 | ENE-WSW cherty | 6.9 | 0.9 | -57 |
| 1-C | ESE-WNW flat | 14.56 | 8.52 | -32 |
| Iso1 | ESE-WNW flat | 14.9 | 8.9 | -36 |
| Iso6 | ESE-WNW flat | 14.8 | 8.8 | -30 |
| Iso9 | ESE-WNW flat | 11.7 | 5.7 | -26 |
| 4-D | NNW-SSE tension | 14.25 | 8.21 | -63 |
| Iso3 | NNW-SSE tension | 15.5 | 9.5 | -60 |
| Iso5 | NNW-SSE tension | 13.1 | 7.1 | -69 |
| Iso7 | NNW-SSE tension | 14.3 | 8.3 | -47 |

# CONCLUSION GÉNÉRALE

Les études minéralogiques couplées à la géochimie ont apporté des avancées significatives dans la compréhension de l'évolution du gisement aurifère de Beattie. Des phases initiales oxydantes ont évolué en conditions plus réduites à la faveur de mélanges de fluides magmatiques (i.e., Bi) et externes (i.e., As dans les sédiments) riches en $CO_2$ qui ont entrainé la précipitation de l'or dans la structure cristalline de la pyrite arsénifère et l'arsénopyrite sous forme de solution solide. Deux phases subséquentes de pyritisation sont dépourvues d'or et d'arsenic. Cela permet de proposer qu'une phase unique d'apport en or est à l'origine de l'anomalie aurifère à Duparquet. Cet or invisible dans les sulfures arsénifères pourrait représenter jusqu'à 85% du minerai. Il est étroitement associé à la syénite de Beattie très carbonatisée à carbonates de fer. Une phase d'altération ultérieure, dominée par des fluides magmatique-hydrothermaux (i.e., isotope O et H) riches en silice, entraine une bréchification des sulfures et leur redistribution dans des corridors siliceux à l'intérieur des zones de failles E-W, ainsi qu'une remobilisation de l'or dans les microfratures des pyrites bréchifiées. L'or expulsé de la structure cristalline de la pyrite et de l'arsénopyrite précipite dans les pièges texturaux de la pyrite avec l'argent sous forme d'éléctrum. L'or est désormais visible au microscope. La géothermométrie appliquée à l'arsénopyrite indique des températures de cristallisation inférieures à 350°C pour l'évènement magmatique-hydrothermal associé à l'or visible. La dominance de régimes en systèmes ouverts a directement affectée le style de cristallisation de l'or, tant au niveau de l'incorporation dans le fluide de l'arsenic qui contrôle la précipitation de l'or invisible, que la circulation tardive de fluides riches en silice qui sont à l'origine de la remobilisation de l'or.

Le modèle génétique, initialement proposé par Robert (2001) a pu être précisé. La mise en place de l'intrusion suivit d'un mélange de fluides magmatiques et externes, qui aboutit à la maturité du magma évolué et à la précipitation de l'or dans les sulfures arsénifères, est contraint entre D1 et D2. L'évènement de redistribution des sulfures et de remobilisation de l'or est syn-métamorphique durant la transition D2-D3. Il est clair désormais que la silicification pervasive des roches spatialement associées aux failles E-W est le dernier évènement d'altération (D3), alors que la séricitisation est plus précoce.

Plusieurs évidences indiquent que le gisement de Beattie a des affinités avec les gisements associés aux intrusions (*Intrusion Related Gold Deposit*; Lang et Baker, 2001; *Syenite Associated Disseminated Gold Deposit*; Robert, 2001), mais aussi avec des gisements de types épithermaux (Sillitoe et Hedenquist, 2003), et possiblement mésothermaux (Groves, 1998). Globalement, le gisement de Douay apparait comme le plus similaire à Beattie, tant sur le plan pétrologique, que sur le plan métallogénique et structural (Gauthier et Arnois, 1994; Dupéré, 2007).

## Références

Dupéré, M., et C. Duplessis. (2007). Technical Report - Resource Evaluation on the Douay Project for SEM Vior Inc.: 188 p.

Gauthier, M., et L. Harnois (1994). Étude sommaire des protolithes, des patrons d'altération et des paragenèses minérales des minéralisations aurifères du canton de Douay (Abitibi). Rapport d'étape soumis à Richard Laplante et Denis Raymond du bureau régional d'Abitibi de SOQUEM, Université du Québec à Montréal.

Groves, D.I., R.J. Goldfarb, M. Gebre-Mariam, S.G. Hagemann, et F. Robert. 1998. «Orogenic gold deposits: A proposed classification in the context of their crustal distribution and relationship to other gold deposit types». *Ore Geology Reviews*, vol. 13, p. 7–27.

Lang, J.R., et T. Baker. 2001. «Intrusion-related gold systems : the present level of understanding». *Mineralium Deposita*, vol. 36, p. 477-489.

Robert, F. 2001. «Syenite associated disseminated gold deposit in the Abitibi greenstone belt, Canada». *Mineralium Deposita*, vol. 36, p. 505-516.

Sillitoe, Richard H., et Jeffrey W. Hedenquist. 2003. «Linkages between volcanotectonic settings, ore-fluid compositions, and epithermal precious metal deposits». *Special Publication [Society of Economic Geologists [U. S.]]*, vol. 10, p. 315-343.

# APPENDICE A

# MÉTHODE ANALYTIQUE POUR LA GÉOCHIMIE, ET RÉSULTATS D'ANALYSES LITHOGEOCHIMIQUES

**Méthodologie pour les analyses lithogéochimiques**

Cinquante-deux échantillons ont été sélectionnés à partir de zones d'affleurement et de forage dans le gisement de Beattie. Des analyses sur roche totale et éléments traces ont été réalisé au laboratoire ACME de Vancouver, et ALS de Val d'or. Les concentrations des éléments majeurs et traces ont été déterminées par Inductively Coupled Plasma Mass Spectrometry (ICP – MS), et par Inductively Coupled Plasma Emission Spectrometry (ICP – ES) suivant la fusion lithium metaborate/tetraborate et la digestion avec un acide nitrique.

**Méthodologie pour les analyses à la microsonde**

Dix lames minces polies préalablement étudiées au microscope optique ont été sélectionnées pour l'analyse microsonde. Ces échantillons sont représentatifs des quatre phases de la paragénèse minérale du gisement de Beattie. Les analyses ont été effectuées au laboratoire de microsonde de l'université McGill. L'appareil utilisé est un JXA JEOL-8900L dans lequel sont intégrés les spectromètres WDS et EDS. Les analyses ont été réalisées sous 20kV, avec un courant de faisceau de 50nA, et un diamètre de faisceau de 3µm. Les éléments Au, As, Ag, Fe, S, Cu, Zn, Hg, Se, et W ont été mesurés dans des pyrites et des arsénopyrites. Les seuils de détection étaient respectivement pour les éléments mentionnés, 0,0065% après 540 secondes, 0,0491% après 60 secondes, 0,035% après 60 secondes, 0,034% après 10 secondes, 0,0121% après 10 secondes, 0,0229% après 60 secondes, 0,0382% après 60 secondes, 0,0337% après 340 secondes, 0,0156% après 60 secondes, et 0,0248% après 100 secondes. Pour les analyses sur électrum, le comptage était de 20 secondes pour l'or et pour l'argent.

**Méthodologie pour les analyses d'isotopes stables d'oxygène et d'hydrogène**

Quatorze échantillons de quartz pur provenant des trois types de veines dans le gisement de Beattie ont été analysés au laboratoire des isotopes stables de l'université Queen's, Ontario. Les isotopes d'hydrogène sont mesurés avec un spectromètre DELTA $^{plus}$ XP. L'analyse est faite par Thermochemical Elemental Analyser (TC/EA) à haute température. Pour les isotopes d'oxygène, le matériel est préparé séparément sur une ligne d'extraction silicatée, puis mesuré avec un spectromètre de masse Finnigan Mat 252.

Résultats lithogéochimiques :

| SAMPLE | D006556 | D009304 | 144103 | D007580 | 144103 | D007601 | 04-A | D047015 | 01-A | D000398 | D023252 |
|---|---|---|---|---|---|---|---|---|---|---|---|
| SiO2 % | 55.1 | 57.9 | 61.1 | 56.1 | 61.1 | 58.4 | 54.66 | 53 | 82.67 | 72.9 | 70.9 |
| Al2O3 | 14.8 | 11.5 | 11.8 | 15.55 | 11.8 | 13.8 | 17.32 | 13.75 | 5.46 | 9.42 | 8.56 |
| Fe2O3 | 4.29 | 6.64 | 4.14 | 4.74 | 4.14 | 4.3 | 4.99 | 4.17 | 4.77 | 2.63 | 3.3 |
| CaO | 4.26 | 4.3 | 6.54 | 4.23 | 6.54 | 4.39 | 3.83 | 4.88 | 0.3 | 2.25 | 3.88 |
| MgO | 1.63 | 1.37 | 1.28 | 1.74 | 1.28 | 1.7 | 1.47 | 2.19 | 0.09 | 0.48 | 1.12 |
| Na2O | 1.7 | 0.21 | 0.98 | 0.22 | 0.98 | 0.86 | 3.75 | 2.31 | 0.38 | 0.15 | 0.36 |
| K2O | 8.84 | 6.43 | 4.07 | 5.24 | 4.07 | 4.71 | 5.43 | 7.45 | 3.79 | 7.02 | 5.62 |
| TiO2 | 0.49 | 1.24 | 0.43 | 0.56 | 0.43 | 0.47 | 0.54 | 0.47 | 0.16 | 0.31 | 0.28 |
| MnO | 0.13 | 0.2 | 0.11 | 0.13 | 0.11 | 0.12 | 0.11 | 0.1 | 0.03 | 0.06 | 0.14 |
| P2O5 | 0.27 | 0.39 | 0.29 | 0.32 | 0.29 | 0.26 | 0.31 | 0.27 | 0.27 | 0.16 | 0.16 |
| C | 1.66 | 1.6 | 2.03 | 1.64 | 2.03 | 1.65 | | 1.91 | | 0.62 | 1.27 |
| S | 1.42 | 1.92 | 0.43 | 0.09 | 0.43 | 0.06 | | 0.91 | | 1.56 | 1.33 |
| LOI | 6.18 | 6.96 | 7.78 | 7.66 | 7.78 | 7.59 | 7.1 | 7 | 1.9 | 2.78 | 5.3 |
| Total | 98.1 | 97.2 | 98.8 | 96.8 | 98.8 | 96.8 | 99.5 | 96 | 99.78 | 98.3 | 99.8 |
| Ba ppm | 2720 | 436 | 1360 | 2270 | 1360 | 1460 | 2028 | 2540 | 790 | 959 | 1185 |
| Ce | 220 | 66.8 | 168 | 245 | 168 | 197 | 250 | 218 | 93.3 | 130 | 133 |
| Eu | 3.69 | 2.21 | 3.17 | 4.35 | 3.17 | 3.87 | 4.07 | 3.65 | 1.65 | 2.43 | 2.58 |
| Cr | 10 | 10 | 10 | 10 | 10 | 10 | | 10 | | 20 | 10 |
| Rb | 195.5 | 137 | 105.5 | 163.5 | 105.5 | 131 | 132.3 | 165.5 | 68.5 | 144.5 | 107.5 |
| Sr | 947 | 413 | 680 | 474 | 680 | 410 | 926 | 1010 | 144.6 | 227 | 422 |
| Sn | 1 | 2 | 1 | 1 | 1 | 1 | 1 | 1 | 0.6 | 1 | 1 |
| Sr | 947 | 413 | 680 | 474 | 680 | 410 | 926 | 1010 | 144.6 | 227 | 422 |
| Th | 22.8 | 2.6 | 17.2 | 23.5 | 17.2 | 19.25 | 29.4 | 22.7 | 9 | 14.9 | 13.35 |
| U | 6.78 | 9.33 | 8.29 | 6.38 | 8.29 | 6.95 | 6.6 | 6.33 | 3.9 | 4.48 | 4.12 |
| V | 144 | 191 | 190 | 148 | 190 | 81 | 105 | 192 | 130 | 179 | 191 |
| W | 12 | 47 | 11 | 10 | 11 | 4 | 2.7 | 13 | 6.8 | 8 | 8 |
| Y | 29.9 | 46.7 | 24.6 | 33.4 | 24.6 | 27.3 | 35.3 | 29.5 | 17.8 | 18.9 | 20.7 |
| Zr | 317 | 255 | 246 | 344 | 246 | 307 | 376 | 301 | 124.3 | 234 | 186 |
| As | 300 | 500 | 93.3 | 3.5 | 93.3 | 6.7 | 8.2 | 200 | 713.8 | >250 | 300 |
| Au | 1.965 | 4.71 | 1.13 | 0.028 | 1.13 | 0.038 | 0.0051 | 2.18 | 9.708 | 7.86 | 3.17 |
| Bi | 0.68 | 0.24 | 0.87 | 0.43 | 0.87 | 0.65 | 0.3 | 0.6 | 0.9 | 0.37 | 0.36 |
| Hg | 1.45 | 1.69 | 1.595 | 0.043 | 1.595 | 10.35 | 0.05 | 1.105 | 2.91 | >25.0 | 22.3 |
| Sb | 3.74 | 12.5 | 10 | 2.8 | 10 | 1.6 | 1 | 2.35 | 4.1 | 26.6 | 10.3 |
| Se | 1.8 | 2.9 | 1.8 | 0.7 | 1.8 | 0.5 | 0.8 | 1.5 | 2.4 | 4 | 4.7 |
| Te | 1.68 | 4.36 | 1.66 | 0.01 | 1.66 | 0.52 | | 0.56 | | >250 | 16.85 |
| Ag | 3.1 | 5.9 | 2.5 | 0.9 | 2.5 | 0.7 | 0.06 | 2 | 5.2 | 149 | 8 |
| Cu | 32 | 88 | 35 | 22 | 35 | 64 | 26.3 | 25 | 21.7 | 168 | 25 |
| Mo | 57 | 103 | 67 | 0.6 | 67 | 1 | 0.3 | 18 | 497.8 | 14 | 67 |
| Ni | 4 | 3 | 4 | 6 | 4 | 6 | 2.2 | 2 | 5.4 | 18 | 3 |
| Pb | 62 | 25 | 89 | 18 | 89 | 20 | 34.9 | 38 | 57.2 | 22 | 30 |
| Zn | 92 | 60 | 70 | 96 | 70 | 73 | 56 | 64 | 46 | 34 | 96 |

| D000396 | 06-A | D009165 | D013071 | D036693 | D039219 | D023142 | D035021 | D048208 | D005117 | D000486 |
|---|---|---|---|---|---|---|---|---|---|---|
| 65.5 | 92.2 | 67.2 | 49.2 | 41.5 | 53.4 | 63.7 | 58.5 | 59.1 | 51.3 | 56.3 |
| 3.08 | 2 | 13.3 | 13.2 | 10.9 | 13.6 | 11.65 | 10.25 | 12.4 | 12.9 | 13.15 |
| 2.03 | 1.78 | 4.1 | 3.92 | 3.19 | 5.33 | 6.64 | 6.44 | 10.9 | 12.65 | 7.38 |
| 1.16 | 0.14 | 0.86 | 12.15 | 19.95 | 7.76 | 0.97 | 4.35 | 3 | 7.13 | 4.81 |
| 0.19 | 0.09 | 0.27 | 1.4 | 0.62 | 2.29 | 0.29 | 1.16 | 0.85 | 2.6 | 1.96 |
| 0.05 | 0.02 | 0.4 | 2.23 | 3.81 | 2.69 | 0.2 | 0.56 | 0.06 | 1.27 | 0.7 |
| 2.16 | 0.89 | 9.53 | 3.84 | 1.6 | 5.11 | 8.91 | 6.94 | 5.49 | 2.41 | 5.56 |
| 0.09 | 0.08 | 0.42 | 0.48 | 0.35 | 0.47 | 1.24 | 1.18 | 1.4 | 1.4 | 0.71 |
| 0.03 | 0.01 | 0.03 | 0.15 | 0.11 | 0.2 | 0.08 | 0.15 | 0.05 | 0.31 | 0.16 |
| 0.07 | 0.06 | 0.31 | 0.24 | 0.23 | 0.28 | 0.43 | 0.37 | 1.11 | 0.3 | 0.11 |
| 0.31 | 0.05 | 0.17 | 3.07 | 4.28 | 1.99 | 0.47 | 1.37 | 0.59 | 2.13 | 1.61 |
| 1.59 | 0.56 | 2.34 | 1.44 | 2.05 | 0.56 | 2.8 | 3.37 | 2.38 | 0.7 | 2.05 |
| 17 | 1.09 | 2.96 | 10.8 | 14.25 | 8.17 | 3.86 | 5.94 | 4.49 | 9.37 | 7.07 |
| 91.4 | 98.4 | 99.7 | 97.8 | 96.7 | 99.6 | 98 | 95.9 | 98.9 | 101.5 | 98 |
| 236 | 124 | 2080 | 705 | 438 | 1790 | 300 | 194.5 | 445 | 324 | 248 |
| 43.1 | 49.4 | 179 | 191 | 159.5 | 210 | 59.7 | 47.8 | 66.7 | 34.2 | 19.7 |
| 0.91 | 1.23 | 2.91 | 3.31 | 2.62 | 3.66 | 2.01 | 1.92 | 2.71 | 1.83 | 0.78 |
| 10 | 30 | 20 | 10 | 10 | 10 | 10 | 6 | 6 | 10 | 50 |
| 42.7 | 23.7 | 172.5 | 98.4 | 49.5 | 110 | 154.5 | 111.5 | 118.5 | 70.1 | 127.5 |
| 82 | 36.5 | 384 | 663 | 1045 | 1145 | 129 | 110.5 | 318 | 122 | 78.2 |
| 3 | 1 | 1 | 1 | 1 | 1 | 2 | 1 | 3 | 1 | 1 |
| 82 | 36.5 | 384 | 663 | 1045 | 1145 | 129 | 110.5 | 318 | 122 | 78.2 |
| 4.28 | 1.81 | 20.4 | 20.1 | 16.8 | 20.6 | 2.46 | 1.82 | 2.59 | 1.2 | 0.86 |
| 1.26 | 3.64 | 9.08 | 6.45 | 4.91 | 5.61 | 3.19 | 0.67 | 1.75 | 0.43 | 0.26 |
| 51 | 260 | 147 | 206 | 334 | 178 | 142 | 188 | 497 | 136 | 220 |
| 2 | 3 | 10 | 9 | 11 | 11 | 47 | 17 | 48 | 9 | 8 |
| 6.7 | 6.7 | 26 | 29.1 | 22.4 | 31.6 | 41.7 | 37.1 | 55.3 | 34.3 | 15.2 |
| 110 | 30 | 287 | 284 | 237 | 307 | 253 | 226 | 258 | 169 | 108 |
| >250 | 223 | 600 | 700 | 300 | 223 | 1900 | 14600 | 5500 | >250 | >250 |
| 120 | 10.6 | 3.14 | 2.97 | 6.35 | 1.995 | 7.04 | 5.41 | 6.64 | 1.29 | 1.895 |
| 1.29 | 0.3 | 0.88 | 0.56 | 0.46 | 0.62 | 0.16 | 0.05 | 0.06 | 0.04 | 0.06 |
| >25.0 | 170 | 2.28 | 1.385 | 50 | 0.741 | 7.96 | 0.372 | 0.594 | >25.0 | >25.0 |
| >250 | 41.1 | 3.76 | 6.3 | 7.1 | 2.57 | 7.62 | 15.35 | 14.25 | 3.41 | 24 |
| 107 | 2.7 | 3.2 | 2.6 | 3.7 | 1.4 | 5.1 | 5.8 | 4.3 | 1.2 | 3.5 |
| >250 | 117.5 | 1.99 | 5.97 | 24.1 | 0.66 | 6.47 | 0.99 | 0.75 | 12.65 | 11.85 |
| 3580 | 44.6 | 2.6 | 5.7 | 4.2 | 2.1 | 2.2 | 1.1 | 2.7 | 4.4 | 2.5 |
| 7920 | 125 | 31 | 22 | 25 | 22 | 124 | 67 | 89 | 38 | 70 |
| 29 | 175 | 103 | 11 | 42 | 4 | 13 | 8 | 81 | 12 | 1 |
| 3 | 6 | 5 | 3 | 3 | 2 | 6 | 1 | 8 | 7 | 48 |
| 22 | 35 | 49 | 23 | 17 | 29 | 69 | 17 | 50 | 3 | 6 |
| 1040 | 38 | 53 | 54 | 17 | 119 | 201 | 24 | 87 | 101 | 71 |

| D0003<br>74 | D0235<br>42 | D0392<br>78 | D0393<br>28 | D0003<br>51 | 56626<br>0 | 56629<br>2 | D0057<br>42 | D0058<br>85 | D0094<br>78 | D0057<br>31 |
|---|---|---|---|---|---|---|---|---|---|---|
| 57.6 | 53.3 | 58.2 | 57.2 | 53.2 | 56.8 | 53.4 | 57.8 | 56.3 | 56.6 | 57.2 |
| 16.2 | 15.15 | 14.3 | 14.95 | 13.8 | 14.7 | 14.9 | 15.8 | 15.5 | 15.7 | 15.65 |
| 4.78 | 4.17 | 4.46 | 5.59 | 4.79 | 4.54 | 4.77 | 5.55 | 4.44 | 5.28 | 5.36 |
| 3.97 | 7.82 | 3.24 | 3.88 | 7.63 | 3.42 | 5.38 | 5.04 | 5.88 | 3.8 | 4.32 |
| 0.59 | 0.57 | 0.96 | 1.04 | 0.86 | 1.22 | 1.55 | 1.5 | 1.13 | 1.56 | 1.92 |
| 0.51 | 0.51 | 1.6 | 1.72 | 0.7 | 1.45 | 0.59 | 4.96 | 4.21 | 5.22 | 5.5 |
| 11.65 | 10.65 | 9.09 | 9.56 | 10.35 | 9.87 | 11.95 | 4.97 | 4.65 | 4.07 | 3.92 |
| 0.54 | 0.5 | 0.44 | 0.5 | 0.45 | 0.47 | 0.48 | 0.61 | 0.53 | 0.56 | 0.59 |
| 0.14 | 0.13 | 0.15 | 0.23 | 0.16 | 0.13 | 0.18 | 0.13 | 0.13 | 0.12 | 0.15 |
| 0.28 | 0.27 | 0.27 | 0.3 | 0.26 | 0.26 | 0.29 | 0.37 | 0.28 | 0.31 | 0.38 |
| 1.13 | 1.67 | 1.15 | 1.45 | 1.82 | 1.25 | 1.7 | 0.92 | 1.66 | 0.65 | 1.46 |
| 1.04 | 1.68 | 0.69 | 0.89 | 1.49 | 0.49 | 1.57 | 0.23 | 0.14 | 0.04 | 0.04 |
| 4.28 | 5.56 | 4.34 | 4.9 | 2.69 | 3.6 | 4.38 | 4.38 | 6.71 | 3.2 | 5.81 |
| 101 | 99 | 97.5 | 100.5 | 95.2 | 96.8 | 98.2 | 101.5 | 100 | 97 | 101.5 |
| 1415 | 1880 | 2890 | 2360 | 1810 | 2380 | 1770 | 2910 | 2130 | 3240 | 2870 |
| 240 | 203 | 204 | 221 | 193 | 202 | 212 | 242 | 231 | 246 | 243 |
| 4.06 | 4.09 | 3.57 | 3.88 | 3.8 | 3.87 | 3.95 | 4.29 | 4.01 | 4.31 | 4.32 |
| 10 | 10 | 10 | 10 | 10 | 10 | 10 | 10 | 10 | 10 | 10 |
| 223 | 189 | 176.5 | 179.5 | 171 | 182.5 | 180 | 102 | 122 | 97 | 101 |
| 461 | 1005 | 772 | 1135 | 706 | 628 | 511 | 2150 | 1075 | 1730 | 1420 |
| 1 | 3 | 1 | 1 | 1 | 1 | 1 | 2 | 2 | 2 | 2 |
| 461 | 1005 | 772 | 1135 | 706 | 628 | 511 | 2150 | 1075 | 1730 | 1420 |
| 25.1 | 21.4 | 21.7 | 23.3 | 19.85 | 21.1 | 22.7 | 23.3 | 23.1 | 23.6 | 23.9 |
| 6.46 | 5.73 | 6.05 | 7.66 | 4.33 | 5.64 | 6.5 | 6.47 | 6.24 | 6.33 | 6.39 |
| 163 | 97 | 124 | 219 | 67 | 105 | 105 | 170 | 145 | 154 | 160 |
| 15 | 10 | 10 | 17 | 9 | 8 | 9 | 4 | 7 | 2 | 4 |
| 32.2 | 28.9 | 29.2 | 32.3 | 27.6 | 27.3 | 28.2 | 34.7 | 33.6 | 35.1 | 33.9 |
| 345 | 332 | 315 | 316 | 307 | 334 | 342 | 335 | 331 | 345 | 330 |
| 400 | 400 | 172 | 300 | >250 | 180 | >250 | 67.5 | 25.4 | 10.5 | 15.4 |
| 1.565 | 2.16 | 1.61 | 2.93 | 2.72 | 1.51 | 2.5 | 0.555 | 0.014 | 0.003 | 0.003 |
| 0.73 | 1.12 | 0.66 | 0.52 | 0.89 | 0.24 | 0.93 | 0.74 | 0.53 | 0.43 | 0.65 |
| 1.66 | 1.27 | 0.722 | 0.862 | 1.34 | 5.55 | 5.04 | 0.886 | 0.114 | 0.059 | 0.128 |
| 3.77 | 2.41 | 2.23 | 4.3 | 2.9 | 1.91 | 4.15 | 2.75 | 0.69 | 1.34 | 0.95 |
| 1.4 | 1.7 | 1.2 | 1.6 | 2 | 1.1 | 2.1 | 1.2 | 0.7 | 0.9 | 0.7 |
| 0.8 | 0.68 | 0.48 | 0.95 | 2.14 | 0.68 | 0.93 | 0.62 | 0.04 | 0.006 | 0.01 |
| 1.3 | 1.9 | 1.4 | 2.3 | 2.5 | 1.5 | 1.6 | 3.3 | 1.4 | 2.2 | 2.1 |
| 31 | 20 | 32 | 23 | 40 | 30 | 29 | 27 | 28 | 16 | 30 |
| 4 | 6 | 11 | 2 | 30 | 5 | 25 | 1 | 0.6 | 0.6 | 0.6 |
| 5 | 5 | 3 | 5 | 8 | 6 | 7 | 5 | 2 | 4 | 5 |
| 32 | 35 | 39 | 38 | 43 | 35 | 33 | 85 | 30 | 40 | 72 |
| 60 | 34 | 59 | 72 | 40 | 59 | 94 | 102 | 54 | 116 | 73 |

| D012839 | D047379 | 144192 | D023338 | D047124 | D010720 | D045826 | D038094 | 01-B | D023348 | 03-A |
|---|---|---|---|---|---|---|---|---|---|---|
| 57.4 | 60.7 | 54.6 | 56.1 | 55.1 | 57.4 | 61 | 62.3 | 60.2 | 56.9 | 58.61 |
| 15.45 | 13.5 | 14.85 | 15.4 | 16.8 | 14.15 | 17.75 | 17.3 | 18.4 | 16.05 | 16.74 |
| 4.97 | 4.12 | 5.12 | 4.8 | 5.16 | 4.55 | 4.9 | 4.57 | 5.55 | 5.03 | 5.41 |
| 4.09 | 6.22 | 4.21 | 3.84 | 4.8 | 4.18 | 2.34 | 0.89 | 0.49 | 4.45 | 3.14 |
| 1.55 | 1.19 | 1.92 | 1.4 | 1.88 | 0.77 | 0.77 | 0.48 | 0.55 | 1.14 | 1.66 |
| 5.44 | 4.63 | 5.38 | 5.07 | 5.05 | 3.47 | 4.38 | 4.5 | 4.44 | 5.46 | 5.47 |
| 3.99 | 3.51 | 4.5 | 4.59 | 4.47 | 4.97 | 5.15 | 7.18 | 7.38 | 3.87 | 5.22 |
| 0.55 | 0.45 | 0.55 | 0.51 | 0.51 | 0.48 | 0.61 | 0.5 | 0.58 | 0.56 | 0.57 |
| 0.12 | 0.12 | 0.13 | 0.15 | 0.08 | 0.12 | 0.03 | 0.05 | 0.08 | 0.13 | 0.09 |
| 0.29 | 0.22 | 0.35 | 0.3 | 0.29 | 0.26 | 0.37 | 0.17 | 0.34 | 0.3 | 0.34 |
| 0.83 | 1.43 | 1.53 | 1.5 | 1.2 | 1.38 | 0.45 | 0.54 | | 0.94 | |
| 0.03 | 0.19 | 0.03 | 0.03 | 0.14 | 0.25 | 0.12 | 0.07 | | 0.04 | |
| 3.65 | 5.89 | 4.76 | 5.15 | 5.53 | 5.19 | 3.09 | 2.5 | 1.5 | 3.97 | 2 |
| 98 | 101 | 96.8 | 97.7 | 100 | 95.8 | 100.5 | 100.5 | 99.5 | 98.4 | 99.22 |
| 3230 | 4710 | 2520 | 1875 | 2300 | 2060 | 2000 | 2100 | 2443 | 2820 | 3109 |
| 237 | 196.5 | 234 | 231 | 237 | 228 | 272 | 243 | 259 | 246 | 239.1 |
| 4.17 | 3.55 | 4.22 | 4.51 | 3.99 | 3.91 | 4.46 | 3.81 | 4.35 | 4.27 | 4.13 |
| 10 | 10 | 10 | 10 | 10 | 10 | 10 | 10 | | 10 | |
| 95 | 84 | 104 | 112 | 93.5 | 140 | 138.5 | 161.5 | 168 | 99.3 | 137.6 |
| 1595 | 1450 | 1430 | 1085 | 1240 | 728 | 551 | 478 | 581 | 1660 | 2258 |
| 2 | 1 | 2 | 2 | 2 | 1 | 2 | 2 | 2 | 2 | 2 |
| 1595 | 1450 | 1430 | 1085 | 1240 | 728 | 551 | 478 | 581 | 1660 | 2258 |
| 23 | 20.6 | 23.5 | 23.7 | 24.3 | 23.1 | 27.2 | 21.9 | 28.8 | 24.4 | 25.9 |
| 6.16 | 5.84 | 6.14 | 6.21 | 6.83 | 6.12 | 7.81 | 5.85 | 5.4 | 6.82 | 6.7 |
| 147 | 113 | 114 | 96 | 149 | 136 | 143 | 122 | 143 | 151 | 115 |
| 2 | 6 | 2 | 3 | 6 | 7 | 5 | 7 | 13 | 2 | 0.9 |
| 34.7 | 31.5 | 32.4 | 33.3 | 32.9 | 30.4 | 36.4 | 30.5 | 33.2 | 35.6 | 33.5 |
| 338 | 284 | 311 | 380 | 342 | 320 | 370 | 388 | 377 | 345 | 368.5 |
| 11.1 | 8.8 | 15.4 | 7.6 | 15 | 47.5 | 16.8 | 21.1 | 92.2 | 5.6 | 12.6 |
| 0.003 | 0.01 | 0.003 | 0.003 | 0.006 | 1.735 | 0.012 | 0.017 | 0.48 | 0.005 | 0.022 |
| 0.39 | 0.51 | 0.66 | 0.19 | 0.23 | 1.43 | 0.59 | 0.69 | 0.8 | 0.44 | 0.4 |
| 0.032 | 0.094 | 0.161 | 4.76 | 0.116 | 50 | 0.128 | 0.217 | 1.14 | 0.053 | 0.05 |
| 0.74 | 0.76 | 2.8 | 0.83 | 0.7 | 1.9 | 2.86 | 1.31 | 1.6 | 1 | 1.6 |
| 0.6 | 0.6 | 0.7 | 0.6 | 0.6 | 1.5 | 0.7 | 0.7 | 0.3 | 0.6 | 0.3 |
| 0.01 | 0.03 | 0.01 | 0.23 | 0.03 | 22.3 | 0.006 | 0.02 | | 0.01 | |
| 1.7 | 1.9 | 1.8 | 1.4 | 1.6 | 4.8 | 0.8 | 0.8 | 0.3 | 2 | 0.06 |
| 21 | 18 | 35 | 27 | 17 | 29 | 30 | 23 | 27.8 | 15 | 22.8 |
| 0.6 | 0.6 | 0.6 | 1 | 0.6 | 111 | 0.6 | 0.6 | 1.5 | 0.6 | 1.6 |
| 2 | 3 | 4 | 6 | 4 | 6 | 6 | 4 | 5.4 | 4 | 6.4 |
| 41 | 29 | 30 | 27 | 19 | 28 | 26 | 43 | 38.2 | 40 | 28.3 |
| 99 | 81 | 65 | 84 | 105 | 73 | 60 | 89 | 41 | 90 | 61 |

| D034717 | D010576 | D048108 | D048158 | D035064 | D023192 | 05-A | 04-C |
|---|---|---|---|---|---|---|---|
| 59.4 | 59.7 | 55.5 | 60.4 | 56.2 | 57 | 75.57 | 59.6 |
| 18.3 | 12.15 | 12.85 | 15.75 | 16.1 | 17.65 | 11.75 | 20.5 |
| 4.59 | 8.49 | 8.81 | 7.63 | 11.3 | 7.26 | 1.93 | 4.31 |
| 0.81 | 2.36 | 5.21 | 1.52 | 1.74 | 2.88 | 0.95 | 0.48 |
| 0.37 | 0.92 | 1.05 | 4.23 | 2.34 | 2.47 | 0.33 | 0.56 |
| 5.37 | 0.51 | 3.69 | 0.87 | 0.69 | 4.68 | 3.31 | 4.39 |
| 5.27 | 3.95 | 2.07 | 2.78 | 3.45 | 2.91 | 3.01 | 6.85 |
| 0.54 | 1.29 | 1.27 | 0.62 | 0.7 | 0.83 | 1.03 | 0.63 |
| 0.07 | 0.14 | 0.16 | 0.04 | 0.2 | 0.09 | 0.03 | 0.02 |
| 0.16 | 0.41 | 0.41 | 0.2 | 0.23 | 0.13 | 0.39 | 0.33 |
| 0.32 | 1.21 | 1.8 | 0.4 | 0.59 | 0.62 | | |
| 0.03 | 1 | 0.27 | 0.17 | 0.78 | 0.39 | | |
| 1.1 | 5.13 | 5.93 | 3.96 | 4.4 | 3.67 | 1.6 | 2 |
| 96.3 | 95.1 | 97 | 98.1 | 97.5 | 99.7 | 99.92 | 99.6 |
| 1855 | 221 | 150 | 569 | 672 | 604 | 166 | 1928 |
| 232 | 65.6 | 71.3 | 61.5 | 142.5 | 22.3 | 56.4 | 251 |
| 4.06 | 2.16 | 2.37 | 1.15 | 2.9 | 0.89 | 1.75 | 4.01 |
| 10 | 6 | 6 | 450 | 390 | 70 | | |
| 140 | 138.5 | 74.3 | 94.4 | 86.9 | 80.4 | 75 | 193 |
| 567 | 121 | 308 | 185 | 110 | 373 | 150.5 | 474 |
| 2 | 2 | 3 | 1 | 1 | 1 | 3 | 2 |
| 567 | 121 | 308 | 185 | 110 | 373 | 150.5 | 474 |
| 20.3 | 2.51 | 2.59 | 6.01 | 13.3 | 1.01 | 2.5 | 31.7 |
| 4.87 | 0.93 | 0.64 | 1.84 | 3.55 | 0.49 | 1.9 | 5.4 |
| 85 | 228 | 101 | 179 | 140 | 138 | 49 | 134 |
| 2 | 17 | 12 | 3 | 5 | 5 | 3.7 | 7.3 |
| 27.9 | 49 | 51.3 | 13.9 | 29 | 15.9 | 36.3 | 28.2 |
| 412 | 268 | 270 | 118 | 262 | 112 | 244.2 | 411 |
| 8.1 | 300 | 39.4 | 68.4 | 300 | 22.2 | 15.1 | 10.6 |
| 0.003 | 3.21 | 0.008 | 0.008 | 0.344 | 0.008 | 0.0061 | 0 |
| 0.33 | 0.06 | 0.07 | 0.29 | 1.62 | 0.18 | 0.1 | 0.5 |
| 0.318 | 0.927 | 0.083 | 0.08 | 0.296 | 7.92 | 0.12 | 0.03 |
| 0.79 | 5.12 | 1.08 | 2.13 | 5.67 | 0.81 | 7 | 0.5 |
| 0.5 | 1.4 | 0.6 | 0.4 | 1.1 | 0.4 | 0.3 | 0.3 |
| 0.006 | 0.38 | 0.006 | 0.04 | 0.35 | 0.48 | | |
| 0.8 | 0.9 | 0.3 | 0.3 | 0.3 | 0.6 | 0.3 | 0.06 |
| 19 | 82 | 88 | 51 | 74 | 9 | 78.7 | 6 |
| 0.6 | 6 | 1 | 1 | 2 | 5 | 1 | 0.8 |
| 5 | 4 | 3 | 222 | 202 | 37 | 1.5 | 2.3 |
| 30 | 7 | 2 | 16 | 15 | 4 | 7.7 | 21.1 |
| 105 | 120 | 119 | 91 | 86 | 92 | 26 | 49 |

# APPENDICE B

# MODÉLISATION 3D DANS LE GISEMENT DE BEATTIE

**Introduction**

La modélisation 3D apparait comme un outil incontournable pour la visualisation de différents paramètres, notamment la minéralisation, l'altération, la structure, et la lithologie. Le logiciel Leapfrog 3D ® est un logiciel axé sur l'exploration minière. Il est développé par la société ARANZ Geo qui est une division de Applied Research Associated New Zealand Limited (ARANZ). L'intérêt de Leapfrog 3D, en comparaison avec ses compétiteurs directs tel que gOcad notamment, est la facilité et la rapidité des traitements de modélisation 3D.

Dans le gisement de Beattie, de nombreux paramètres semblent influencer la minéralisation, qu'ils soient structuraux, lithologiques, ou géochimiques. Notre intérêt est de visualiser les relations, mais aussi d'utiliser le logiciel à son plein potentiel pour mettre en évidence des composantes non visibles initialement. En appliquant par exemple un poids à une faille, elle va influencer selon la valeur du poids la quantité de déformation dans le gisement. Ces outils permettent l'affinement du modèle. D'autres paramètres pertinents sont les calculs des volumes, ou encore la possibilité de réaliser des films à partir du modèle 3D.

**Méthode**

L'importation de données se fait à partir de tableur excel convertit en format CSV. Trois tables essentielles sont à integrer pour la réalisation d'un modèle de base, *collar* (holeID, x, y, z, max depth), *survey* (holeID, depth, dip, azimuth), et *assay* (holeID, from, to, assay) (Figure 1).

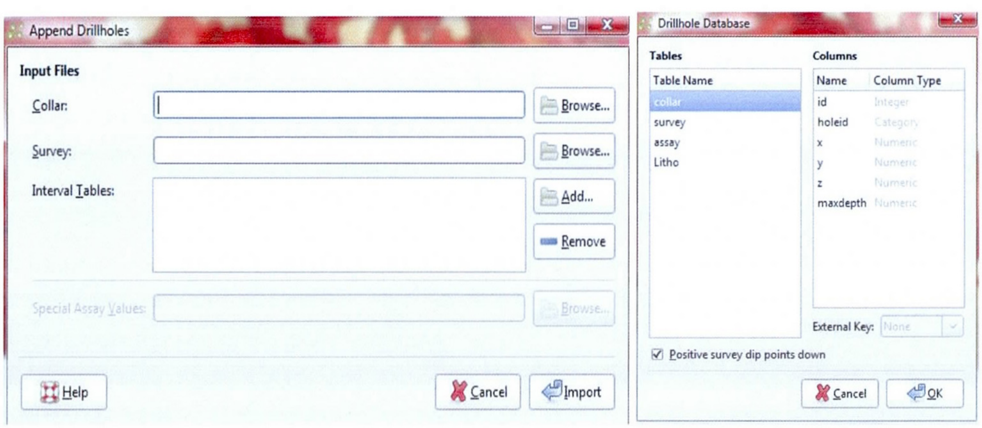

**Figure 1.** Importation de la base de données

Une fois la base de données importée, les forages sont immédiatement visualisable (Figure 2).

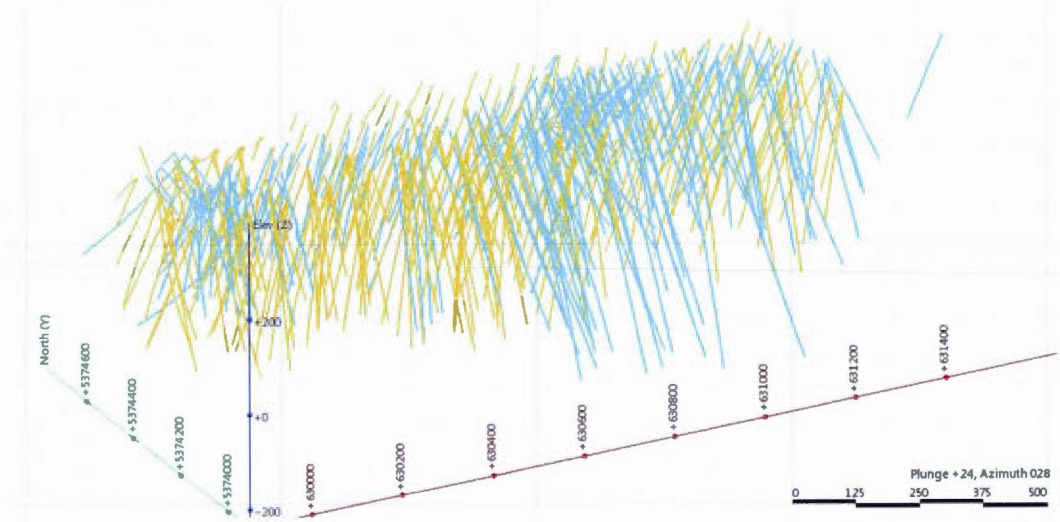


**Figure 2.** Visualisation des forages

Des domaines qui définissent la zone d'influence des forages doivent être déterminés par l'utilisateur. De cette valeur dépend la forme et le volume des corps qui vont être créées. La figure 3 présente que le domaine est contraint sous la surface et la zone d'influence des forages s'étend à 100m au maximum. Il s'agit du domaine que nous avons choisi pour réaliser l'étude.

A

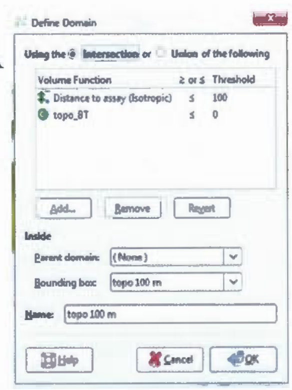


B

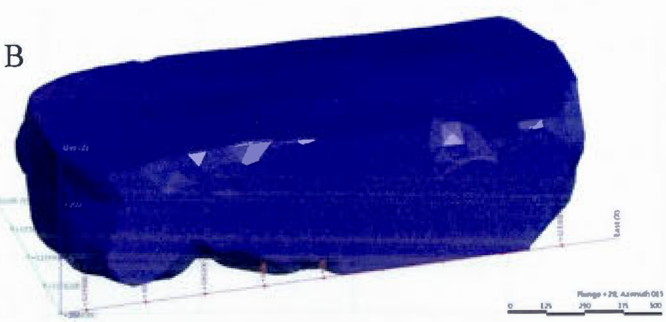

**Figure 3**. (a) Définition du domaine d'étude et du champ d'influence des forages. (b) visualisation du champ d'influence.

Après la définition du domaine d'étude, les volumes sont intégrés et rendu visibles : Les altérations, les zones minéralisées en fonction de la teneur donnée, et les lithologies (Figure 4,5,6).

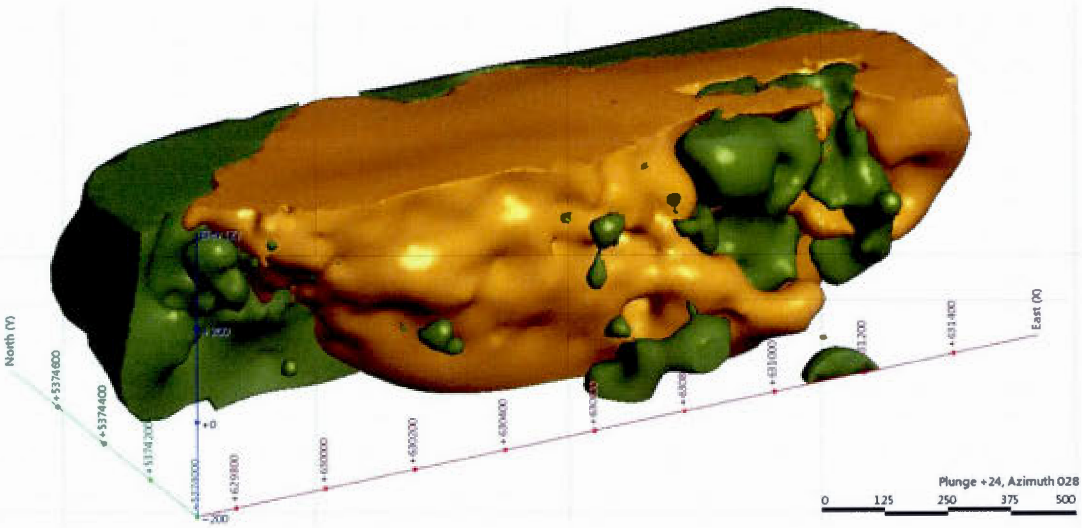


**Figure 1.** Lithologies : volcanites du Kinojévis en vert, et la syénite de Beattie en orange.

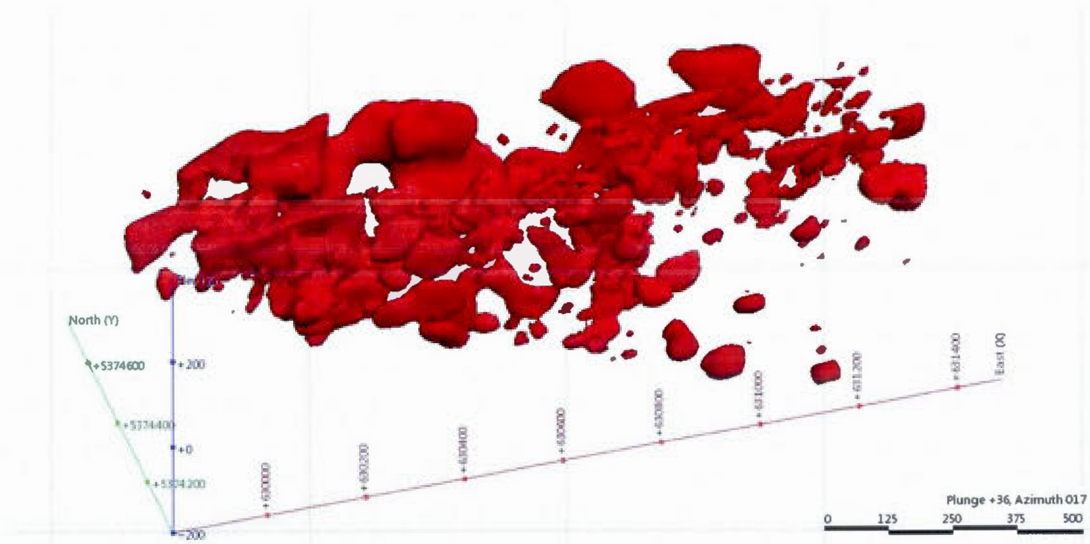


**Figure 2.** Zones minéralisées pour une teneur de 0.67g/t Au.

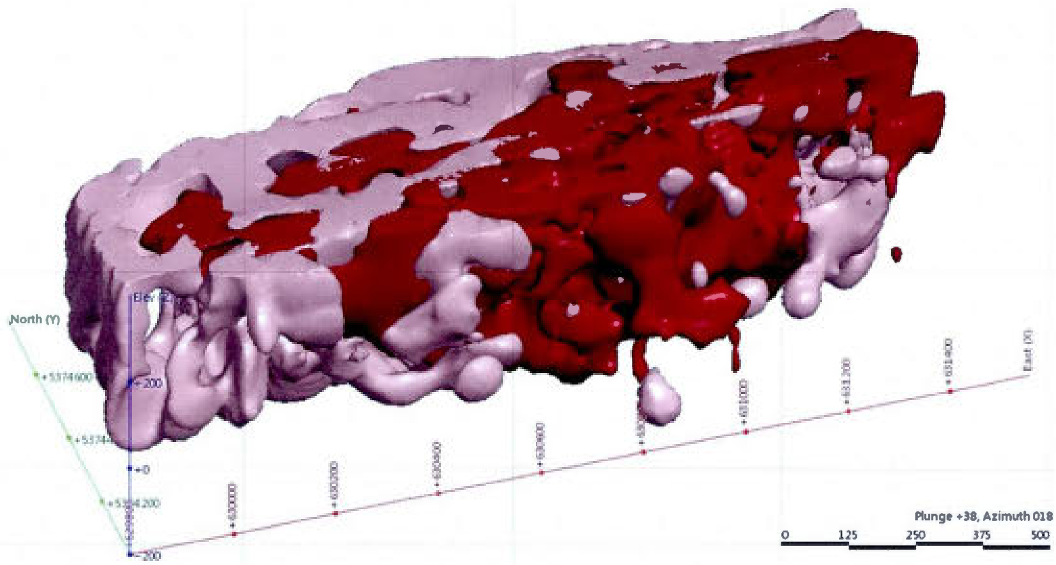


**Figure 3.** Zones d'altération : carbonatation en rose, hématisation en rouge vin.

Un module de dessin est intégré dans le logiciel. De nombreux objets structuraux peuvent ainsi être dessinés, notamment les failles (Figure 7). Il s'agit d'une interprétation en profondeur de la géologie en surface. Un moyen plus précis pour intégrer la structure est d'avoir une base de données de la structure à partir des forages. Il s'agit d'une base de données similaire à *assay* avec l'information sur la structure à chaque intervalle.

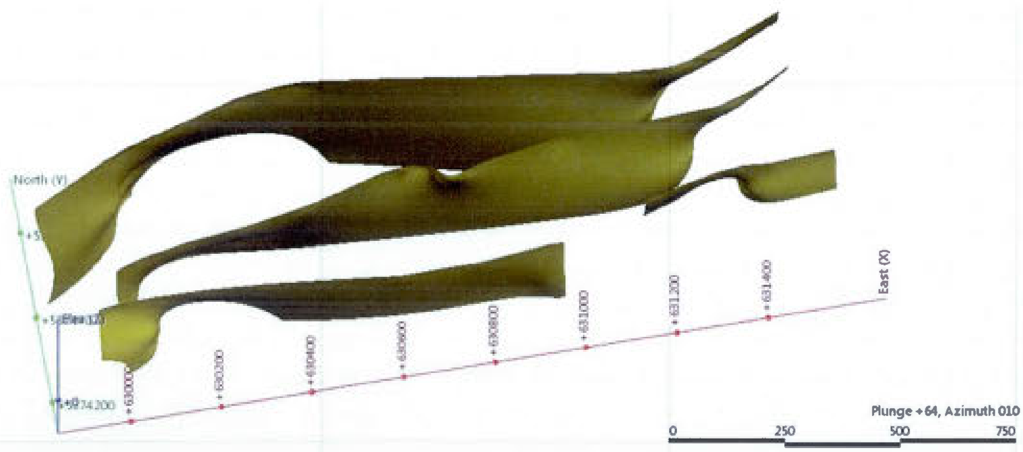


**Figure 4.** Système de failles dessiné à partir de la géologie de surface.

Lorsque la structure est dessinée, il est possible d'affiner le modèle 3D en le soumettant à l'influence d'une faille. Un poids et une zone d'influence va être donné à chaque faille (Figure 8a). La déformation sera d'autant plus intense qu'un corps est proche de la zone de faille (Figure 8b).

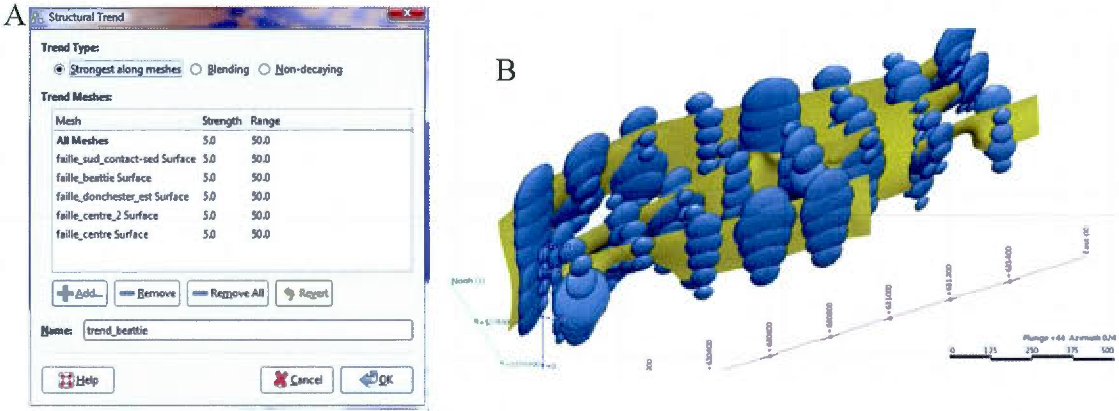


**Figure 8.** Structural trend, zone d'influence de chaque faille. (a) Définition du control structural – réglage des paramètres. (b) Visualisation de l'intensité de la déformation de long des failles.

Il est possible de définir des sous-domaines pour faire du traitement de données plus précis. Pour prendre un exemple, on veut connaitre le volume de l'altération à carbonate à l'extérieur de la syénite (Figure 9).

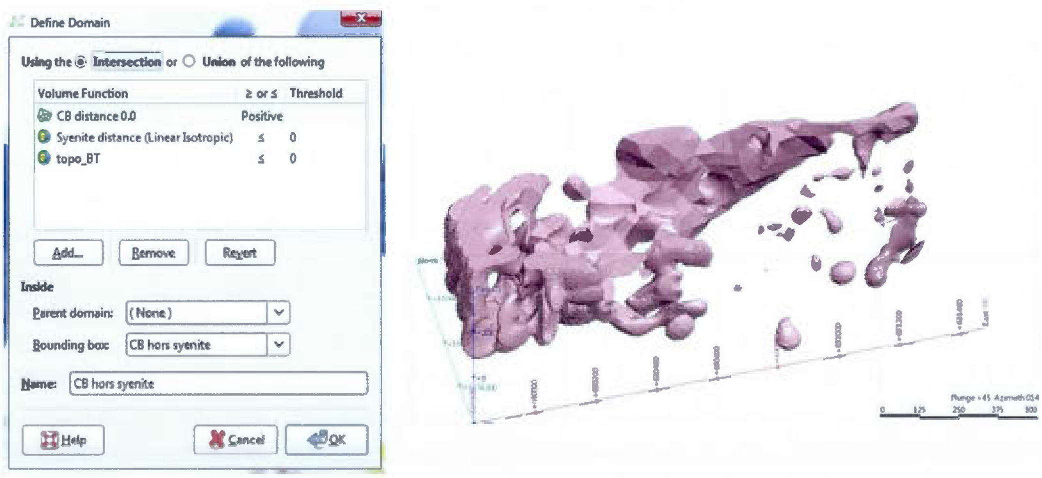


**Figure 9.** Sous domaine de carbonatation à l'extérieur de la syénite.

La phase ultime du traitement du modèle 3D est l'exportation d'image et de vidéo. Cette application est très intéressante dans le cadre de présentation du projet. Une vidéo du modèle 3D du gisement de Beattie est disponible. Pour l'obtenir, veuillez contacter l'auteur à l'adresse suivante : ludovic.bigot@gmail.com

# APPENDICE C

# ANALYSE DES BRÈCHES DU GISEMENT DE BEATTIE

## Introduction

Les brèches sont des objets géologiques qui sont communément présent dans les gisements. Elles sont présentent aussi bien dans les gisements magmatiques (Porphyres, épithermaux, IOCG), profonds et superficiels, que dans les gisements hydrothermaux (veines et shear zones), ou encore dans les gisements sédimentaires (MVT). La propagation des fluides à l'origine de la bréchification sont très variées (Jébrak, 1997): hydraulique, tectonique, explosion, et décompression. En association à ces processus de fracturation, la mobilité des fragments résulte de différents mécanismes: le broyage, l'effondrement, la fluidisation, et la dissolution.

## Méthode

Jébrak (1997) propose une classification des brèches selon deux paramètres principaux, la description des clastes et du ciment, et la description générale de l'organisation de la brèche. Des paramètres non-dimensionnels sont nécessaires pour décrire la brèche (Figure 1), tels que la nature des clastes, l'espacement entre les clastes, la présence d'une fabrique, la distribution des particules, et la circularité ou complexité du claste.

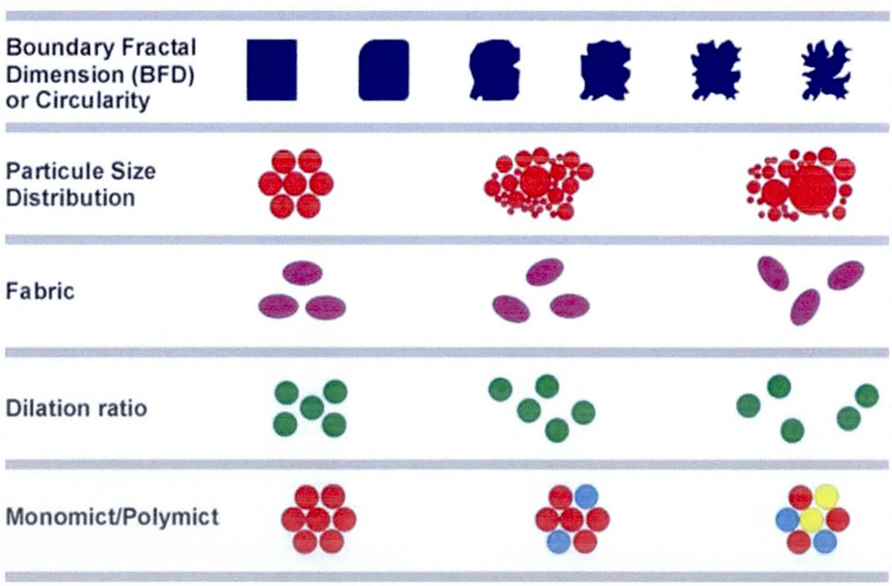


**Figure 1.** Paramètres non-dimensionnelles pour la classification des brèches.

En connaissant cette méthode d'analyse, il faut un échantillon pour l'analyse. Cet échantillon est une brèche minéralisée d'une teneur de 6g/t Au (Figure 2; B08-78 ; 95.6m). Le traitement se fait par analyse d'image en utilisant le logiciel imageJ. Le traitement consiste en une séparation des fragments et de la matrice (Figure 3). Pour ce, le contraste et les couleurs sont retouchés. Puis le logiciel fait l'analyse des particules (résultats reportés dans le tableau.2). L'analyse se fait sur les fragments, et consiste-en des mesures de longueur, largeur, périmètre, et de circularité entre autres. Une fois l'analyse complète, l'image de brèche est observable sous forme de contour de fragments.

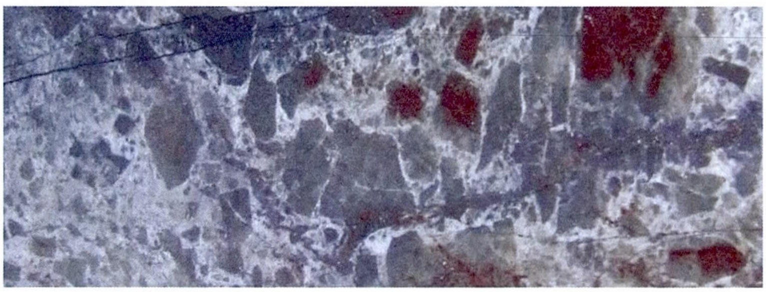

**Figure 2.** Brèche minéralisée du gisement de Beattie – exemple pour l'analyse.

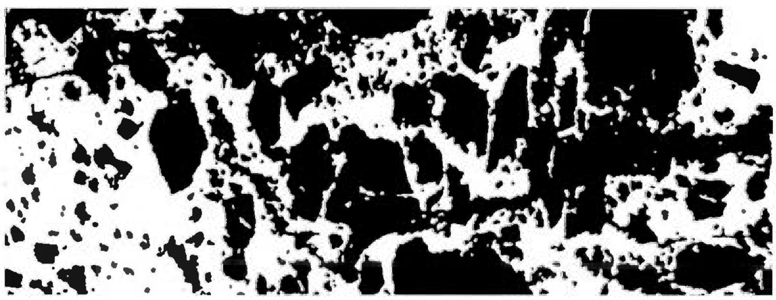

**Figure 3.** Image (Fig.2) retouchée pour l'analyse.

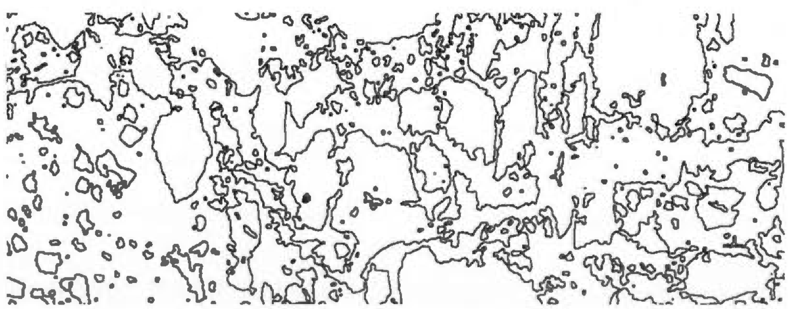

**Figure 4.** Contour des fragments isolés.

**Traitement des résultats de l'exemple de la brèche de Beattie**

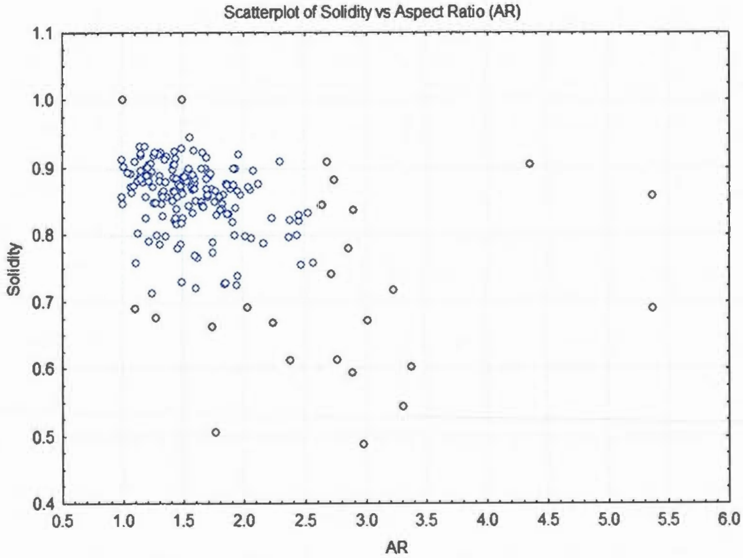


**Figure 5.** Solidité vs l'aspect ratio

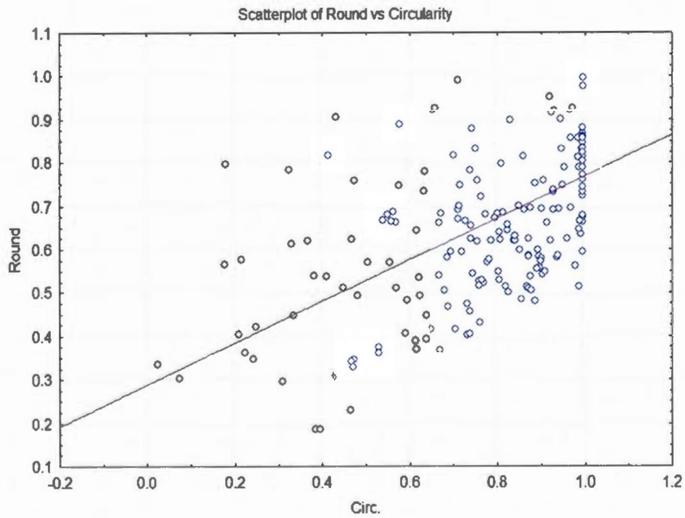


**Figure 6.** Arrondissement vs la circularité (complexité des fragments)

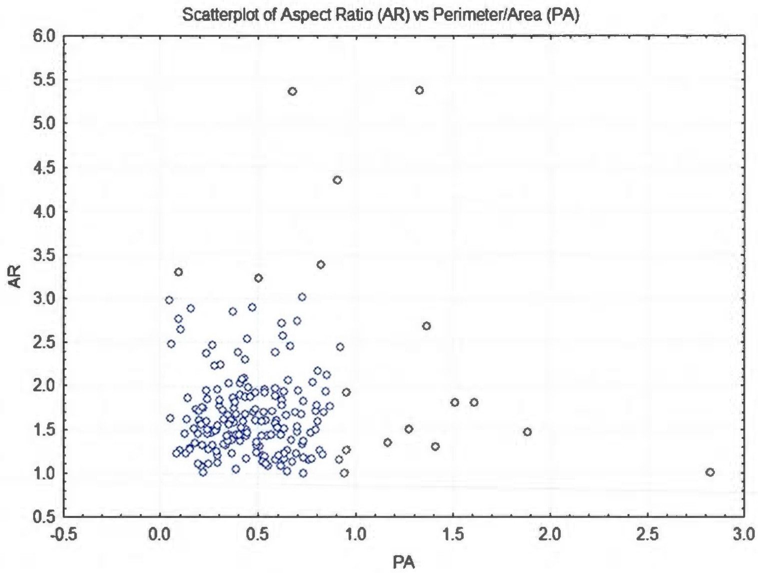


**Figure 5.** Aspect Ratio vs Périmètre/Surface

**Table 1.** Résultat de l'analyse de l'exemple de brèche à Beattie

| Parameter | Beattie breccia |
|---|---|
| Mono/Poly | Mono -syenite or volcanite |
| Dilatation Ratio | low to medium |
| Fabric Intensity | inherited to medium |
| Particles Size Distribution | normal - mm to cm |
| Aspect Ratio | medium - 1.66 |
| Solidity | 0.85 |
| Perimeter/Area | 0.59 |
| Circularity | low |

## Conclusions

Des paramètres de propagation hydraulique et tectonique peuvent être interprétés comme à l'origine de la fracturation de la roche. Pour la propagation hydraulique, la mobilité est très faible, considérée in-situ. Pour la propagation tectonique, la mobilité des clastes semble résulter du broyage étant donné la variation de la taille des fragments. La propagation hydraulique est nécessairement précoce, suivie par des processus tectonique. Les fluides auraient donc d'abord circulé dans les zones de faiblesse des failles Beattie, Donchester, et de la Fracture zone. Par la suite, les mouvements tectoniques sur ces mêmes failles auraient entrainé une seconde bréchification.

Résultats de l'analyse des fragments de brèche par ImageJ :

| | Area | Mean | Min | Max | X | Y | Perim. | Major | Minor | Angle | Circ. | AR | Round | Solidity | PA |
|---|---|---|---|---|---|---|---|---|---|---|---|---|---|---|---|
| 1 | 200690 | 255 | 255 | 255 | 649.396 | 168.18 | 10176.56 | 871.94 | 293.05 | 175.459 | 0.02 | 2.975 | 0.336 | 0.487 | 0.051 |
| 2 | 425 | 255 | 255 | 255 | 226.832 | 9.164 | 90.184 | 24.176 | 22.382 | 41.323 | 0.66 | 1.08 | 0.926 | 0.892 | 0.212 |
| 3 | 6 | 255 | 255 | 255 | 377 | 0.833 | 9.071 | 3.718 | 2.055 | 0 | 0.92 | 1.809 | 0.553 | 0.857 | 1.512 |
| 4 | 6456 | 255 | 255 | 255 | 752.638 | 40.277 | 673.879 | 101.53 | 80.964 | 21.58 | 0.18 | 1.254 | 0.797 | 0.714 | 0.104 |
| 5 | 6 | 255 | 255 | 255 | 725 | 0.833 | 9.071 | 3.718 | 2.055 | 0 | 0.92 | 1.809 | 0.553 | 0.857 | 1.512 |
| 6 | 25 | 255 | 255 | 255 | 734.98 | 1.58 | 21.314 | 8.227 | 3.869 | 173.87 | 0.69 | 2.127 | 0.47 | 0.877 | 0.853 |
| 7 | 324 | 255 | 255 | 255 | 833.29 | 7.722 | 86.426 | 24.791 | 16.64 | 144.717 | 0.55 | 1.49 | 0.671 | 0.787 | 0.267 |
| 8 | 21 | 255 | 255 | 255 | 859.643 | 2.167 | 15.899 | 5.538 | 4.828 | 140.392 | 1 | 1.147 | 0.872 | 0.933 | 0.757 |
| 9 | 951 | 255 | 255 | 255 | 1123.48 | 20.885 | 138.711 | 47.534 | 25.473 | 94.861 | 0.62 | 1.866 | 0.536 | 0.877 | 0.146 |
| 10 | 12 | 255 | 255 | 255 | 255 | 6 | 11.314 | 3.909 | 3.909 | 0 | 1 | 1 | 1 | 0.857 | 0.943 |
| 11 | 14 | 255 | 255 | 255 | 197.714 | 9.143 | 13.314 | 4.746 | 3.756 | 24.358 | 0.99 | 1.264 | 0.791 | 0.848 | 0.951 |
| 12 | 51 | 255 | 255 | 255 | 822.48 | 15.343 | 27.556 | 10.202 | 6.365 | 95.775 | 0.84 | 1.603 | 0.624 | 0.879 | 0.540 |
| 13 | 24 | 255 | 255 | 255 | 180.375 | 18.167 | 16.728 | 6.111 | 5.001 | 109.605 | 1 | 1.222 | 0.818 | 0.906 | 0.697 |
| 14 | 62 | 255 | 255 | 255 | 210.597 | 23.161 | 29.799 | 11.569 | 6.824 | 95.653 | 0.88 | 1.695 | 0.59 | 0.899 | 0.481 |
| 15 | 53 | 255 | 255 | 255 | 669.538 | 31.104 | 32.87 | 13.532 | 4.987 | 51.784 | 0.62 | 2.713 | 0.369 | 0.741 | 0.620 |
| 16 | 36 | 255 | 255 | 255 | 694.75 | 34.778 | 22.728 | 9.426 | 4.863 | 83.003 | 0.88 | 1.939 | 0.516 | 0.9 | 0.631 |
| 17 | 49 | 255 | 255 | 255 | 841.153 | 36.582 | 26.142 | 10.304 | 6.055 | 93.75 | 0.9 | 1.702 | 0.588 | 0.916 | 0.534 |
| 18 | 12 | 255 | 255 | 255 | 1086 | 35 | 11.314 | 3.909 | 3.909 | 0 | 1 | 1 | 1 | 0.857 | 0.943 |
| 19 | 366 | 255 | 255 | 255 | 653.396 | 51.309 | 91.154 | 26.104 | 17.852 | 115.612 | 0.55 | 1.462 | 0.684 | 0.78 | 0.249 |
| 20 | 746 | 255 | 255 | 255 | 672.763 | 69.582 | 229.907 | 41.004 | 23.164 | 68.165 | 0.18 | 1.77 | 0.565 | 0.506 | 0.308 |
| 21 | 246 | 255 | 255 | 255 | 1103.92 | 49.695 | 72.912 | 18.715 | 16.736 | 13.375 | 0.58 | 1.118 | 0.894 | 0.759 | 0.296 |
| 22 | 20 | 255 | 255 | 255 | 695.2 | 45 | 16.971 | 7.014 | 3.631 | 129.806 | 0.87 | 1.932 | 0.518 | 0.8 | 0.849 |
| 23 | 21 | 255 | 255 | 255 | 111.405 | 47.024 | 16.142 | 6.258 | 4.272 | 118.684 | 1 | 1.465 | 0.683 | 0.857 | 0.769 |
| 24 | 17 | 255 | 255 | 255 | 687.794 | 49.324 | 14.728 | 6.19 | 3.497 | 159.699 | 0.99 | 1.77 | 0.565 | 0.85 | 0.866 |
| 25 | 28 | 255 | 255 | 255 | 606.286 | 54 | 18.142 | 6.024 | 5.918 | 90 | 1 | 1.018 | 0.982 | 0.903 | 0.648 |
| 26 | 19 | 255 | 255 | 255 | 75.342 | 55.658 | 14.728 | 5.301 | 4.564 | 135 | 1 | 1.161 | 0.861 | 0.884 | 0.775 |
| 27 | 50 | 255 | 255 | 255 | 576.52 | 58.42 | 36.284 | 13.838 | 4.6 | 33.324 | 0.48 | 3.008 | 0.332 | 0.671 | 0.726 |
| 28 | 186 | 255 | 255 | 255 | 105.129 | 66.871 | 55.598 | 16.845 | 14.059 | 140.337 | 0.76 | 1.198 | 0.835 | 0.825 | 0.299 |
| 29 | 32 | 255 | 255 | 255 | 59.438 | 63.656 | 20.142 | 6.883 | 5.919 | 179.302 | 0.99 | 1.163 | 0.86 | 0.889 | 0.629 |
| 30 | 160 | 255 | 255 | 255 | 1185.98 | 71.888 | 56.77 | 20.318 | 10.026 | 89.619 | 0.62 | 2.026 | 0.493 | 0.798 | 0.355 |
| 31 | 21 | 255 | 255 | 255 | 82.595 | 65.119 | 16.728 | 6.763 | 3.954 | 119.62 | 0.94 | 1.711 | 0.585 | 0.857 | 0.797 |
| 32 | 110 | 255 | 255 | 255 | 632.955 | 70.218 | 42.042 | 15.612 | 8.971 | 82.686 | 0.78 | 1.74 | 0.575 | 0.87 | 0.382 |
| 33 | 26 | 255 | 255 | 255 | 689.577 | 66.538 | 18.142 | 7.134 | 4.64 | 69.548 | 0.99 | 1.537 | 0.65 | 0.881 | 0.698 |

| | | | | | | | | | | | | | | | |
|---|---|---|---|---|---|---|---|---|---|---|---|---|---|---|---|
| 34 | 111 | 255 | 255 | 255 | 595.05 | 72.086 | 49.355 | 14.549 | 9.714 | 85.571 | 0.57 | 1.498 | 0.668 | 0.73 | 0.445 |
| 35 | 122 | 255 | 255 | 255 | 578.221 | 74.025 | 41.456 | 14.334 | 10.836 | 83.864 | 0.89 | 1.323 | 0.756 | 0.924 | 0.340 |
| 36 | 39 | 255 | 255 | 255 | 711.423 | 73.192 | 25.799 | 11.055 | 4.492 | 125.168 | 0.74 | 2.461 | 0.406 | 0.821 | 0.662 |
| 37 | 33 | 255 | 255 | 255 | 1153.53 | 70.379 | 21.556 | 9.321 | 4.508 | 167.522 | 0.89 | 2.068 | 0.484 | 0.868 | 0.653 |
| 38 | 52 | 255 | 255 | 255 | 1105.23 | 77.615 | 32.627 | 13.05 | 5.073 | 99.676 | 0.61 | 2.572 | 0.389 | 0.759 | 0.627 |
| 39 | 31 | 255 | 255 | 255 | 1200.89 | 74.919 | 20.142 | 7.055 | 5.594 | 178.535 | 0.96 | 1.261 | 0.793 | 0.873 | 0.650 |
| 40 | 44 | 255 | 255 | 255 | 533.864 | 78.682 | 24.385 | 7.802 | 7.181 | 58.717 | 0.93 | 1.087 | 0.92 | 0.863 | 0.554 |
| 41 | 72 | 255 | 255 | 255 | 55.736 | 81.694 | 48.527 | 22.174 | 4.134 | 30.3 | 0.38 | 5.364 | 0.186 | 0.689 | 0.674 |
| 42 | 163 | 255 | 255 | 255 | 612.715 | 83.739 | 53.355 | 16.618 | 12.488 | 22.209 | 0.72 | 1.331 | 0.751 | 0.847 | 0.327 |
| 43 | 1956 | 255 | 255 | 255 | 1159.74 | 102.51 | 214.208 | 81.128 | 30.698 | 158.056 | 0.54 | 2.643 | 0.378 | 0.843 | 0.110 |
| 44 | 46 | 255 | 255 | 255 | 295.957 | 86.63 | 23.556 | 8.761 | 6.686 | 155.705 | 1 | 1.31 | 0.763 | 0.92 | 0.512 |
| 45 | 179 | 255 | 255 | 255 | 709.366 | 91.494 | 52.527 | 16.875 | 13.506 | 47.751 | 0.82 | 1.249 | 0.8 | 0.895 | 0.293 |
| 46 | 47 | 255 | 255 | 255 | 797.734 | 88.011 | 27.799 | 10.617 | 5.636 | 68.77 | 0.76 | 1.884 | 0.531 | 0.832 | 0.591 |
| 47 | 12 | 255 | 255 | 255 | 94 | 90 | 11.314 | 3.909 | 3.909 | 0 | 1 | 1 | 1 | 0.857 | 0.943 |
| 48 | 75 | 255 | 255 | 255 | 535.58 | 94.687 | 33.213 | 11.647 | 8.199 | 107.244 | 0.85 | 1.421 | 0.704 | 0.898 | 0.443 |
| 49 | 22 | 255 | 255 | 255 | 677.773 | 93 | 16.142 | 5.741 | 4.879 | 90 | 1 | 1.176 | 0.85 | 0.88 | 0.734 |
| 50 | 631 | 255 | 255 | 255 | 596.614 | 114.99 | 156.167 | 32.016 | 25.094 | 95.856 | 0.33 | 1.276 | 0.784 | 0.676 | 0.247 |
| 51 | 12 | 255 | 255 | 255 | 175 | 95 | 11.314 | 3.909 | 3.909 | 0 | 1 | 1 | 1 | 0.857 | 0.943 |
| 52 | 12 | 255 | 255 | 255 | 278 | 97 | 11.314 | 3.909 | 3.909 | 0 | 1 | 1 | 1 | 0.857 | 0.943 |
| 53 | 12297 | 255 | 255 | 255 | 698.546 | 155.66 | 683.394 | 159.87 | 97.936 | 163.107 | 0.33 | 1.632 | 0.613 | 0.766 | 0.056 |
| 54 | 203 | 255 | 255 | 255 | 772.224 | 104.75 | 59.012 | 19.642 | 13.159 | 22.844 | 0.73 | 1.493 | 0.67 | 0.864 | 0.291 |
| 55 | 111 | 255 | 255 | 255 | 660.662 | 104.43 | 39.213 | 14.239 | 9.926 | 55.82 | 0.91 | 1.435 | 0.697 | 0.925 | 0.353 |
| 56 | 28 | 255 | 255 | 255 | 638.714 | 102 | 18.142 | 6.024 | 5.918 | 90 | 1 | 1.018 | 0.982 | 0.903 | 0.648 |
| 57 | 552 | 255 | 255 | 255 | 569.205 | 120.94 | 134.953 | 36.1 | 19.469 | 110.21 | 0.38 | 1.854 | 0.539 | 0.728 | 0.244 |
| 58 | 292 | 255 | 255 | 255 | 183.51 | 115.03 | 70.184 | 24.32 | 15.287 | 93.698 | 0.75 | 1.591 | 0.629 | 0.868 | 0.240 |
| 59 | 122 | 255 | 255 | 255 | 322.385 | 107.34 | 42.284 | 16.047 | 9.68 | 141.919 | 0.86 | 1.658 | 0.603 | 0.9 | 0.347 |
| 60 | 115 | 255 | 255 | 255 | 348.561 | 112.34 | 57.941 | 21.729 | 6.738 | 92.538 | 0.43 | 3.225 | 0.31 | 0.717 | 0.504 |
| 61 | 25 | 255 | 255 | 255 | 580.42 | 106.18 | 18.142 | 6.511 | 4.889 | 177.444 | 0.95 | 1.332 | 0.751 | 0.862 | 0.726 |
| 62 | 78 | 255 | 255 | 255 | 292.577 | 114.74 | 34.87 | 12.035 | 8.252 | 173.8 | 0.81 | 1.458 | 0.686 | 0.839 | 0.447 |
| 63 | 663 | 255 | 255 | 255 | 106.934 | 129.04 | 120.368 | 33.64 | 25.094 | 133.481 | 0.58 | 1.341 | 0.746 | 0.829 | 0.182 |
| 64 | 35 | 255 | 255 | 255 | 1152.53 | 120.73 | 21.556 | 7.991 | 5.577 | 76.427 | 0.95 | 1.433 | 0.698 | 0.886 | 0.616 |
| 65 | 96 | 255 | 255 | 255 | 542.729 | 125.28 | 39.456 | 15.226 | 8.028 | 121.127 | 0.78 | 1.897 | 0.527 | 0.869 | 0.411 |
| 66 | 13 | 255 | 255 | 255 | 65.885 | 124.89 | 11.899 | 4.38 | 3.779 | 135 | 1 | 1.159 | 0.863 | 0.897 | 0.915 |
| 67 | 42 | 255 | 255 | 255 | 1105.86 | 127.07 | 24.971 | 9.26 | 5.775 | 79.012 | 0.85 | 1.603 | 0.624 | 0.884 | 0.595 |
| 68 | 229 | 255 | 255 | 255 | 1095.3 | 142.29 | 60.77 | 20.627 | 14.135 | 72.591 | 0.78 | 1.459 | 0.685 | 0.884 | 0.265 |
| 69 | 191 | 255 | 255 | 255 | 516.081 | 142.66 | 54.77 | 18.988 | 12.808 | 126.363 | 0.8 | 1.483 | 0.675 | 0.876 | 0.287 |
| 70 | 34 | 255 | 255 | 255 | 549.5 | 138.24 | 20.142 | 7.074 | 6.12 | ####### | 1 | 1.156 | 0.865 | 0.919 | 0.592 |
| 71 | 185 | 255 | 255 | 255 | 6.468 | 149.16 | 69.598 | 25.921 | 9.087 | 96.562 | 0.48 | 2.853 | 0.351 | 0.779 | 0.376 |
| 72 | 477 | 255 | 255 | 255 | 192.798 | 153.75 | 118.125 | 25.881 | 23.466 | 176.638 | 0.43 | 1.103 | 0.907 | 0.689 | 0.248 |

| | | | | | | | | | | | | | | | |
|---|---|---|---|---|---|---|---|---|---|---|---|---|---|---|---|
| 73 | 29 | 255 | 255 | 255 | 213.466 | 140.67 | 20.385 | 8.466 | 4.362 | 131.823 | 0.88 | 1.941 | 0.515 | 0.841 | 0.703 |
| 74 | 6 | 255 | 255 | 255 | 69 | 140.5 | 7.657 | 3.385 | 2.257 | 90 | 1 | 1.5 | 0.667 | 1 | 1.276 |
| 75 | 16 | 255 | 255 | 255 | 90.5 | 141 | 13.314 | 4.963 | 4.105 | 0 | 1 | 1.209 | 0.827 | 0.889 | 0.832 |
| 76 | 36 | 255 | 255 | 255 | 359.5 | 147 | 21.314 | 8.468 | 5.413 | 90 | 1 | 1.565 | 0.639 | 0.947 | 0.592 |
| 77 | 20 | 255 | 255 | 255 | 529.5 | 146 | 18.385 | 7.893 | 3.226 | 137.043 | 0.74 | 2.446 | 0.409 | 0.8 | 0.919 |
| 78 | 16 | 255 | 255 | 255 | 1074 | 146.5 | 13.314 | 4.963 | 4.105 | 90 | 1 | 1.209 | 0.827 | 0.889 | 0.832 |
| 79 | 901 | 255 | 255 | 255 | 60.085 | 176.9 | 213.522 | 52.218 | 21.969 | 139.623 | 0.25 | 2.377 | 0.421 | 0.613 | 0.237 |
| 80 | 12 | 255 | 255 | 255 | 507 | 154 | 11.314 | 3.909 | 3.909 | 0 | 1 | 1 | 1 | 0.857 | 0.943 |
| 81 | 594 | 255 | 255 | 255 | 1137.8 | 166.18 | 105.296 | 33.718 | 22.431 | 11.349 | 0.67 | 1.503 | 0.665 | 0.825 | 0.177 |
| 82 | 12 | 255 | 255 | 255 | 522 | 158 | 11.314 | 3.909 | 3.909 | 0 | 1 | 1 | 1 | 0.857 | 0.943 |
| 83 | 45 | 255 | 255 | 255 | 147.3 | 165.3 | 23.799 | 8.285 | 6.916 | 134.999 | 1 | 1.198 | 0.835 | 0.9 | 0.529 |
| 84 | 37 | 255 | 255 | 255 | 539.5 | 169.26 | 22.971 | 9.324 | 5.052 | 145.619 | 0.88 | 1.846 | 0.542 | 0.86 | 0.621 |
| 85 | 42 | 255 | 255 | 255 | 1102.24 | 171.45 | 24.142 | 9.578 | 5.583 | 101.584 | 0.91 | 1.716 | 0.583 | 0.894 | 0.575 |
| 86 | 151 | 255 | 255 | 255 | 523.076 | 177.81 | 49.941 | 17.6 | 10.924 | 101.976 | 0.76 | 1.611 | 0.621 | 0.851 | 0.331 |
| 87 | 827 | 255 | 255 | 255 | 196.525 | 186.63 | 127.924 | 36.761 | 28.644 | 18.282 | 0.64 | 1.283 | 0.779 | 0.848 | 0.155 |
| 88 | 28 | 255 | 255 | 255 | 151.786 | 177.61 | 18.728 | 7.002 | 5.092 | 97.047 | 1 | 1.375 | 0.727 | 0.918 | 0.669 |
| 89 | 20 | 255 | 255 | 255 | 1151 | 179.5 | 16.142 | 6.363 | 4.002 | 26.921 | 0.97 | 1.59 | 0.629 | 0.833 | 0.807 |
| 90 | 32 | 255 | 255 | 255 | 588.156 | 182.16 | 20.142 | 7.07 | 5.763 | 96.969 | 0.99 | 1.227 | 0.815 | 0.889 | 0.629 |
| 91 | 6 | 255 | 255 | 255 | 598.5 | 182 | 7.657 | 3.385 | 2.257 | 0 | 1 | 1.5 | 0.667 | 1 | 1.276 |
| 92 | 21 | 255 | 255 | 255 | 1143.98 | 184.41 | 16.142 | 6.258 | 4.272 | 28.684 | 1 | 1.465 | 0.683 | 0.857 | 0.769 |
| 93 | 74 | 255 | 255 | 255 | 20.838 | 188.89 | 33.456 | 13.661 | 6.897 | 148.08 | 0.83 | 1.981 | 0.505 | 0.86 | 0.452 |
| 94 | 34 | 255 | 255 | 255 | 1112.88 | 189.24 | 21.556 | 8.074 | 5.362 | 78.677 | 0.92 | 1.506 | 0.664 | 0.861 | 0.634 |
| 95 | 77 | 255 | 255 | 255 | 5.708 | 192.05 | 41.213 | 13.841 | 7.083 | 33.443 | 0.57 | 1.954 | 0.512 | 0.74 | 0.535 |
| 96 | 651 | 255 | 255 | 255 | 121.2 | 227.07 | 132.51 | 36.449 | 22.741 | 118.437 | 0.47 | 1.603 | 0.624 | 0.769 | 0.204 |
| 97 | 107 | 255 | 255 | 255 | 58.855 | 211.56 | 39.456 | 12.904 | 10.557 | 68.079 | 0.86 | 1.222 | 0.818 | 0.881 | 0.369 |
| 98 | 56 | 255 | 255 | 255 | 391 | 213.54 | 27.799 | 9.676 | 7.369 | 90 | 0.91 | 1.313 | 0.762 | 0.889 | 0.496 |
| 99 | 12 | 255 | 255 | 255 | 819 | 210 | 11.314 | 3.909 | 3.909 | 0 | 1 | 1 | 1 | 0.857 | 0.943 |
| 100 | 1712 | 255 | 255 | 255 | 169.762 | 242.33 | 315.304 | 61.517 | 35.434 | 131.422 | 0.22 | 1.736 | 0.576 | 0.663 | 0.184 |
| 101 | 26 | 255 | 255 | 255 | 208.538 | 215.42 | 18.142 | 7.134 | 4.64 | 159.548 | 0.99 | 1.537 | 0.65 | 0.881 | 0.698 |
| 102 | 6 | 255 | 255 | 255 | 25 | 216.5 | 7.657 | 3.385 | 2.257 | 90 | 1 | 1.5 | 0.667 | 1 | 1.276 |
| 103 | 12 | 255 | 255 | 255 | 77 | 219 | 11.314 | 3.909 | 3.909 | 0 | 1 | 1 | 1 | 0.857 | 0.943 |
| 104 | 199 | 255 | 255 | 255 | 76.575 | 235.73 | 61.012 | 21.58 | 11.741 | 90.721 | 0.67 | 1.838 | 0.544 | 0.847 | 0.307 |
| 105 | 65 | 255 | 255 | 255 | 397.238 | 227.38 | 28.971 | 9.801 | 8.444 | 138.233 | 0.97 | 1.161 | 0.861 | 0.922 | 0.446 |
| 106 | 12 | 255 | 255 | 255 | 28 | 227 | 11.314 | 3.909 | 3.909 | 0 | 1 | 1 | 1 | 0.857 | 0.943 |
| 107 | 151 | 255 | 255 | 255 | 382.944 | 232.29 | 49.113 | 18.188 | 10.571 | 162.361 | 0.79 | 1.721 | 0.581 | 0.888 | 0.325 |
| 108 | 25 | 255 | 255 | 255 | 60.18 | 233.82 | 17.556 | 6.852 | 4.645 | 135 | 1 | 1.475 | 0.678 | 0.877 | 0.702 |
| 109 | 21 | 255 | 255 | 255 | 409.5 | 237.5 | 15.314 | 5.171 | 5.171 | 0 | 1 | 1 | 1 | 0.913 | 0.729 |
| 110 | 12 | 255 | 255 | 255 | 337 | 240 | 11.314 | 3.909 | 3.909 | 0 | 1 | 1 | 1 | 0.857 | 0.943 |
| 111 | 446 | 255 | 255 | 255 | 38.993 | 259.04 | 95.397 | 29.7 | 19.12 | 89.36 | 0.62 | 1.553 | 0.644 | 0.844 | 0.214 |

| | | | | | | | | | | | | | | | |
|---|---|---|---|---|---|---|---|---|---|---|---|---|---|---|---|
| 112 | 116 | 255 | 255 | 255 | 794.052 | 248.97 | 45.113 | 14.575 | 10.134 | 148.086 | 0.72 | 1.438 | 0.695 | 0.823 | 0.389 |
| 113 | 43 | 255 | 255 | 255 | 813.221 | 247.76 | 23.556 | 8.842 | 6.192 | 31.36 | 0.97 | 1.428 | 0.7 | 0.905 | 0.548 |
| 114 | 6 | 255 | 255 | 255 | 0.833 | 249 | 9.657 | 3.718 | 2.055 | 90 | 0.81 | 1.809 | 0.553 | 0.857 | 1.610 |
| 115 | 503 | 255 | 255 | 255 | 335.335 | 263.72 | 111.882 | 33.485 | 19.126 | 119.177 | 0.51 | 1.751 | 0.571 | 0.789 | 0.222 |
| 116 | 49 | 255 | 255 | 255 | 347.541 | 253.54 | 24.385 | 8.796 | 7.093 | 96.8 | 1 | 1.24 | 0.806 | 0.907 | 0.498 |
| 117 | 357 | 255 | 255 | 255 | 120.847 | 262.74 | 79.497 | 21.431 | 21.21 | 146.066 | 0.71 | 1.01 | 0.99 | 0.847 | 0.223 |
| 118 | 3798 | 255 | 255 | 255 | 1107.85 | 291.69 | 337.605 | 76.846 | 62.928 | 155.156 | 0.42 | 1.221 | 0.819 | 0.791 | 0.089 |
| 119 | 278 | 255 | 255 | 255 | 141.759 | 274.33 | 69.841 | 22.931 | 15.436 | 99.978 | 0.72 | 1.486 | 0.673 | 0.874 | 0.251 |
| 120 | 103 | 255 | 255 | 255 | 783.432 | 272.49 | 39.113 | 14.38 | 9.12 | 44.947 | 0.85 | 1.577 | 0.634 | 0.873 | 0.380 |
| 121 | 17 | 255 | 255 | 255 | 962.088 | 268.38 | 13.899 | 5.229 | 4.14 | 74.828 | 1 | 1.263 | 0.792 | 0.919 | 0.818 |
| 122 | 230 | 255 | 255 | 255 | 999.509 | 273.62 | 61.698 | 19.608 | 14.935 | 4.734 | 0.76 | 1.313 | 0.762 | 0.881 | 0.268 |
| 123 | 19 | 255 | 255 | 255 | 805.342 | 270.66 | 14.728 | 5.301 | 4.564 | 135 | 1 | 1.161 | 0.861 | 0.884 | 0.775 |
| 124 | 456 | 255 | 255 | 255 | 979.649 | 283.95 | 91.054 | 31.514 | 18.424 | 92.78 | 0.69 | 1.71 | 0.585 | 0.86 | 0.200 |
| 125 | 5708 | 255 | 255 | 255 | 369.35 | 342.69 | 566.441 | 141.72 | 51.28 | 92.446 | 0.22 | 2.764 | 0.362 | 0.613 | 0.099 |
| 126 | 10 | 255 | 255 | 255 | 0.9 | 273 | 13.657 | 5.848 | 2.177 | 90 | 0.67 | 2.686 | 0.372 | 0.909 | 1.366 |
| 127 | 24 | 255 | 255 | 255 | 1025.67 | 276.21 | 18.728 | 7.909 | 3.863 | 172.154 | 0.86 | 2.047 | 0.488 | 0.873 | 0.780 |
| 128 | 205 | 255 | 255 | 255 | 49.978 | 289.15 | 61.355 | 22.617 | 11.541 | 92.223 | 0.68 | 1.96 | 0.51 | 0.867 | 0.299 |
| 129 | 501 | 255 | 255 | 255 | 1046.49 | 289.17 | 118.711 | 35.295 | 18.073 | 7.877 | 0.45 | 1.953 | 0.512 | 0.726 | 0.237 |
| 130 | 19 | 255 | 255 | 255 | 313.342 | 282.34 | 14.728 | 5.301 | 4.564 | 45.001 | 1 | 1.161 | 0.861 | 0.884 | 0.775 |
| 131 | 12 | 255 | 255 | 255 | 662 | 282 | 11.314 | 3.909 | 3.909 | 0 | 1 | 1 | 1 | 0.857 | 0.943 |
| 132 | 79 | 255 | 255 | 255 | 1018.97 | 287.93 | 32.627 | 11.695 | 8.601 | 90.555 | 0.93 | 1.36 | 0.735 | 0.913 | 0.413 |
| 133 | 81 | 255 | 255 | 255 | 296.377 | 292.24 | 35.456 | 13.911 | 7.414 | 51.47 | 0.81 | 1.876 | 0.533 | 0.876 | 0.438 |
| 134 | 121 | 255 | 255 | 255 | 32.822 | 302.22 | 48.284 | 19.161 | 8.041 | 113.529 | 0.65 | 2.383 | 0.42 | 0.823 | 0.399 |
| 135 | 170 | 255 | 255 | 255 | 10.618 | 306.63 | 50.77 | 18.282 | 11.84 | 115.561 | 0.83 | 1.544 | 0.648 | 0.895 | 0.299 |
| 136 | 483 | 255 | 255 | 255 | 123.084 | 317.74 | 104.711 | 32.823 | 18.736 | 106.033 | 0.55 | 1.752 | 0.571 | 0.774 | 0.217 |
| 137 | 87 | 255 | 255 | 255 | 174.121 | 307.56 | 36.284 | 12.953 | 8.552 | 16.631 | 0.83 | 1.515 | 0.66 | 0.888 | 0.417 |
| 138 | 84 | 255 | 255 | 255 | 439.619 | 309.01 | 36.042 | 13.067 | 8.185 | 77.911 | 0.81 | 1.596 | 0.626 | 0.87 | 0.429 |
| 139 | 12 | 255 | 255 | 255 | 687 | 305 | 11.314 | 3.909 | 3.909 | 0 | 1 | 1 | 1 | 0.857 | 0.943 |
| 140 | 26 | 255 | 255 | 255 | 93.577 | 310.46 | 18.142 | 7.134 | 4.64 | 110.452 | 0.99 | 1.537 | 0.65 | 0.881 | 0.698 |
| 141 | 307 | 255 | 255 | 255 | 304.663 | 320.19 | 75.497 | 23.852 | 16.388 | 69.967 | 0.68 | 1.455 | 0.687 | 0.816 | 0.246 |
| 142 | 17200 | 255 | 255 | 255 | 1091.31 | 399.51 | 1710.209 | 269.01 | 81.41 | 5.201 | 0.07 | 3.304 | 0.303 | 0.543 | 0.099 |
| 143 | 293 | 255 | 255 | 255 | 847.336 | 326.47 | 79.012 | 30.315 | 12.306 | 97.769 | 0.59 | 2.463 | 0.406 | 0.83 | 0.270 |
| 144 | 22 | 255 | 255 | 255 | 1169 | 314.5 | 16.142 | 6.173 | 4.537 | 148.799 | 1 | 1.361 | 0.735 | 0.88 | 0.734 |
| 145 | 119 | 255 | 255 | 255 | 1044.69 | 319.9 | 43.456 | 15.595 | 9.716 | 97.356 | 0.79 | 1.605 | 0.623 | 0.869 | 0.365 |
| 146 | 56 | 255 | 255 | 255 | 25.25 | 319.27 | 27.556 | 10.678 | 6.678 | 107.917 | 0.93 | 1.599 | 0.625 | 0.926 | 0.492 |
| 147 | 36 | 255 | 255 | 255 | 788.583 | 319.11 | 22.385 | 9.028 | 5.077 | 49.846 | 0.9 | 1.778 | 0.562 | 0.867 | 0.622 |
| 148 | 19 | 255 | 255 | 255 | 91.763 | 319.97 | 15.899 | 6.41 | 3.774 | 101.564 | 0.94 | 1.699 | 0.589 | 0.884 | 0.837 |
| 149 | 41 | 255 | 255 | 255 | 411.5 | 324.5 | 22.142 | 7.892 | 6.615 | 134.999 | 1 | 1.193 | 0.838 | 0.932 | 0.540 |
| 150 | 34 | 255 | 255 | 255 | 30.647 | 329.06 | 21.799 | 8.475 | 5.108 | 55.87 | 0.9 | 1.659 | 0.603 | 0.85 | 0.641 |

| | | | | | | | | | | | | | | | |
|---|---|---|---|---|---|---|---|---|---|---|---|---|---|---|---|
| 151 | 58 | 255 | 255 | 255 | 779.397 | 331.69 | 28.385 | 11.319 | 6.524 | 9.464 | 0.91 | 1.735 | 0.576 | 0.892 | 0.489 |
| 152 | 55 | 255 | 255 | 255 | 144.118 | 335.85 | 27.213 | 9.725 | 7.201 | 176.121 | 0.93 | 1.351 | 0.74 | 0.866 | 0.495 |
| 153 | 17666 | 255 | 255 | 255 | 727.791 | 403.27 | 1033.661 | 235.95 | 95.33 | 1.8 | 0.21 | 2.475 | 0.404 | 0.756 | 0.059 |
| 154 | 52 | 255 | 255 | 255 | 1126.02 | 338.62 | 27.213 | 9.724 | 6.809 | 36.286 | 0.88 | 1.428 | 0.7 | 0.867 | 0.523 |
| 155 | 391 | 255 | 255 | 255 | 20.63 | 350.88 | 77.497 | 26.874 | 18.525 | 126.085 | 0.82 | 1.451 | 0.689 | 0.914 | 0.198 |
| 156 | 41 | 255 | 255 | 255 | 531.061 | 340.45 | 24.142 | 10.13 | 5.153 | 171.763 | 0.88 | 1.966 | 0.509 | 0.921 | 0.589 |
| 157 | 120 | 255 | 255 | 255 | 179.267 | 350.26 | 44.284 | 14.503 | 10.535 | 94.545 | 0.77 | 1.377 | 0.726 | 0.857 | 0.369 |
| 158 | 203 | 255 | 255 | 255 | 113.204 | 353.26 | 63.255 | 24.053 | 10.746 | 138.975 | 0.64 | 2.238 | 0.447 | 0.825 | 0.312 |
| 159 | 97 | 255 | 255 | 255 | 77.809 | 349.21 | 43.698 | 17.701 | 6.977 | 178.69 | 0.64 | 2.537 | 0.394 | 0.833 | 0.450 |
| 160 | 117 | 255 | 255 | 255 | 3.218 | 359.73 | 55.799 | 20.785 | 7.167 | 100.869 | 0.47 | 2.9 | 0.345 | 0.836 | 0.477 |
| 161 | 82 | 255 | 255 | 255 | 198.878 | 351.65 | 33.213 | 12.252 | 8.522 | 126.806 | 0.93 | 1.438 | 0.696 | 0.906 | 0.405 |
| 162 | 19 | 255 | 255 | 255 | 1064.66 | 348.66 | 14.728 | 5.301 | 4.564 | 45.001 | 1 | 1.161 | 0.861 | 0.884 | 0.775 |
| 163 | 370 | 255 | 255 | 255 | 305.305 | 358.57 | 90.811 | 26.521 | 17.763 | 22.443 | 0.56 | 1.493 | 0.67 | 0.818 | 0.245 |
| 164 | 215 | 255 | 255 | 255 | 224.063 | 363.09 | 81.154 | 22.572 | 12.128 | 80.933 | 0.41 | 1.861 | 0.537 | 0.729 | 0.377 |
| 165 | 388 | 255 | 255 | 255 | 523.969 | 360.51 | 76.426 | 23.407 | 21.105 | 122.851 | 0.84 | 1.109 | 0.902 | 0.91 | 0.197 |
| 166 | 2004 | 255 | 255 | 255 | 285.322 | 394.54 | 322.919 | 85.805 | 29.737 | 125.948 | 0.24 | 2.885 | 0.347 | 0.593 | 0.161 |
| 167 | 13 | 255 | 255 | 255 | 1090.12 | 357.89 | 11.899 | 4.38 | 3.779 | 45 | 1 | 1.159 | 0.863 | 0.897 | 0.915 |
| 168 | 57 | 255 | 255 | 255 | 327.605 | 363.62 | 30.627 | 11.798 | 6.152 | 161.307 | 0.76 | 1.918 | 0.521 | 0.82 | 0.537 |
| 169 | 993 | 255 | 255 | 255 | 66.358 | 379.33 | 133.054 | 39.256 | 32.207 | 167.973 | 0.71 | 1.219 | 0.82 | 0.901 | 0.134 |
| 170 | 153 | 255 | 255 | 255 | 877.958 | 370.69 | 63.255 | 19.889 | 9.794 | 178.005 | 0.48 | 2.031 | 0.492 | 0.691 | 0.413 |
| 171 | 113 | 255 | 255 | 255 | 157.881 | 371.13 | 44.284 | 15.514 | 9.274 | 144.102 | 0.72 | 1.673 | 0.598 | 0.843 | 0.392 |
| 172 | 1 | 255 | 255 | 255 | 135.5 | 367.5 | 2.828 | 1.128 | 1.128 | 0 | 1 | 1 | 1 | 1 | 2.828 |
| 173 | 26 | 255 | 255 | 255 | 95.538 | 371.15 | 18.971 | 7.785 | 4.252 | 35.792 | 0.91 | 1.831 | 0.546 | 0.839 | 0.730 |
| 174 | 6 | 255 | 255 | 255 | 1067.67 | 370.33 | 8.485 | 3.14 | 2.433 | 45 | 1 | 1.291 | 0.775 | 0.8 | 1.414 |
| 175 | 24 | 255 | 255 | 255 | 247 | 373.5 | 17.314 | 7.142 | 4.279 | 90 | 1 | 1.669 | 0.599 | 0.923 | 0.721 |
| 176 | 14 | 255 | 255 | 255 | 449 | 377.5 | 13.314 | 5.862 | 3.041 | 53.23 | 0.99 | 1.928 | 0.519 | 0.875 | 0.951 |
| 177 | 30 | 255 | 255 | 255 | 348.4 | 380.07 | 20.728 | 8.065 | 4.736 | 84.323 | 0.88 | 1.703 | 0.587 | 0.87 | 0.691 |
| 178 | 26 | 255 | 255 | 255 | 1211.73 | 378.92 | 20.971 | 8.476 | 3.905 | 142.824 | 0.74 | 2.17 | 0.461 | 0.788 | 0.807 |
| 179 | 22 | 255 | 255 | 255 | 1042.18 | 380.23 | 17.556 | 7.071 | 3.961 | 27.905 | 0.9 | 1.785 | 0.56 | 0.83 | 0.798 |
| 180 | 89 | 255 | 255 | 255 | 978.455 | 387.5 | 34.87 | 10.915 | 10.382 | 144.694 | 0.92 | 1.051 | 0.951 | 0.894 | 0.392 |
| 181 | 90 | 255 | 255 | 255 | 1052.73 | 389.83 | 39.213 | 15.481 | 7.402 | 75.941 | 0.74 | 2.091 | 0.478 | 0.896 | 0.436 |
| 182 | 114 | 255 | 255 | 255 | 439.018 | 392.05 | 43.698 | 16.257 | 8.928 | 140.753 | 0.75 | 1.821 | 0.549 | 0.838 | 0.383 |
| 183 | 1749 | 255 | 255 | 255 | 462.561 | 419.13 | 244.936 | 59.96 | 37.139 | 55.186 | 0.37 | 1.614 | 0.619 | 0.722 | 0.140 |
| 184 | 61 | 255 | 255 | 255 | 174.057 | 397.86 | 32.042 | 9.385 | 8.276 | 137.335 | 0.75 | 1.134 | 0.882 | 0.803 | 0.525 |
| 185 | 63 | 255 | 255 | 255 | 875.468 | 396.14 | 30.971 | 12.435 | 6.451 | 170.894 | 0.83 | 1.928 | 0.519 | 0.9 | 0.492 |
| 186 | 10 | 255 | 255 | 255 | 1214.1 | 399 | 13.657 | 5.848 | 2.177 | 90 | 0.67 | 2.686 | 0.372 | 0.909 | 1.366 |
| 187 | 1289 | 255 | 255 | 255 | 111.665 | 419.27 | 168.995 | 48.757 | 33.661 | 135.946 | 0.57 | 1.448 | 0.69 | 0.826 | 0.131 |
| 188 | 162 | 255 | 255 | 255 | 145.846 | 405.07 | 56.77 | 16.758 | 12.308 | 127.811 | 0.63 | 1.362 | 0.734 | 0.798 | 0.350 |
| 189 | 12 | 255 | 255 | 255 | 78 | 403 | 11.314 | 3.909 | 3.909 | 0 | 1 | 1 | 1 | 0.857 | 0.943 |

| | | | | | | | | | | | | | | | |
|---|---|---|---|---|---|---|---|---|---|---|---|---|---|---|---|
| 190 | 12 | 255 | 255 | 255 | 837 | 403 | 11.314 | 3.909 | 3.909 | 0 | 1 | 1 | 1 | 0.857 | 0.943 |
| 191 | 119 | 255 | 255 | 255 | 197.256 | 407.42 | 50.184 | 17.731 | 8.545 | 156.679 | 0.59 | 2.075 | 0.482 | 0.796 | 0.422 |
| 192 | 34 | 255 | 255 | 255 | 236.647 | 406.15 | 20.971 | 6.837 | 6.332 | 77.196 | 0.97 | 1.08 | 0.926 | 0.872 | 0.617 |
| 193 | 700 | 255 | 255 | 255 | 13.464 | 419.71 | 108.77 | 33.691 | 26.454 | 144.357 | 0.74 | 1.274 | 0.785 | 0.923 | 0.155 |
| 194 | 76 | 255 | 255 | 255 | 887.539 | 413.63 | 35.213 | 13.468 | 7.185 | 117.423 | 0.77 | 1.874 | 0.534 | 0.831 | 0.463 |
| 195 | 125 | 255 | 255 | 255 | 324.028 | 416.95 | 44.042 | 15.734 | 10.116 | 91.487 | 0.81 | 1.555 | 0.643 | 0.899 | 0.352 |
| 196 | 36 | 255 | 255 | 255 | 512.056 | 413.67 | 21.799 | 7.408 | 6.187 | 171.674 | 0.95 | 1.197 | 0.835 | 0.857 | 0.606 |
| 197 | 563 | 255 | 255 | 255 | 411.699 | 430.51 | 122.468 | 30.747 | 23.314 | 120.402 | 0.47 | 1.319 | 0.758 | 0.787 | 0.218 |
| 198 | 26 | 255 | 255 | 255 | 165.846 | 417.15 | 17.556 | 6.12 | 5.409 | 45 | 1 | 1.131 | 0.884 | 0.881 | 0.675 |
| 199 | 484 | 255 | 255 | 255 | 60.579 | 431.86 | 134.953 | 37.102 | 16.609 | 159.441 | 0.33 | 2.234 | 0.448 | 0.669 | 0.279 |
| 200 | 12 | 255 | 255 | 255 | 521 | 422 | 11.314 | 3.909 | 3.909 | 0 | 1 | 1 | 1 | 0.857 | 0.943 |
| 201 | 149 | 255 | 255 | 255 | 511.802 | 430.5 | 51.113 | 16.418 | 11.555 | 108.78 | 0.72 | 1.421 | 0.704 | 0.851 | 0.343 |
| 202 | 45 | 255 | 255 | 255 | 903.656 | 425.83 | 25.556 | 9.079 | 6.311 | 99.211 | 0.87 | 1.439 | 0.695 | 0.865 | 0.568 |
| 203 | 16 | 255 | 255 | 255 | 523 | 429.5 | 13.314 | 4.963 | 4.105 | 90 | 1 | 1.209 | 0.827 | 0.889 | 0.832 |
| 204 | 9 | 255 | 255 | 255 | 359.389 | 431.83 | 10.485 | 3.919 | 2.924 | 110.301 | 1 | 1.34 | 0.746 | 0.857 | 1.165 |
| 205 | 45 | 255 | 255 | 255 | 227.211 | 436.99 | 24.385 | 7.956 | 7.202 | 46.719 | 0.95 | 1.105 | 0.905 | 0.874 | 0.542 |
| 206 | 19 | 255 | 255 | 255 | 140.658 | 436.34 | 14.728 | 5.301 | 4.564 | 135 | 1 | 1.161 | 0.861 | 0.884 | 0.775 |
| 207 | 93 | 255 | 255 | 255 | 854.758 | 439.35 | 40.87 | 14.079 | 8.41 | 177.853 | 0.7 | 1.674 | 0.597 | 0.842 | 0.439 |
| 208 | 51 | 255 | 255 | 255 | 606.245 | 439.66 | 30.042 | 12.435 | 5.222 | 136.309 | 0.71 | 2.381 | 0.42 | 0.797 | 0.589 |
| 209 | 24 | 255 | 255 | 255 | 96.5 | 438 | 17.314 | 7.142 | 4.279 | 0 | 1 | 1.669 | 0.599 | 0.923 | 0.721 |
| 210 | 3 | 255 | 255 | 255 | 285.833 | 437.17 | 5.657 | 2.365 | 1.615 | 135 | 1 | 1.464 | 0.683 | 0.857 | 1.886 |
| 211 | 53 | 255 | 255 | 255 | 10.689 | 442.16 | 27.556 | 10.361 | 6.513 | 173.673 | 0.88 | 1.591 | 0.629 | 0.891 | 0.520 |
| 212 | 60 | 255 | 255 | 255 | 320.25 | 442.43 | 49.355 | 16.06 | 4.757 | 172.186 | 0.31 | 3.376 | 0.296 | 0.603 | 0.823 |
| 213 | 86 | 255 | 255 | 255 | 1146.49 | 441.88 | 37.556 | 15.87 | 6.9 | 179.829 | 0.77 | 2.3 | 0.435 | 0.91 | 0.437 |
| 214 | 47 | 255 | 255 | 255 | 493.989 | 442.39 | 28.142 | 9.534 | 6.277 | 11.686 | 0.75 | 1.519 | 0.658 | 0.887 | 0.599 |
| 215 | 48 | 255 | 255 | 255 | 375.604 | 443.13 | 33.556 | 12.944 | 4.721 | 0.356 | 0.54 | 2.742 | 0.365 | 0.881 | 0.699 |
| 216 | 20 | 255 | 255 | 255 | 86.8 | 443.25 | 15.899 | 6.168 | 4.128 | 170.604 | 0.99 | 1.494 | 0.669 | 0.93 | 0.795 |
| 217 | 33 | 255 | 255 | 255 | 1103.32 | 443.71 | 29.899 | 13.524 | 3.107 | 1.861 | 0.46 | 4.353 | 0.23 | 0.904 | 0.906 |
| 218 | 6 | 255 | 255 | 255 | 307 | 444.17 | 9.071 | 3.718 | 2.055 | 0 | 0.92 | 1.809 | 0.553 | 0.857 | 1.512 |
| 219 | 6 | 255 | 255 | 255 | 514 | 444.17 | 9.071 | 3.718 | 2.055 | 0 | 0.92 | 1.809 | 0.553 | 0.857 | 1.512 |
| 220 | 18 | 255 | 255 | 255 | 1088.33 | 444.11 | 23.899 | 11.094 | 2.066 | 179.345 | 0.4 | 5.37 | 0.186 | 0.857 | 1.328 |

# APPENDICE D

# APPORT DE LA SUSCEPTIBILITÉ MAGNÉTIQUE À L'EXPLORATION DU GISEMENT DE BEATTIE

**Introduction**

Les travaux minéralogiques ont montré que les concentrations en or sur la propriété de Beattie semblent associées à la destruction de magnétite, et dans une certaine mesure l'absence d'hématite.

Un levé géophysique aéroporté à haute résolution, commandé par Corporation Minière Osisko, a été réalisé sur la propriété de Beattie. L'objectif de cette étude était de mettre en évidence les zones minéralisées, à l'échelle du gisement (Wares, 2010). L'utilisation d'un susceptibilimètre magnétique est efficace sur une plus faible échelle; c'est le cas pour les carottes de forage qui ont un volume connu. L'intérêt de la présente étude est de caractériser par les mesures de susceptibilité magnétique les différents faciès d'altération de la syénite de Beattie, et de les comparer avec les teneurs en or. La connaissance des valeurs types de chaque faciès d'altération serait un moyen complémentaire au loggage pour distinguer les roches.

**Méthode**

Les mesures de susceptibilité magnétique ont été réalisées sur douze demi-carottes de forages et six échantillons de surface provenant de la propriété Beattie à Duparquet (Figure 1). Les carottes de forages sont de type NQ; la largeur est 4,6cm pour environ 10cm de longueur; les échantillons de surface ont des volumes comparables aux demi-carottes de forage. Six faciès lithologiques ont été distingués : le faciès de syénite/volcanite silicifiée-bréchifiée-remplacée (SISY-BRSY-RESY), le faciès de syénite fraîche très peu altéré à chlorite-carbonate (INSY), le faciès de syénite séricitisée (SRSY), le faciès de syénite carbonatée (CBSY), le faciès de syénite hématisée (HMSY) un peu carbonaté (transition entre martite et carbonatisation), et le faciès de syénite martitisée (HMSY).

Les résultats de susceptibilité magnétiques ont été associés aux teneurs en or dans chaque faciès; des observations pétrographiques ont permis une bonne distinction de deux faciès d'alteration : le faciès de syénite martitisée non aurifère, et le faciès de syénite hématisée (dusty hematite) qui peut être associé à des valeurs en or.

Le susceptibilimètre magnétique utilisé est une sonde MPP-EM2S+ - sonde multi-paramètres - de la compagnie Instrumentation GDD inc. La sonde détecte la susceptibilité magnétique avec une précision de 10-6 SI, ainsi que les valeurs de conductivité relative et absolue (MHOS/M). Les mesures ont été faites dans le laboratoire de recherche en géologie économique de l'UQAM. Le « bruit magnétique », ou bruit de fond, durant l'analyse était de 0,0001 SI.

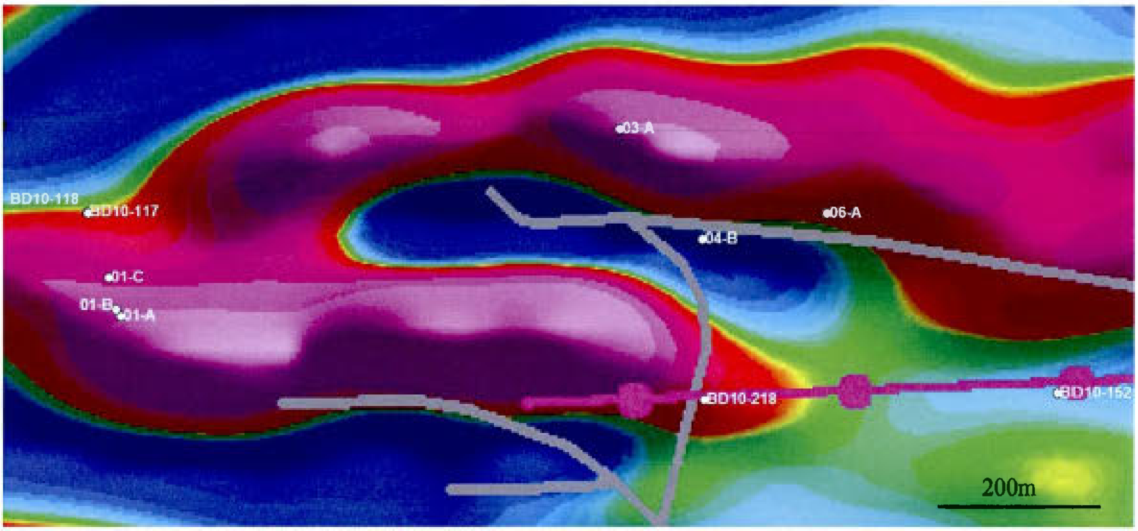


**Figure 6.** Localisation des échantillons de surface et des trous de forage (BD...) une carte géophysique SVD de Duparquet.

**Résultats**

La susceptibilité magnétique varie grandement dans les faciès lithologiques de Beattie (Table 1); il y a un ordre de grandeur de quasiment 1000 entre le faciès de syénite silicifiée-bréchifiée-remplacée, et le faciès de syénite fraîche.

Les observations pétrographiques ont permis de constater que le faciès martitisé est dépourvu de pyrite, alors que dans le faciès hématisé il y a une faible quantité de pyrite (inférieur à 2%).

**Table 1.** Comparaison des différents faciès d'altération à Beattie

| Facies d'alteration | moyenne Au (g/t) | Susceptibilité Magnétique (0,001 SI) | Texture de Minéralisation | Type de Minéralisation |
|---|---|---|---|---|
| Syénite/volcanites silicifiée-bréchifiée-remplacée (SISY-BRSY-RESY - dans shear zones) | 6,24 | 0,12 | pyrite (15%) fine cataclasée dans des corridors siliceux | très aurifère; inclus dans pyrite, parfois à l'état libre |
| Syénite carbonatée (CBSY - dans intrusif) | 2,7 | 0,43 | pyrite (8%) disséminée dans la roche | aurifère; inclus dans pyrite et arsénopyrite |
| Syénite séricitisée (SRSY - dans shear zones) | 2,35 | 1,05 | pyrite (2%) souvent concentrée dans des corridors à séricite | aurifère; inclus dans pyrite et arsénopyrite |
| Syénite hématisée (HMSY - dans intrusif) | 1,06 | 33,25 | hématite disséminée, faible pyrite (inf 2%) | Aurifère parfois; inclus dans pyrite |
| Syénite martitisée (HMSY - dans intrusif) | 0,2 | 60 | martite (5%) disséminée dans la roche | très faible aurifère |
| Syénite fraîche peu altérée à chlorite (INSY - dans intrusif) | 0,0224 | 98,2 | magnétite (5%) disséminée dans la roche | non aurifère |

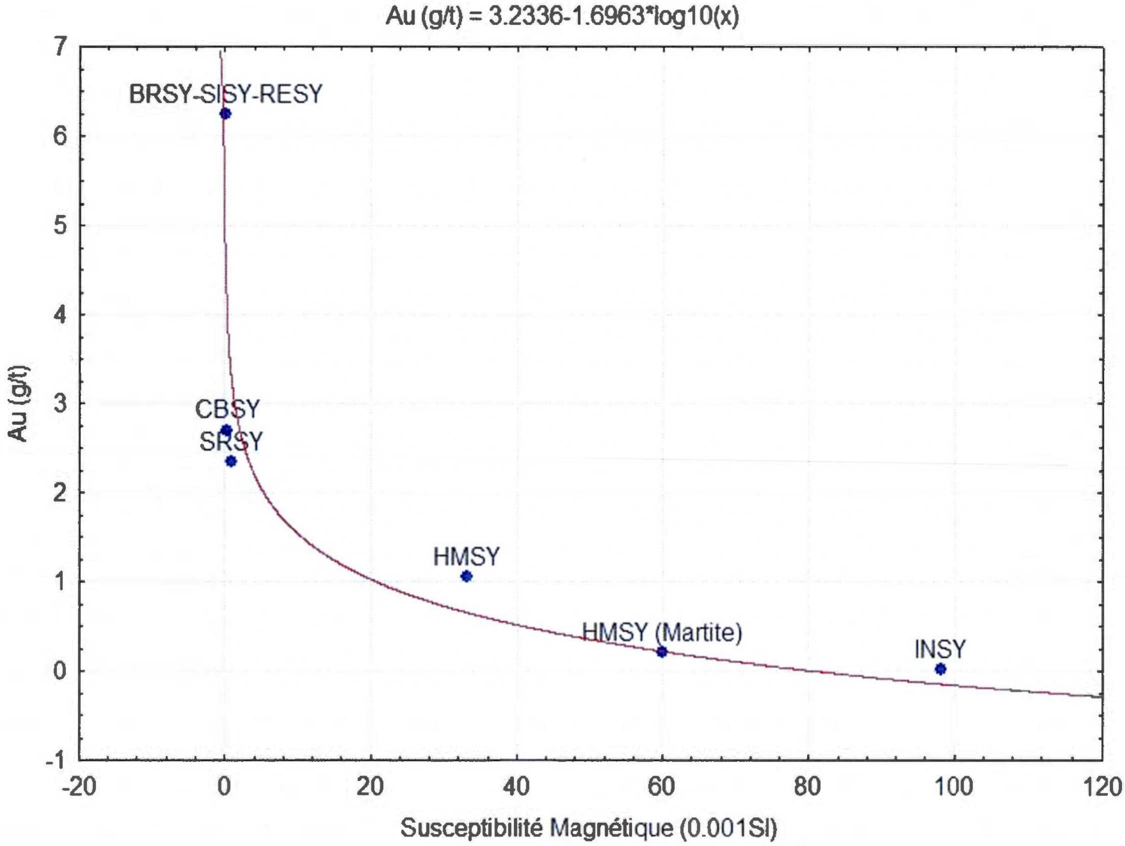


**Figure 2.** Teneur en or versus la susceptibilité magnétique mesurée dans les différents faciès d'altération

**Discussion**

La distribution des sulfures, disséminée dans l'intrusion ou contrôlée dans des failles cisaillantes, n'est pas déterminante pour la valeur de la susceptibilité magnétique. C'est la concentration en fer dans la roche (naturelle ou par altération) qui contrôle les valeurs de susceptibilité magnétique. Plus elle est forte, plus la susceptibilité magnétique sera élevée. Une étude minéralogique a mis en évidence les fortes concentrations en fer, marquées par la magnétite (supérieur à 55% des minéraux métalliques), dans les faciès non altérés de la syénite de Beattie. Ainsi, à Beattie, plus l'altération est prononcée (marquée par la disparition des oxydes de fer magnétite et hématite), plus la valeur de susceptibilité magnétique est faible.

À partir des mesures de susceptibilité magnétique, il serait possible d'établir une évaluation qualitative de l'altération des roches (Figure 3). La méthode serait basée sur une numérotation de 1 à 5 selon la valeur de susceptibilité magnétique : (1) susceptibilité magnétique d'environ 100.10-3 SI. La roche est fraîche, pas ou très peu altérée; (2) susceptibilité magnétique d'environ 60.10-3 SI. La martitisation témoigne du départ du fer; (3) susceptibilité magnétique d'environ 30.10-3 SI correspondant à l'hématisation de la roche sous forme de dusty hématite résultant de la destruction de l'hématite avec un peu de carbonatation; (4) susceptibilité magnétique entre 1 et 0,4.10-3 SI correspondant à la carbonatation et la séricitisation sans dusty hematite; (5) susceptibilité magnétique inférieure à 0,4.10-3 SI correspondant au remplacement total de la roche par la silice, il n'y a plus de fer sauf dans les sulfures.

| Susceptibilité magnétique (10-3 SI) | 100 | 60 | 30 | <1 et >0,4 | <0,4 |
|---|---|---|---|---|---|
| Degré d'altération | 1 | 2 | 3 | 4 | 5 |
| Évolution de l'altération | frais (INSY) | martitisation (HMSY) | hématisation (HMSY) | carbonatation & sericitisation (CB-SRSY) | remplacement par silice (SI-RESY) |
| | *intensité d'altération* → | | | | |

**Figure 3.** Méthode qualitative pour caractériser l'altération à Beattie

Cette méthode de caractérisation de l'altération, basée sur des paramètres géophysiques, peut être un outil efficace pour les roches de la syénite de Beattie. L'utilisation du logiciel NORMAT (Piché and Jébrak, 2004), dont les fondements sont géochimiques, peut être utilisé de façon complémentaire à la méthode géophysique. La rareté de roches à quartz normatif dans le secteur de Beattie a notamment permis à Legault et al. (2005), avec le logiciel NORMAT, de déceler les zones fortement altérées par silicification. Ce sont les mêmes zones identifiées dans ce rapport comme ayant un degré d'altération très avancé, numéro cinq.

L'étude de la paragénèse métallique du gîte de Beattie montre que l'or, et la pyrite, ne sont pas associés au faciès de martitisation mais sont tardifs par rapport à la martite. Ici, la présence d'or associée au faciès d'hématisation (±carbonatation), et la faible quantité de pyrite, témoignent que l'altération à hématite est tardive par rapport à la martitisation.

**Conclusions**

Dans le gisement de Beattie, la minéralisation aurifère n'a aucune affinité avec la magnétite; en revanche, l'or se trouve parfois en faibles concentrations (1g/t) dans les roches hématisées associé à un degré de carbonatation. La magnétite est un métallotecte négatif pour l'or à Beattie. La susceptibilité magnétique dans les roches du gisement de Beattie est inversement corrélée (décroissance logarithmique) avec la teneur en or et l'intensité d'altération des roches. Une susceptibilité magnétique d'environ 100.10-3 SI correspond à une roche non altérée avec une teneur en or d'environ 0,02g/t Au. Une susceptibilité magnétique d'environ 30.10-3 SI correspond à une altération « partielle » (dusty hématite) avec une teneur en or d'environ 1g/t Au. Une susceptibilité magnétique inférieure à 0,4.10-3 SI correspond à une altération très intense (remplacement) avec une teneur en or supérieure à 6,2g/t Au. Ces valeurs de susceptibilité magnétiques peuvent servir d'indicateurs pour le caractère aurifère des roches à Beattie.

Une nouvelle méthode de caractérisation de l'altération des roches par les mesures de susceptibilité magnétique peut être développée pour le gisement de Beattie. Il s'agit d'attribuer un numéro à la roche selon les valeurs de susceptibilité magnétique. Plus les valeurs sont élevées (proche de 100.10-3 SI), plus les numéros tendent vers 1 qui caractérise l'état de fraîcheur des roches; plus les valeurs sont faibles (inférieur à 0,4.10-3 SI), plus les numéros tendent vers 5 qui caractérise l'état d'altération très intense des roches, marqué par la silicification pervasive et le remplacement total.

# APPENDICE E

# ANALYSE STRUCTURALE DES PHASES TARDIVES CASSANTES

## Introduction

Lorsque la mine Beattie était en activité de 1936 à 1954, l'exploitation était exclusivement concentrée au niveau de la faille Beattie marquant le contact entre la syénite au sud et les roches volcaniques mafiques au nord. Des forages effectués en 2009 et 2010 par les compagnies minières Osisko et Clifton Star ont mis en évidence que les minéralisations aurifères à fortes teneurs se distribuent le long de failles, soulignant un contrôle structural important. L'étroite relation entre la minéralisation aurifère et les failles nécessite une étude structurale approfondie afin d'établir une meilleure compréhension de l'évolution structurale à Beattie.

## Méthode

### *Échantillonnage*

Des observations structurales basées sur les relations de recoupement et la géométrie des objets ont été faites sur des affleurements à proximité de la Fracture zone dans la syénite de Beattie. Des attitudes de plans de failles et de stries ont été collectées sur ces mêmes affleurements. La prise de mesure s'est faite rigoureusement; (1) déterminer l'indice de certitude de la mesure – C-certain, P-probable, S-supposé, (2) déterminer le type de mouvement sur la faille – N-normal, I-inverse, D-dextre, S-senestre, (3) déterminer l'azimuth de la faille, (4) déterminer le pendage de la faille, (5) déterminer le plongement de la strie le long du plan de faille, (6) déterminer l'orientation de la strie. Des mesures de veines et de joints ont aussi été faites.

### *Intégration des données*

L'analyse des données s'est faites avec le logiciel d'analyse de failles T-TECTO 3.0® basé sur l'inversion de données et permettant la reconstitution du tenseur des contraintes. Lorsque les données sont intégrées au logiciel (Table 1, Table 2), il faut fixer des paramètres (Figure 1) propres à chaque cas. Les paramètres qui influencent le plus le modèle sont le type d'inversion et le paramètre de dispersion. Les paramètres secondaires sont le facteur de certitude des mesures, l'angle de friction, le type de régime, et le paramètre de contrainte entres autres.

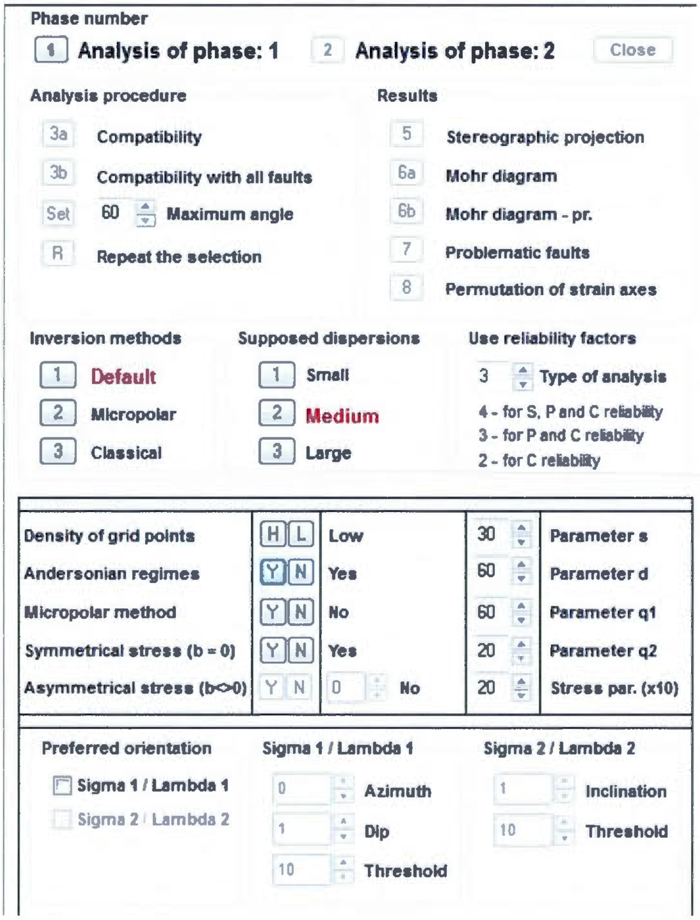


**Figure 1.** Paramètres à fixer pour effectuer une reconstitution du tenseur des contraintes - logiciel T-TECTO

*Paramètres fixés*

Les paramètres ont été fixés selon les observations de terrain. Le type d'inversion utilisé est la méthode conventionnelle basée sur la symétrie des contraintes. Le paramètre de dispersion est moyen car il y a des orientations dominantes dans les plans de failles et non une distribution totalement hétérogène qui aurait indiqué une dispersion large. Le facteur de certitude des mesures est fixé à 3, ce qui signifie que seuls « certain » et « probable » sont conservés dans l'analyse. Le paramètre de dispersion est fixé à 30, valeur arbitraire pour les dispersions moyennes. L'angle de friction est ici fixé par défaut à une valeur de 60 degré. Étant donné qu'il y a plus d'une strie sur un même plan de faille, il faut considérer la réactivation de ces failles, ce qui dans ce cas exclut le régime Andersonian qui implique uniquement les failles néoformées.

**Table 1.** Mesures des failles et stries associés

| | | | | | | | | |
|---|---|---|---|---|---|---|---|---|
| C | I | 134 | 66 | 55 | N | 1.00E+0000 | 1.00E+0000 | 1 |
| C | I | 178 | 89 | 54 | E | 1.00E+0000 | 1.00E+0000 | 2 |
| C | I | 197 | 88 | 49 | E | 1.00E+0000 | 1.00E+0000 | 3 |
| C | D | 335 | 88 | 35 | E | 1.00E+0000 | 1.00E+0000 | 4 |
| S | D | 120 | 72 | 35 | N | 1.00E+0000 | 1.00E+0000 | 5 |
| S | I | 134 | 70 | 60 | N | 1.00E+0000 | 1.00E+0000 | 6 |
| C | D | 336 | 86 | 46 | E | 1.00E+0000 | 1.00E+0000 | 7 |
| C | D | 258 | 73 | 46 | E | 1.00E+0000 | 1.00E+0000 | 8 |
| C | D | 356 | 81 | 38 | E | 1.00E+0000 | 1.00E+0000 | 9 |
| S | I | 266 | 81 | 51 | W | 1.00E+0000 | 1.00E+0000 | 10 |
| P | D | 360 | 69 | 35 | E | 1.00E+0000 | 1.00E+0000 | 11 |
| C | D | 190 | 67 | 38 | E | 1.00E+0000 | 1.00E+0000 | 12 |
| C | D | 187 | 25 | 12 | W | 1.00E+0000 | 1.00E+0000 | 13 |
| C | D | 30 | 69 | 25 | E | 1.00E+0000 | 1.00E+0000 | 14 |
| C | D | 195 | 40 | 54 | W | 1.00E+0000 | 1.00E+0000 | 15 |
| C | D | 200 | 49 | 52 | E | 1.00E+0000 | 1.00E+0000 | 16 |
| C | D | 205 | 60 | 57 | E | 1.00E+0000 | 1.00E+0000 | 17 |
| C | D | 200 | 59 | 75 | E | 1.00E+0000 | 1.00E+0000 | 18 |
| C | D | 167 | 62 | 85 | E | 1.00E+0000 | 1.00E+0000 | 19 |
| C | D | 174 | 60 | 84 | E | 1.00E+0000 | 1.00E+0000 | 20 |
| P | D | 165 | 66 | 65 | E | 1.00E+0000 | 1.00E+0000 | 21 |
| S | S | 335 | 88 | 65 | W | 1.00E+0000 | 1.00E+0000 | 22 |
| S | S | 150 | 79 | 45 | E | 1.00E+0000 | 1.00E+0000 | 23 |
| S | S | 260 | 56 | 15 | S | 1.00E+0000 | 1.00E+0000 | 24 |
| P | S | 208 | 65 | 77 | W | 1.00E+0000 | 1.00E+0000 | 25 |
| S | S | 270 | 66 | 30 | S | 1.00E+0000 | 1.00E+0000 | 26 |
| S | S | 175 | 60 | 63 | W | 1.00E+0000 | 1.00E+0000 | 27 |
| C | S | 180 | 78 | 56 | W | 1.00E+0000 | 1.00E+0000 | 28 |
| C | S | 270 | 85 | 16 | N | 1.00E+0000 | 1.00E+0000 | 29 |
| C | S | 280 | 80 | 17 | N | 1.00E+0000 | 1.00E+0000 | 30 |
| C | S | 262 | 82 | 18 | N | 1.00E+0000 | 1.00E+0000 | 31 |
| P | I | 83 | 82 | 82 | N | 1.00E+0000 | 1.00E+0000 | 32 |

| | | |
|---|---|---|
| P S 108 51 4 N | 1.00E+0000 | 1.00E+0000 33 |
| C D 296 89 19 N | 1.00E+0000 | 1.00E+0000 34 |
| C D 278 73 46 N | 1.00E+0000 | 1.00E+0000 35 |
| P S 172 81 38 E | 1.00E+0000 | 1.00E+0000 36 |
| C D 280 86 36 N | 1.00E+0000 | 1.00E+0000 37 |
| C D 290 66 14 N | 1.00E+0000 | 1.00E+0000 38 |
| C S 165 70 65 E | 1.00E+0000 | 1.00E+0000 39 |
| P D 299 85 26 N | 1.00E+0000 | 1.00E+0000 40 |
| P S 165 89 33 E | 1.00E+0000 | 1.00E+0000 41 |
| P D 290 84 20 N | 1.00E+0000 | 1.00E+0000 42 |
| C D 286 76 23 N | 1.00E+0000 | 1.00E+0000 43 |
| P S 160 79 45 E | 1.00E+0000 | 1.00E+0000 44 |
| P S 163 60 55 E | 1.00E+0000 | 1.00E+0000 45 |
| P S 170 66 30 E | 1.00E+0000 | 1.00E+0000 46 |
| P S 154 75 18 E | 1.00E+0000 | 1.00E+0000 47 |
| P D 358 45 35 E | 1.00E+0000 | 1.00E+0000 48 |
| P D 340 55 35 E | 1.00E+0000 | 1.00E+0000 49 |

**Table 2.** Mesures de veines et joints

| |
|---|
| T 218 60 |
| T 271 62 |
| T 254 69 |
| T 215 70 |
| T 240 80 |
| T 206 70 |
| T 265 65 |
| T 265 44 |
| T 260 86 |
| T 245 65 |
| T 260 35 |
| T 270 50 |
| T 283 64 |
| T 260 70 |
| T 295 75 |
| J 191 69 |
| J 176 80 |
| J 024 78 |

J 015 76
J 030 70
J 186 70
J 002 75
J 005 75
J 155 81
J 360 76
J 020 88
J 006 77
J 170 66
J 184 66
J 172 75
J 012 83

**Traitement des données**

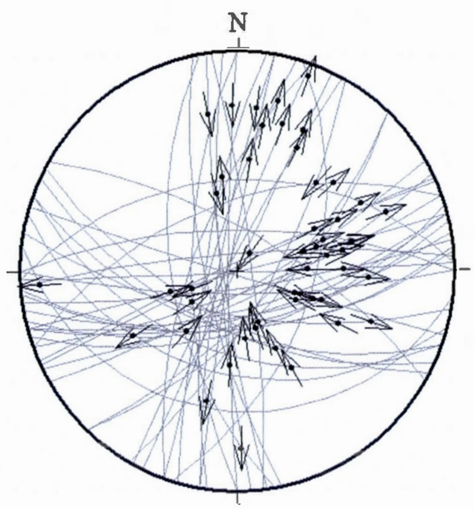


**Figure 2.** Stéréonet de toutes les failles mineures tardives avec les stries

*Reconstitution du tenseur des contraintes*

Le logiciel T-TECTO distingue deux phases structurales : (1) un axe de raccourcissement maximal NNO-SSE avec la contrainte maximale σ1 plongeant de 33 degrés vers le N155 (Figure 3a,b), (2) un axe de raccourcissement maximal ENE-OSO avec la contrainte maximale σ1 plongeant de 34 degré vers le N060 (Figure 4a,b).

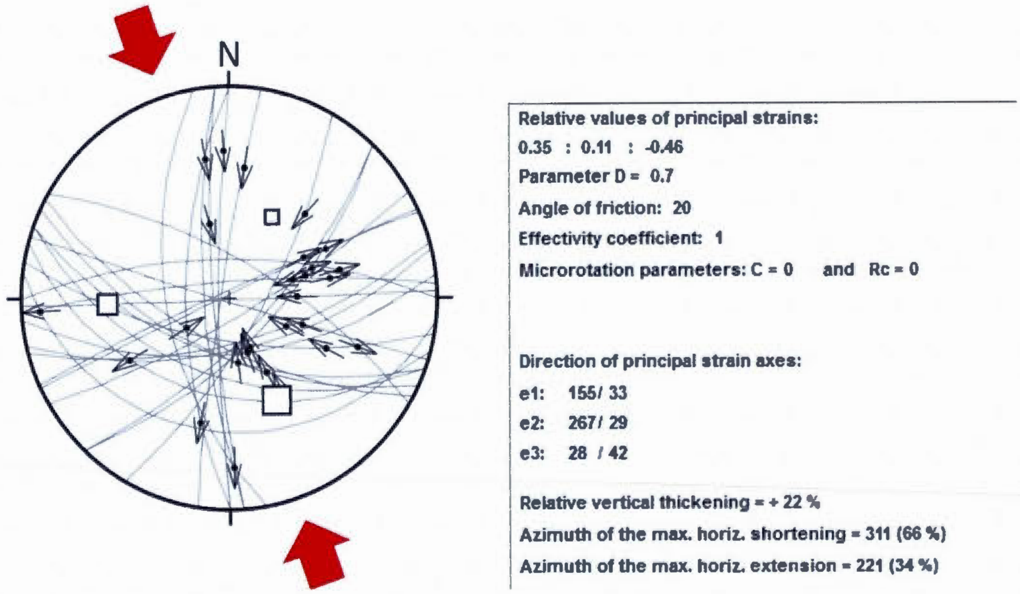


**Figure 3.** Phase 1

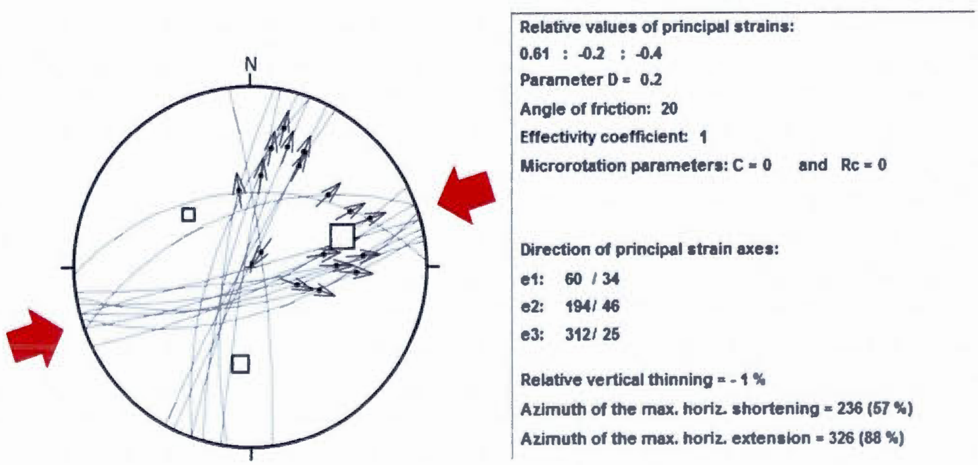


**Figure 4.** Phase 2

# APPENDICE F

# CALCULS DES VOLUMES DE FLUIDE POUR LES ALTÉRATIONS

Résultats des volumes de fluides des altérations avec les paramètres :

| **Objet** | **Volume ($m^3$)** | **densité (rho)** | **Masse de Roche altérée (t)** | **Gain en éléments (%)** | **Solubilité des éléments (ppm)** | **volume minimal de fluide ($m^3$)** | **Ratio Eau/Roche** |
|---|---|---|---|---|---|---|---|
| Syénite | 247 980 000 | 2.7 | 669 546 000 | | | | |
| Hématisation | 62 399 000 | 2.6 | 162 237 400 | Oxydation in-situ | | | |
| Carbonatisation | 151 470 000 | 2.66 | 402 910 200 | 3.83 | 10 | 154 314 606 600.0 | 1 018.78 |
| Silicification | 4 068 600 | 2.69 | 10 944 534 | 17.74 | 500 | 388 312 066.3 | 95.44 |
| Sericitisation | 9 924 300 | 2.79 | 27 688 797 | 4.29 | 379 | 313 416 725.9 | 31.58 |

Solubilité des minéraux à 300°C : Quartz et Calcite d'après Dolejs et Manning (2010); Séricite d'après Mexias et al. (2005). Le volume de carbonatisation est global, il comprend les 2 phases d'altération : (1) à calcite, (2) à carbonate de fer.

# APPENDICE G

# ANALYSE DE L'OR INVISIBLE AU MICROSCOPE ÉLÉCTRONIQUE À TRANSMISSION

**Introduction**

La cristallisation de l'or essentiellement sous forme invisible est un problème de majeure pour une étude minéralogique. En effet, l'observation se fait généralement au microsccope optique et microscope à balayage éléctronique (MEB), mais très rarement avec d'autres outils. Comprenant qu'il y a de l'or dans les pyrites arsénifères et arsénopyrite, mais que sa dimension est nécessairement inférieur au micron (limite du MEB), il a fallu trouver une méthode d'analyse alternative. Seul le microscope éléctronique à transmition (TEM) permet une étude très fine grâce à des grossissements jusqu'à 470000 fois, ce qui donne une échelle d'environ 2 nanomètres.

**Méthode**

Les analyses ont été réalisées au département de physique de l'université de McGill, au sein du FEMR (Facility for Electron Microscopy Research). Les manipulations, incluant préparation d'échantillons et utilisation du TEM, ont été faites par Dirk Schuman, étudiant en post-doc avec le professeur Hojatolla Vali.

*Préparation*

Le support initial est une lame mince polie régulière (échantillon B2 – faciès à contrôle lithologique à 2,4g/t Au). Cette lame est trempée dans un acide durant 24 heures afin de retirer l'époxy. Par la suite, nous avons découpé avec un scalpel des surfaces d'environ 3mm de diamètre contenant les pyrites à analyser. Une fois les échantillons sélectionnés, il faut réduire l'épaisseur de la section polie à 80 nm. Pour cela, nous avons utilisé le procédé « Ion-milling » qui consiste à envoyer un faisceau sur une petite partie de l'échantillon afin d'en réduire son épaisseur. Malheureusement, compte tenu de la forte concentration en carbonate dans la roche, cette méthode fut un échec car le faisceau détruisait bien plus rapidement les carbonates (la matrice), alors que les pyrites étaient moins affectées. Il en résultait un déséquilibre entre l'épaisseur des pyrites, supérieur au 80 nm requis, et les carbonates quasiment totalement détruit. Il a fallu trouver une autre méthode de préparation. Cette méthode consiste à placer les échantillons découpés et sélectionnés dans une résine. Puis les techniciens du FEMR ont fait de très fines sections d'épaisseur de 80 nm requis pour placer l'échantillon dans l'appareil. Cette méthode s'est révélée bien meilleur dans la préservation à la fois de la matrice carbonatée et des pyrites. Une fois les sections découpées, elles sont placées sur une grille (« grid ») en cuivre d'environ 1mm de diamètre. Ce support en cuivre avec l'échantillon est ensuite inséré dans le TEM.

*Procédé analytique*

Le TEM utilisé est un Philips CM200. Le voltage appliqué est de 200 kV. Les autres propriétés de l'appareil sont les suivantes : AMT XR-80C 2k x 2k CCD, avec Camera System et EDAX Genesis EDS. Les analyses se faisait généralement à des grossissements entre 300000 fois et jusqu'à 470000 fois.

**Résultats**

A

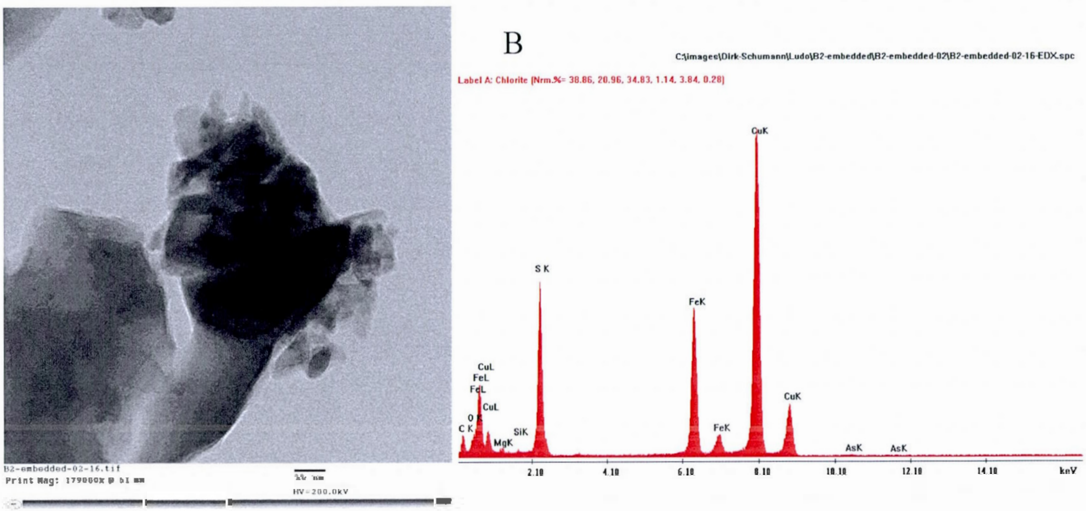


**Figure 1.** (a) Image d'une pyrite non arsénifère. (b) Analyse élémentaire avec EDAX; à noter que les anomalies en Cu sont dus à la grille de cuivre qui perturbe en partie le signal.

A

B

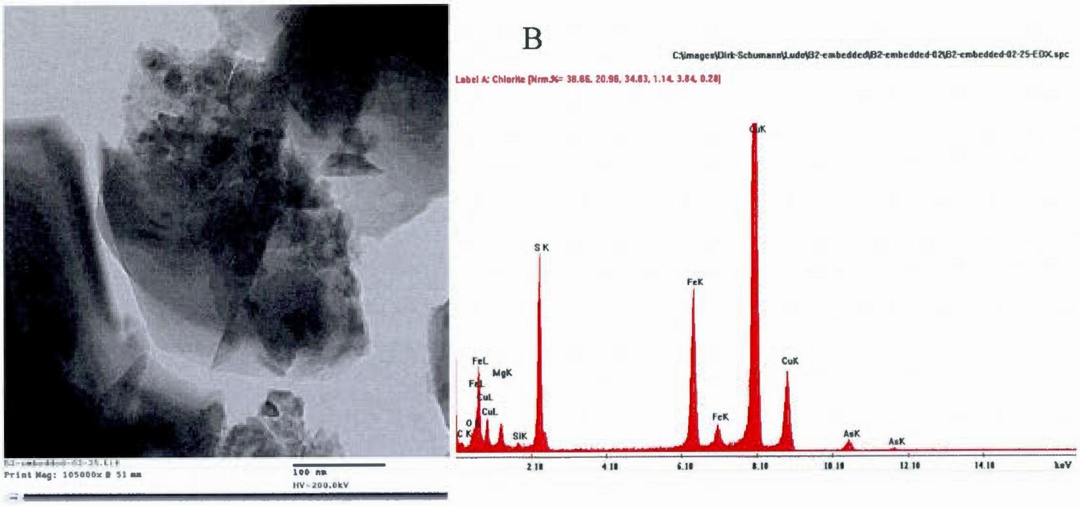


**Figure 2.** (a) Pyrite arsénifère, aurifère, et poreuse. (b) Analyse élémentaire de la pyrite. Noter les pics en arsenic, et l'absence des pics en or. Cela s'explique par le degré de detection de l'EDAX de l'ordre du %. En revanche les analyses à la microsonde, avec un seuil de détection de 60ppm Au, avaient confirmées la présence d'or dans cette pyrite.

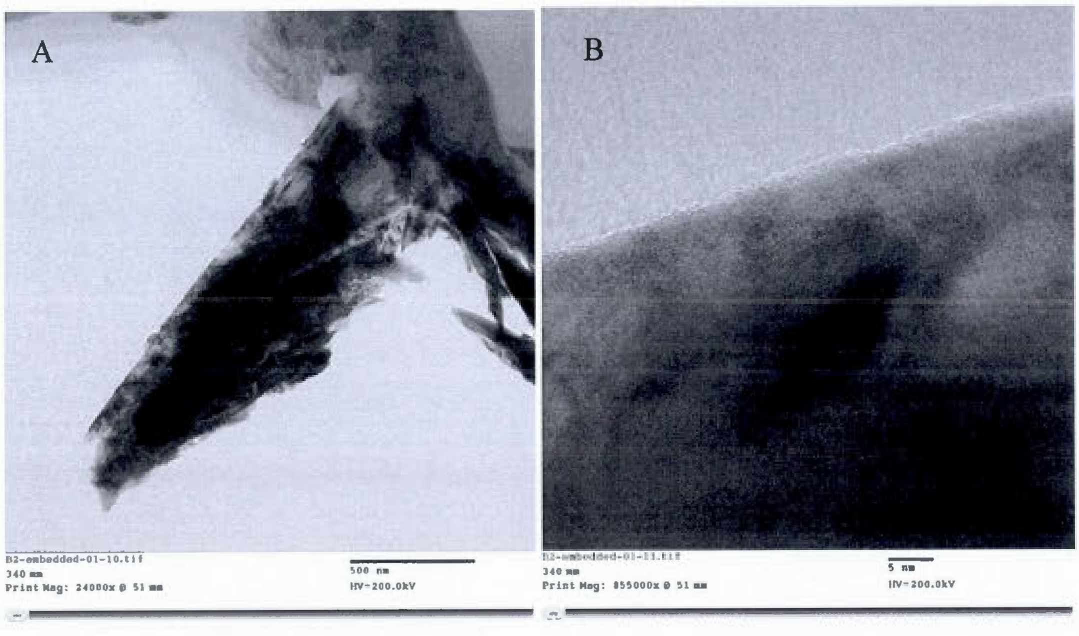

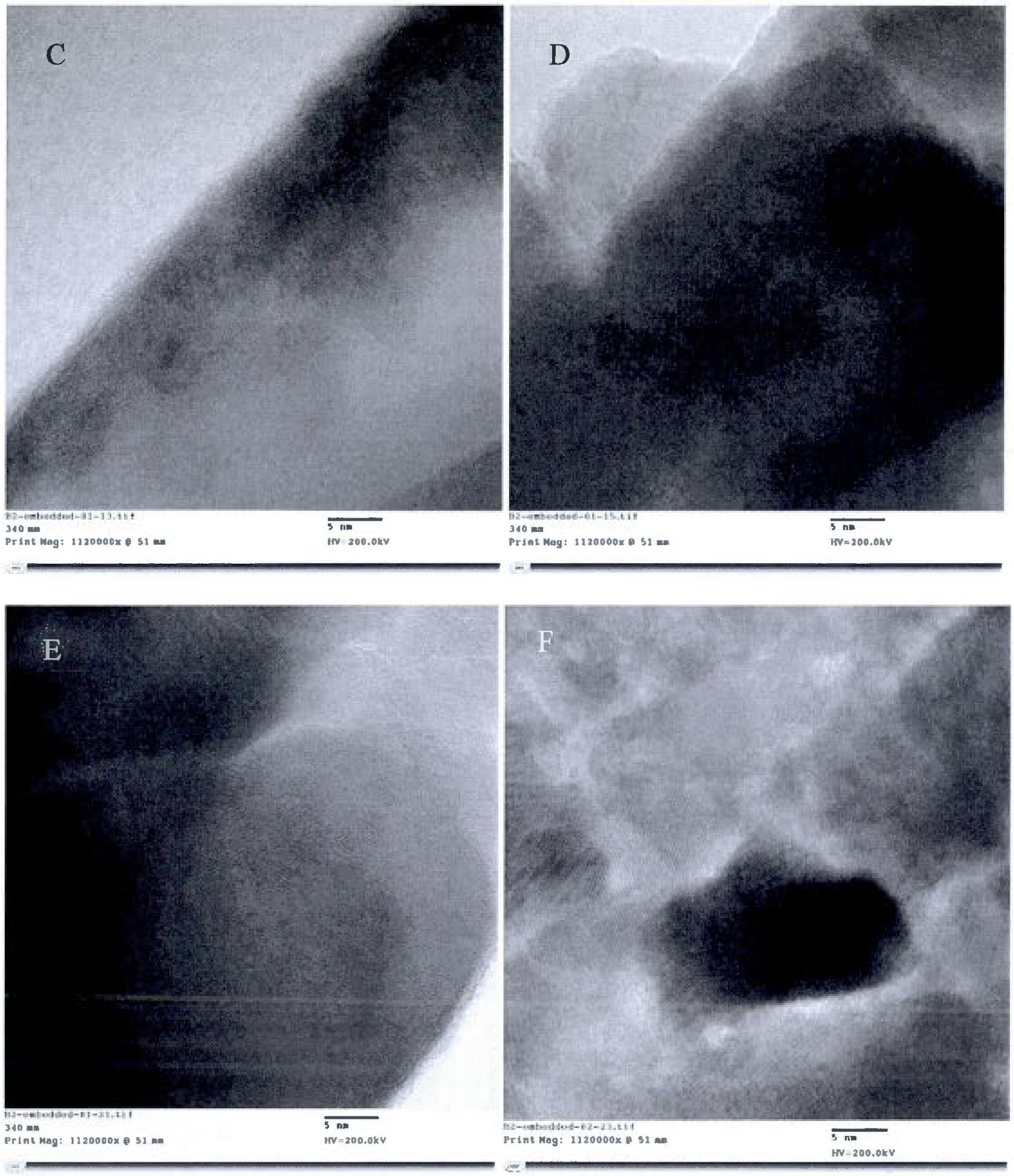


**Figure 3.** (a) pyrite. (b), (c), (d), et (e) fort grossissement sur (a); visualisation des structures cristallines de la pyrite; les différentes teintes de gris indiquent des changements de composition. (f) Structure cristallines d'une autre pyrite; hétérogénéité des structures bien visibles.

BIBLIOGRAPHIE GÉNÉRALE


Ashley, P. M. , C. J. Creagh, et C. G. Ryan. 2000. «Invisible gold in ore and mineral concentrates from the Hillgrove gold-antimony deposits, NSW, Australia». *Mineralium Deposita*, vol. 35, p. 285-301.

Ayer, J. A., P. C. Thurston, R. Bateman, B. Dube, H. L. Gibson, M. A. Hamilton, B. Hathway, S. M. Hocker, M. G. Houle, G. Hudak, V. O. Ispolatov, B. Lafrance, C. M. Lesher, P. J. MacDonald, A. S. Peloquin, S. J. Piercey, L. E. Reed, et P. H. Thompson (2005). Overview of results from the Greenstone Architecture Project; Discover Abitibi Initiative. Open File Report - Ontario Geological Survey. Canada, Ontario Geological Survey : Toronto, ON, Canada.

Ayer, J., Y. Amelin, F. Corfu, S. Kamo, J. Ketchum, K. Kwok, et N. Trowell. 2002. «Evolution of the southern Abitibi greenstone belt based on U–Pb geochronology: autochthonous volcanic construction followed by plutonism, regional deformation and sedimentation». *Precambrian Research*, vol. 115, p. 63-95.

Baker, T., P. J. Pollard, R. Mustard, G. Mark, et J. L. Graham. 2005. «A comparison of granite-related tin, tungsten, and gold-bismuth deposits; implications for exploration». *SEG Newsletter*, vol. 61, p. 5.

Barron, K.M. 1998. «The Petrological and Metallogenic Signifiance of the Alkaline Igneous Centre at the Springpole Gold Prospect, Northwestern Ontario». Ph.D. Thesis, Department of Earth Sciences, Univerity of Western Ontario, London, Ontario.

Barton, P.B.Jr. 1969. «Thermochemical study of the system Fe-As-S». *Geochimica et Cosmochimica Acta*, vol. 33, no 7, p. 841-857.

Bedart, J.H., L. B. Harris, et P. Thurston. 2012. «The hunting of the snARC». *Precambrian Research.*

Benn, K., et A. Peschler. 2005. «A detachment fold model for fault zones in the Late Archean Abitibi greenstone belt». *Tectonophysics*, vol. 400, no 1-4, p. 85-104.

Bevan, P.A. (2009). Technical Report on Beattie-Donchester Gold Mine Property, Duparquet, Quebec. NI 43-101 Report: 42 p.

Bi, S. J., J. W. Li, M. F. Zhou, et Z. K. Li. 2011. «Gold distribution in As-deficient pyrite and telluride mineralogy of the Yangzhaiyu gold deposit, Xiaoqinling district, southern North China craton». *Mineralium Deposita*, vol. 46, no 8, p. 1-17.

Bleeker, W., et R.R. Parrish. 1996. «Stratigraphy and U - Pb zircon geochronology of Kidd Creek: implications for the formation of giant volcanogenic massive sulphide deposits and the tectonic history of the Abitibi greenstone belt». *Canadian Journal of earth Sciences*, vol. 33, p. 1213-1231.

Boivin, P. 1974. «Pétrographie, stratigraphie et structure de la ceinture de schistes verts de Noranda, dans les cantons de Hébécourt, de Duparquet et de Destor, Québec.». Clermont-Ferrand, Université de Clermont-Ferrand, France, 133 p.

Bonnemaison, M., et E. Marcoux. 1990. «Auriferous mineralization in some shear-zones: A three-stage model of metallogenesis». *Mineralium Deposita*, vol. 25, no 2, p. 96-104.

Bourdeau, J., A.E. Lalonde, et J. Goutier. 2011. «Petrology, mineralogy, and geochemistry of the Beattie syenite, Porcupine-Destor fault zone, Abitibi Subprovince, Québec». *Association géologique du Canada - Association minéralogique du Canada*, vol. 34, p. 24.

Brown, S. M., C.A. Johnson, R.J. Watling, et W. R. Premo. 2003. «Constraints on the composition of ore fluids and implications for mineralising events at the Cleo gold deposit, Eastern Goldfields Province, Western Australia». *Australian Journal of Earth Sciences*, vol. 50, no 1, p. 19-38.

Cabri, L.J., S.L. Chryssoulis, J.P.R. De Villiers, J.H. Gilles Laflamme, et Peter R. Buseck. 1989. «The Nature of "Invisible" Gold in Arsenopyrite». *The Canadian Mineralogist*, vol. 27, p. 353-362.

Cameron, E.M., et K. Hattori. 1987. «Archean gold mineralization and oxidized hydrothermal fluids». *Economic Geology and the Bulletin of the Society of Economic Geologists*, vol. 82, no 5, p. 1177-1191.

Cathelineau, M., M.C. Boiron, P. Holliger, P. Marion, et M. Denis. 1989. «Gold in Arsenopyrites : Crystal Chemistry, Location and State, Physical and Chemical Conditions of Deposition». *Economic Geology Monography*, vol. 6, p. 328–341.

Cathles, L. M., et R. Shannon. 2007. «How potassium silicate alteration suggests the formation of porphyry ore deposits begins with the nearly explosive but barren expulsion of large volumes of magmatic water». *Earth and Planetary Science Letters*, vol. 262, no 1-2, p. 92-108.

Cepedal, A., M. Fuertes-Fuente, A. Martin-Izard, S. Gonzalez-Nistal, et M. Barrero. 2008. «Gold-bearing As-rich pyrite and arsenopyrite from the El Valle gold deposit, Asturias, northwestern Spain». *The Canadian Mineralogist*, vol. 46, p. 233-247.

Chown, E.H. 1992. «Tectonic evolution of the Northern Volcanic Zone, Abitibi Belt, Quebec». *Canadian Journal of Earth Sciences = Revue Canadienne des Sciences de la Terre*, vol. 29, no 10, p. 2211-2225.

Ciobanu, C. L., N.J. Cook, F. Damian, et G. Damian. 2006. «Gold scavenged by bismuth melts; an example from Alpine shear-remobilizates in the Highis Massif, Romania». *Mineralogy and Petrology*, vol. 87, no 3-4, p. 351-384.

Colvine, A.C. 1989. «An empirical model for the formation of Archean gold deposits: products of final cratonization of the Superior province, Canada». *In:*, vol. Keays RR, Ramsay WRH, Groves DI (eds). The geology of gold deposits: the perspective in 1988. Economic Geology Monography 6, p. 37-53.

Cook, N. J., C. L. Ciobanu, et J. Mao. 2009. «Textural control on gold distribution in As-free pyrite from the Dongping, Huangtuliang and Hougou gold deposits, North China Craton (Hebei Province, China)». *Chemical Geology*, vol. 264, no 1-4, p. 101-121.

Cook, N.J., et S.L. Chryssoulis. 1990. «Concentration of "Invisible Gold" in the common sulfides». *The Canadian Mineralogist*, vol. 28, p. 1-16.

Cooke, D.R., C.L. Deyell, P.J. Waters, R.I. Gonzales, et K. Zaw. 2011. «Evidence for magmatic-hydrothermal fluids and ore-forming processes in epithermal and porphyry deposits of the Baguio District, Philippines». *Economic Geology and the Bulletin of the Society of Economic Geologists*, vol. 106, no 8, p. 1399-1424.

Corbett, G. 2009. «Anatomy of porphyry-related Au-Cu-Ag-Mo mineralised systems: Some exploration implications». In *Australian Institute of Geoscientists North Queensland Exploration*, p. 13.

Daigneault, R., W.U. Mueller, et E.H. Chown. 2002. «Oblique Archean subduction: accretion and exhumation ofan oceanic arc during dextral transpression, Southern Volcanic Zone, Abitibi Subprovince Canada». *Precambrian Research*, vol. 115, p. 261–290.

David, J., C. Dion, J. Goutier, P. Roy, D. Bandyayera, M. Legault, et P. Rhéaume (2006). Datations U-Pb effectuées dans la Sous-province de l'Abitibi à la suite des travaux de 2004-2005, Ministère des Ressources Naturelles et Faune; RP 2006-04: 22 p.

Davidson, S., et A. F. Banfield. 1944. «Geology of the Beattie Gold Mine, Duparquet, Quebec». *Economic Geology*, vol. 39, p. 535-556.

Dimroth, E. 1982. «Evolution of the south-central part of the Archean Abitibi Belt, Quebec; Part I, Stratigraphy and paleogeographic model». *Canadian Journal of Earth Sciences = Revue Canadienne des Sciences de la Terre*, vol. 19, no 9, p. 1729-1758.

Dinel, E., A.D. Fowler, J. Ayer, A. Still, K. Tylee, et E. Barr. 2008. «Lithogeochemical and Stratigraphic Controls on Gold Mineralization within the Metavolcanic Rocks of the Hoyle Pond Mine, Timmins, Ontario». *Economic Geology*, vol. 103, no 6, p. 1341-1363.

Dolejs, D., et C. E. Manning. 2010. «Thermodynamic model for mineral solubility in aqueous fluids; theory, calibration and application to model fluid flow systems». *Geofluids [Oxford]*, vol. 10, no 1-2, p. 20-40.

Doucet, P., J. Goutier, M. Melaçon, et L. Ste-Croix (2000). L'Abitibi: Un centenaire d'exploration et de succès minier, Ministère des Ressources naturelles, faune et parcs, Québec. DV 2000-03: 44 p.

Dupéré, M., et C. Duplessis (2007). Technical Report - Resource Evaluation on the Douay Project for SEM Vior Inc.: 188 p.

Dupéré, M., C. Duplessis, et J. Gagné (2011). NI 43-101 Technical Report Mineral Resource Estimation Duparquet – Beattie Property For Osisko Mining Corporation and Clifton Star Resources Inc.: 125 p.

Duuring, P., K. Cassidy, et S. Hagemann. 2007. «Granitoid-associated orogenic, intrusion-related, and porphyry style metal deposits in the Archean Yilgarn Craton, Western Australia». *Ore Geology Reviews*, vol. 32, no 1-2, p. 157-186.

Fleet, M. E., S. L. Chryssoulis, R. Davidson, C. G. Weisener, et P. J. Maclean. 1993. «Arsenian pyrite from gold deposits: Au and As distribution investigated by SIMS and EMP, and color staining and surface oxidation by XPS and LIMS». *Canadian Mineralogist*, vol. 31, no 1, p. 1-17.

Gauthier, M., et L. Harnois (1994). Étude sommaire des protolithes, des patrons d'altération et des paragenèses minérales des minéralisations aurifères du canton de Douay (Abitibi). Rapport d'étape soumis à Richard Laplante et Denis Raymond du bureau régional d'Abitibi de SOQUEM, Université du Québec à Montréal.

Genkin, A.D., N.S. Bortnikov, L.J. Cabri, F. E. Wagner, C.J. Stanley, Y.G. Safonov, G. McMahon, J. Friedl, A.L. Kerzin, et G.N. Gamyanin. 1998. «A multidisciplinary study of invisible gold in arsenopyrite from four mesothermal gold deposits in Siberia, Russian Federation». *Economic Geology and the Bulletin of the Society of Economic Geologists*, vol. 93, no 4, p. 463-487.

Goutier, J., et S. Lacroix (1992). Géologie du secteur de la faille de Porcupine-Destor dans les cantons de Destor et Duparquet, Ministère de l'Énergie et des Ressources, Québec; MB 92-06: 67 p.

Grant, J. 2005. «Isocon analysis: A brief review of the method and applications». *Physics and Chemistry of the Earth, Parts A/B/C*, vol. 30, no 17-18, p. 997-1004.

Groves, D.I., R.J. Goldfarb, M. Gebre-Mariam, S.G. Hagemann, et F. Robert. 1998. «Orogenic gold deposits: A proposed classification in the context of their crustal distribution and relationship to other gold deposit types». *Ore Geology Reviews*, vol. 13, p. 7–27.

Groves, D.I., R.J. Goldfarb, F. Robert, et C. J. R. Hart. 2003. «Gold Deposits in Metamorphic Belts: Overview of Current Understanding, Outstanding Problems, Future Research, and Exploration Significance». *Economic Geology*, vol. 98, p. 1–29.

Hart, C.J.R. 2005. «Classifying, distinguishing and exploring for intrusion-related gold systems». *Program with Abstracts - Geological Association of Canada; Mineralogical Association of Canada: Joint Annual Meeting*, vol. 30, p. 81-81.

Hart, C.J.R. (2007). Reduced Intrusion-Related Gold Systems. W.D. *in* Goodfellow, ed., Mineral deposits of Canada: A Synthesis of Major Deposit Types, District et the Evolution of Geological Provinces Metallogeny, and Exploration Methods: Geological Association of Canada, Mineral Deposits Division. Special publication No 5: 95-112 p.

Jébrak, M. 1997. «Hydrothermal breccias in vein type ore deposit : A review of mechanisms, morphology and size distribution». *Ore Geology Reviews*, vol. 12, p. 111-134.

Jébrak, M., et E. Marcoux. 2008. *Géologie des ressources minérales*, Denis L. Lefebvre, ing.: Ministère des Ressources Naturelles et de la Faune. Québec, 667 p.

Kerrich, R., A. Polat, et Q. Xie. 2008. «Geochemical systematics of 2.7 Ga Kinojevis Group (Abitibi), and Manitouwadge and Winston Lake (Wawa) Fe-rich basalt–rhyolite associations: Backarc rift oceanic crust?». *Lithos*, vol. 101, no 1-2, p. 1-23.

Kovalev, K. R., Y. Kalinin, E. A. Naumov, M. K. Kolesnikova, et V. N. Korolyuk. 2011. «Gold-bearing arsenopyrite in eastern Kazakhstan gold-sulfide deposits». *Russian Geology and Geophysics*, vol. 52, no 2, p. 178-192.

Kretschmar, U., et S. D. Scott. 1976. «Phase relations involving arsenopyrite in the system Fe-As-S and their application». *Canadian Mineralogist*, vol. 14, Part 3, p. 364-386.

Lafrance, B. 2011. «À la recherche d'IOCG et de porphyres à Cu-Au alcalins-calciques en Abitibi: utilisation de la typologie des intrusions». In *Forum Technologique Consorem-Divex*, Rouyn-Noranda, Québec.

Lang, J.R., et T. Baker. 2001. «Intrusion-related gold systems : the present level of understanding». *Mineralium Deposita*, vol. 36, p. 477-489.

Legault, M., J. Goutier, G. Baudoin, et M. Aucoin (2005). Synthese-metallogenique-de-la-faille-Destor-Porcupine, Ministère des Ressources Naturelles et de la Faune, Québec; ET 2005-01: 37 p.

Legault, M., et A.E. Lalonde (2009). Discrimination des syenites associées aux gisements aurifères de la sous province de l'Abitibi, Québec, Canada, Ministère des Ressources Naturelles et de la Faune, Québec; RP 2009-04: 10 p

Linnen, R. 2012. «Syenite-Hosted Gold Mineralization at the Young-Davidson Deposit». In *Short Course Intrusion Related Gold in the Abitibi : Theory and Application to Exploration* (University of Western Ontario, London, Ontario, Canada). Resource Geoscience Wester London Student Chapter. University of Western Ontario, London, Ontario, Canada.

Martin-Izard, A., et L. Rodríguez-Terente. 2009. *Invisible gold at the Salave Deposit, NW Spain: Proceedings of the Tenth Biennial SGA Meeting* (Townsville).

McCuaig, T. C., et R. Kerrich. 1998. «P-T-t-deformation-fluid characteristics of lode gold deposits: Evidence from alteration systematics». *Ore Geology Reviews*, vol. 12, no 6, p. 381-453.

Mexias, A.S., G. Berger, M.E.B. Gomes, M.L.L. Formoso, N. Dani, J.C. Frantz, et E.M. Bongiolo. 2005. «Geochemical modeling of gold precipitation conditions in the Bloco do Butia Mine, Lavras do Sul, Brazil». *Anais da Academia Brasileira de Ciencias*, vol. 77, no 4, p. 717-728.

Mikucki, E.J. 1998. «Hydrothermal transport and depositional processes in Archean lode-gold systems; a review». *Ore Geology Reviews*, vol. 13, no 1-5, p. 307-321.

Mikucki, E.J., et F.I. Roberts (2004). Metamorphic petrography of the Kalgoorlie region, Eastern Goldfields granite-greenstone terrane: METPET database. Geological Survey of Western Australia Record 2003/12: 40 p.

Morey, A.A., A.G. Tomkins, F.P. Bierlein, R.F. Weinberg, et G.J. Davidson. 2008. «Bimodal Distribution of Gold in Pyrite and Arsenopyrite: Examples from the Archean Boorara and Bardoc Shear Systems, Yilgarn Craton, Western Australia». *Economic Geology*, vol. 103, no 3, p. 599-614.

Müller, D., K. Kaminski, S. Uhlig, T. Graupner, P. Herzig, et S. Hunt. 2002. «The transition from porphyry- to epithermal-style gold mineralization at Ladolam, Lihir Island, Papua New Guinea: a reconnaissance study». *Mineralium Deposita*, vol. 37, no 1, p. 61-74.

Mueller, W.U., R. Daigneault, J.K. Mortensen, et E.H. Chown. 1996. «Archean terrane docking: upper crust collision tectonics, Abitibi greenstone belt, Quebec, Canada». *Tectonophysics*, vol. 265, p. 127-150.

Mumin, A.H., M.E. Fleet, et S. Chryssoulis. 1994. «Gold mineralization in As-rich mesothermal gold ores of the Bogosu-Prestea mining district of the Ashanti gold belt, Ghana; remobilization of 'invisible' gold». *Mineralium Deposita*, vol. 29, no 6, p. 445-460.

Mutschler, F.E. 1985. «Precious metal deposits related to alkaline rocks in the North American Cordillera; an interpretive review». *Verhandelinge van die Geologiese*

*Vereniging van Suid Afrika = Transactions of the Geological Society of South Africa*, vol. 88, no 2, p. 355-377.

Neumayr, P. 2007. «Fluid chemistry and evolution of hydrothermal fluids in an Archaean transcrustal fault zone network; the case of the Cadillac tectonic zone, Abitibi greenstone belt, Canada». *Canadian Journal of earth Sciences*, vol. 44, no 6, p. 745-773.

O'Neill, J.J. (1932). La mine d'or Beattie, canton de Duparquet. Service des mines du québec, Service des Mines de Québec.

Palenik, C.S., S. Utsunomiya, M. Reich, S.E. Kesler, L. Wang, et R.C. Ewing. 2004. «"Invisible" gold revealed: Direct imaging of gold nanoparticles in a Carlin-type deposit». *American Mineralogist*, vol. 89, no 10, p. 1359-1366.

Panina, L.I., et I.V. Motorina. 2008. «Liquid Immiscibility in Deep-Seated Magmas and the Generation of Carbonatite Melts». *Geochemistry International*, vol. 46, no 5, p. 443-464.

Pelissonnier, H. 2001. *Réflexion sur la métallogénie*. Paris: Société de l'industrie minérale, 413 p.

Peschler, A. P., K. Benn, et W. R. Roest. 2006. «Gold-bearing fault zones related to Late Archean orogenic folding of upper and middle crust in the Abitibi granite-greenstone belt, Ontario». *Precambrian Research*, vol. 151, no 3-4, p. 143-159.

Piché, M., et M. Jébrak. 2004. «Normative minerals and alteration indices developed for mineral exploration». *Journal of Geochemical Exploration*, vol. 82, no 1-3, p. 59-77.

Powell, W.G., D.M. Carmichael, et C.J. Hodgson. 1995. «Conditions and timing of metamorphism in the southern Abitibi greenstone belt, Quebec». *Canadian Journal of earth Sciences*, vol. 32, p. 787-805.

Putnis, A. 2002. «Mineral replacement reactions; from macroscopic observations to microscopic mechanisms». *Mineralogical Magazine*, vol. 66, no 5, p. 689-708.

Rabeau, O. 2010. «Distribution de l'or de type orogénique le long de grands couloirs de déformation archéens: modélisation numérique sur l'exemple de la ceinture de l'Abitibi». Université du Québec à Montréal et Institut National Polytechnique de Lorraine (France), 155 p.

Reich, M., S. Kesler, S. Utsunomiya, C. Palenik, S. Chryssoulis, et R. Ewing. 2005. «Solubility of gold in arsenian pyrite». *Geochimica et Cosmochimica Acta*, vol. 69, no 11, p. 2781-2796.

Richards, J.P. 1992. «Magmatic-epithermal transitions in alkalic systems; Porgera gold deposit, Papua New Guinea». *Geology [Boulder]*, vol. 20, no 6, p. 547-550.

Robert, F. 2001. «Syenite associated disseminated gold deposit in the Abitibi greenstone belt, Canada». *Mineralium Deposita*, vol. 36, p. 505-516.

Robert, F. (1994). Vein fields in gold districts; the example of Val d'Or, southeastern Abitibi Subprovince, Quebec. Canada, Geological Survey of Canada : Ottawa, ON, Canada: 295-302 p.

Robert, F., K.H. Poulsen, K.F. Cassidy, et C.J. Hodgson. 2005. «Gold Metallogeny of the Superior and Yilgarn Cratons». *Economic Geology*, vol. 100th Anniversary Volume, p. 1001-1033.

Romberger, S.B. 1986. «The Solution Chemistry of Gold Applied to the Origin of Hydrothermal Deposits». *Canad. Inst. Mining Special*, vol. 38, p. 168-186.

Sharp, Z.D., E.J. Essene, et W.C. Kelly. 1985. «A re-examination of the arsenopyrite geothermometer: Pressure considerations and applications to natural assemblages». *The Canadian Mineralogist*, vol. 23, p. 517–534.

Sillitoe, R. H. 2010. «Porphyry copper systems». *Economic Geology*, vol. 105, no 1, p. 3-41.

Sillitoe, R.H., et J.W. Hedenquist. 2003. «Linkages between volcanotectonic settings, ore-fluid compositions, and epithermal precious metal deposits». *Special Publication [Society of Economic Geologists [U. S.]]*, vol. 10, p. 315-343.

Sung, Y. H., J. Brugger, C. L. Ciobanu, A. Pring, W. Skinner, et M. Nugus. 2009. «Invisible gold in arsenian pyrite and arsenopyrite from a multistage Archaean gold deposit: Sunrise Dam, Eastern Goldfields Province, Western Australia». *Mineralium Deposita*, vol. 44, no 7, p. 765-791.

Thompson, T.B., A.D. Tbippel, et P.C. Dwelley. 1985. «Mineralized Veins and Breccias of the Cripple Creek District, Colorado». *Economic Geology*, vol. 80, p. 1669-1688.

Tooth, B., C. L. Ciobanu, L. Green, B. O'Neill, et J. Brugger. 2011. «Bi-melt formation and gold scavenging from hydrothermal fluids: An experimental study». *Geochimica et Cosmochimica Acta*, vol. 75, no 19, p. 5423-5443.

Vaughan, J. P., et A. Kyin. 2004. «Refractory gold ores in Archaean greenstones, Western Australia; mineralogy, gold paragenesis, metallurgical characterization and classification». *Mineralogical Magazine*, vol. 68, no 2, p. 255-277.

Wares, R. 2010. «Communiqué de presse : Osisko et Clifton Star recoupent 42 mètres à une teneur moyenne de 3,38g/t Au à Duparquet ». En ligne :

http://www.osisko.com/en/press/2010/12/06/563/osisko-and-clifton-star-intersect-42-metres-averaging-3-38-g-t-au-at-duparquet.html.

Williams-Jones, A. E., et C. A. Heinrich. 2005. «100th Anniversary Special Paper: Vapor transport of metals and the formation of magmatic-hydrothermal ore deposits». *Economic Geology*, vol. 100, no 7, p. 1287-1312.

Witt, W.K. 1992. «Porphyry intrusions and albitites in the Bardoc-Kalgoorlie area, Western Australia and their role in the Archean epigenetic gold mineralization». *Canadian Journal of earth Sciences*, vol. 29, p. 1609-1622.

Zhang, P.L., N. Machado, J. Ludden, et D. Moore. 1993. «Geotectonic constraints fro U-Pb ages from the Black River Group, the Kinojévis Group and the Normétal mine area, Abitibi, Québec». *Association géologique du Canada - Association minéralogique du Canada*, vol. 18, p. A114.